SUPPORTING INFORMARION

Supramolecular Chiroptical Sensing by Achiral AIE-active Thiols

Xueyan Zhang, [a,b]* Yang Li[a], Li Wang[b], Hongcheng Liu[b]

a. Wenzhou Key Laboratory of Biophysics, Wenzhou Institute, University of Chinese Academy of Sciences, Wenzhou, Zhejiang 325000, P. R. China.
*E-mail: cpuzhangxueyan@163.com.
b. Institute of Quality Standard and Testing Technology, Yunnan Academy of Agricultural Science, Supervision and Testing Center for Farm Product Quality, Ministry of Agriculture, Kunming 650205, PR China

Contents

Experimental Section

Materials and Instrumentations

All other chemicals and regents were purchased from energy-chemical and used as received without further purification. ^{1}H and ^{13}C NMR spectra were measured on a QUANTUM-I-400 MHz spectrometer in $CDCl_3$ and DMSO-d_6 using tetramethylsilane (TMS; $\delta = 0$) as internal reference. UV-*vis* absorption spectra were obtained by using a TU-1901 spectrophotometer. Fluorescence spectra were measured by using a HORIBA Scientific Fluoro-max-4 Spectrofluorometer. Circular dichroism (CD) spectra were obtained on a Chirascan Plus spectropolarimeter. Circularly polarized luminescence (CPL) spectra were recorded by a JASCO CPL-300 spectrofluoropolarimeter. LC-MS analyses were performed with a Dionex UltiMate 3000 connected to a thermo scientific MSQ PLUS mass spectrometer using a Thermo Scientific C18 (1.9 µm, 2.1 × 100 mm) analytical column. Flash chromatography columns were packed with 300-400 C18 packing material with MeOH and H_2O as eluents. FT-IR spectra were recorded on a Bruker Tensor 27 FTIR spectrometer at room temperature. SEM images were recorded on a Hitachi S-4800 FE-SEM instrument with an accelerating voltage of 10 kV. Sensors **1-3** or chiroptical sensing products solution were cast onto single-crystal silica plates, the solvent evaporated under the ambient conditions, and then vacuum-dried. The sample surface was coated with a thin layer of Pt to increase the contrast. All measurements were performed at room temperature unless otherwise stated.

Synthesis Procedures

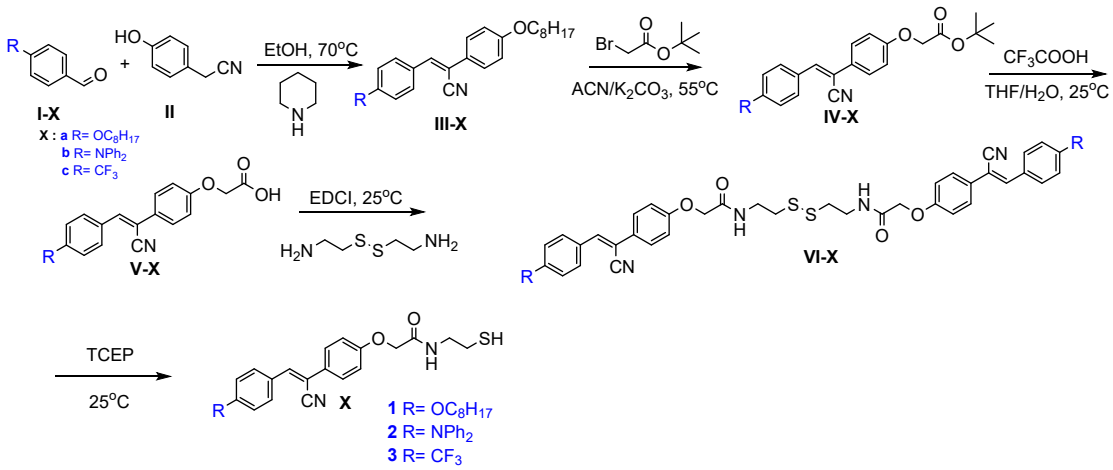

Scheme S1 The synthesis procedures of probes **1-3**

Probes **1-3** were synthesized according to the reference literature [1] to yield two pale yellow solids (**1** and **3**) and a yellow solid (**2**).

Synthesis of probe 1

4-octyloxy benzaldehyde (2.34 g, 10.0 mmol) and 2-(4-hydroxyphenyl) acetonitrile (1.33 g,

10.0 mmol) were dissolved in ethanol (100 mL) at 70°C. Then 2.02 mL piperidine (1.75 g, 20.5 mmol) was added into the mixture and stirred overnight. A yellow precipitate (2.70 g) was obtained after filtration and used for next step without purification. Intermediate **III-a** and 1.6 mL of tert-butyl 2-bromoacetate (2.15 g, 11.0 mmol) were dissolved in 100 mL of acetone, then K_2CO_3 (6.90 g, 50.0 mmol) was added to the above solution, heated to 55°C, and the resulting mixture was stirred at this temperature overnight. After cooling to room temperature, the mixture was filtered by filter paper and the solvent was removed under reduced pressure to give a crude product **IV-a**. This crude product was dissolved in mixed solution (THF/H_2O = 3:1, v/v), 3.71 mL CF_3COOH (5.70 g, 50.0 mmol) was added and then stirred at room temperature for 6 h. The reaction mixture was extracted with CH_2Cl_2 for 3 times. The organic phase was collected and dried with anhydrous Na_2SO_4, after being filtered, the solvent was removed using rotary evaporator and gave crude product, which was purified by recrystallization. 3.75 g of **V-a** white solid was obtained. Then cystamine dihydrochloride (1.04 g, 4.6 mmol) was dissolved in CH_2Cl_2, and triethylamine (0.9 g, 5.0 mmol) was added to the above solution, **V-a** (3.75 g, 9.2 mmol) and 1-(3-dimethylaminopropyl)-3-ethylcarbodiimide hydrochloride (EDC-HCl) (0.96 g, 5.0 mmol) were added to the solution, the mixed solution was stirred at room temperature overnight. Saturated aqueous Na_2CO_3 solution was added to the above reaction solution to remove triethylamine hydrochloride and EDC, then the organic phase was collected and dried with anhydrous Na_2SO_4, after filtering, the organic solvent was removed using a rotary evaporator to give the crude product **VI-a**, which was further purified by recrystallisation to give a pale-yellow solid (6.98 g, 7.5 mmol), yield 81.0 %.

Intermediates **III-a** and **IV-a** were simply purified by filtration or precipitation, were used directly in the next step. Intermediate **V-a** was simply purified via precipitation and characterized by ^{1}H NMR. Intermediate **VI-a** was well characterized by ^{1}H NMR, ^{13}C NMR, and EI-MS. Intermediate **VI-a** (5×10^{-4} M) and 1.2 eq amount of tris(2-carboxyethyl)phosphine hydrochloride (TCEP) were dissolved in mixed solution (THF/H_2O = 9:1, v/v) to make probe **1** solution to participate in the subsequent chiral compound detection reaction.

Intermediate V-a

^{1}H NMR (400 MHz, DMSO-d_6) δ (ppm): 7.92-7.90 (d, 2H, J = 8 Hz), 7.83 (s, 1H), 7.67-7.65 (d, 2H, J = 8 Hz), 7.10-7.04 (m, 4H), 4.76 (s, 2H), 4.07-4.03 (m, 2 H), 1.78-1.71 (m, 2H), 1.46-1.41 (m, 2H), 1.34-1.28 (m, 8H), 0.92-0.86 (t, 3H, J =12 Hz)).

Intermediate VI-a

^{1}H NMR (400 MHz, DMSO-d_6) δ (ppm): 7.92-7.90 (d, 2H, J = 8 Hz), 7.83 (s, 1H), 7.69-7.67 (d, 2H, J = 8 Hz), 7.10-7.07 (m, 4H), 4.89 (s, 2H), 4.08-4.04 (m, 2 H), 3.73 (s, 2H), 3.35 (s, 2H), 1.77-1.73 (m, 2H), 1.45-1.41 (m, 2H), 1.34-1.26 (m, 8H), 0.90-0.86 (t, 3H, J =12 Hz); ^{13}C NMR

(100 MHz, DMSO-d_6) δ (ppm): 169.44, 160.89, 158.58, 141.39, 131.33, 129.82, 127.81, 126.70, 119.06, 115.64, 107.10, 68.28, 65.16, 52.49, 31.98, 29.26, 25.84, 22.73, 14.58; EI-MS: calculated for $C_{54}H_{66}N_4O_6S_2$, 930.44, found 1009.49 [$C_{54}H_{66}N_4O_6S_2$+Br^-].

Intermediate V-b

Compound **V-b** was synthesized also according to the reference literature[1] to afford **V-b** as a yellow solid (2.9 g, yield: 70%). ^{1}H NMR (400 MHz, DMSO-d_6) δ (ppm): 7.82-7.79 (d, 2H, J = 12 Hz), 7.75 (s, 1H), 7.63-7.60 (d, 2H, J = 12 Hz), 7.42-7.38 (m, 4H), 7.20-7.13 (m, 6H), 6.98-6.96 (m, 4 H), 4.44 (s, 2H).

Synthesis of compound VI-b

Compound **VI-b** was synthesized according to the procedure of **VI-a** to give **VI-b** as a yellow solid (0.39 g, yield: 58%). ^{1} H NMR (400 MHz, DMSO-d_6) δ (ppm): 7.78-7.76 (m, 2H), 7.69-7.66 (m, 2H), 7.44-7.40 (m, 5H), 7.20-7.11 (m, 8H),7.08-6.96 (m, 3 H), 4.55 (s, 2H), 3.49-3.43 (q, 2H, J_1 = 8 Hz, J_2 = 12 Hz), 2.89-2.84 (q, 2H, J_1 = 8 Hz, J_2 = 12 Hz). ^{13}C NMR (100 MHz, DMSO-d_6) δ (ppm): 168.03, 158.58, 157.58, 146.61, 140.88, 131.03, 130.43, 129.82, 127.81, 127.21, 126.0, 124.99, 120.77, 119.97, 119.16, 115.64, 106.49, 67.57, 38.31, 22.02; EI-MS: calculated for $C_{62}H_{52}N_6O_4S_2$, 1008.35, found 1009.55 [$C_{62}H_{52}N_6O_4S_2$+H^+].

Intermediate V-c

Compound **V-c** was synthesized also according to the reference literature[1] to afford **V-c** as a yellow solid (2.96 g, yield: 85.3%). ^{1}H NMR (400 MHz, DMSO-d_6) δ (ppm):8.10-8.04 (m, 4H), 7.92-7.90 (m, 2H), 7.74-7.72 (m, 3H), 4.58 (s, 2H).

Synthesis of compound VI-c

Compound **VI-c** was synthesized according to the procedure of **VI-a** to afford **VI-c** as a white solid (0.62 g, yield: 76%). ^{1} H NMR (400 MHz, DMSO-d_6) δ (ppm): 8.12-8.06 (m, 3H), 7.94-7.88 (m, 2H), 7.78-7.75 (m, 2H), 7.15-7.10 (m, 2H), 4.60 (s, 2H), 3.49-3.46 (m, 2H), 2.91-2.84 (m, 2H). ^{13}C NMR (100 MHz, DMSO-d_6) δ (ppm): 167.92, 159.32, 139.48, 138.52, 130.03, 128.01, 126.42, 117.92, 115.91, 113.05, 67.40, 38.32,37.58; ^{19}F NMR (376 MHz, DMSO-d_6) δ (ppm): -56.51, -68.70; EI-MS: calculated for $C_{40}H_{32}F_6N_4O_4S_2$, 810.18, found 833.26 [$C_{40}H_{32}F_6N_4O_4S_2$+Na^+].

NMR Spectra

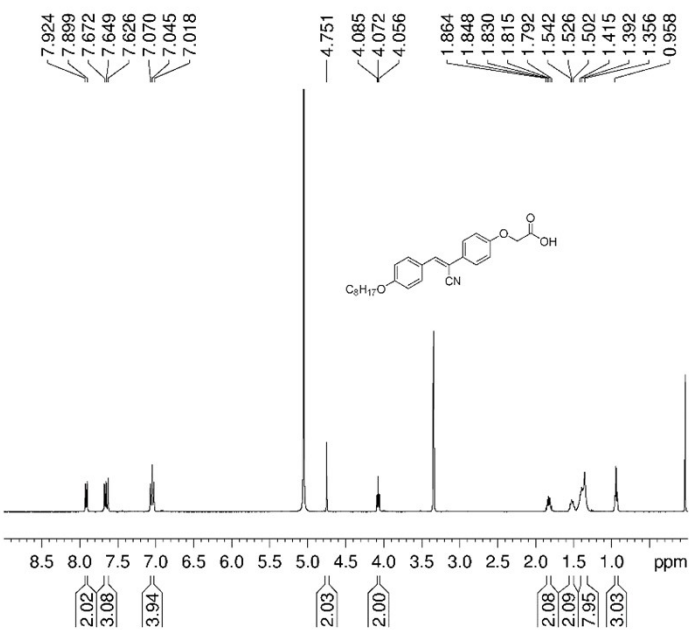

Figure S1 ^{1}H NMR (400 MHz, DMSO-d_6)

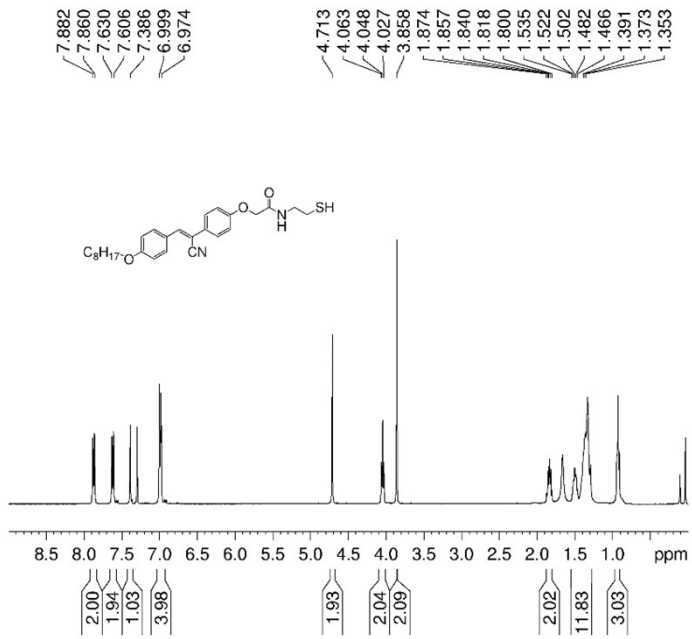

Figure S2 ^{1}H NMR of **VI-a** (400 MHz, DMSO-d_6)

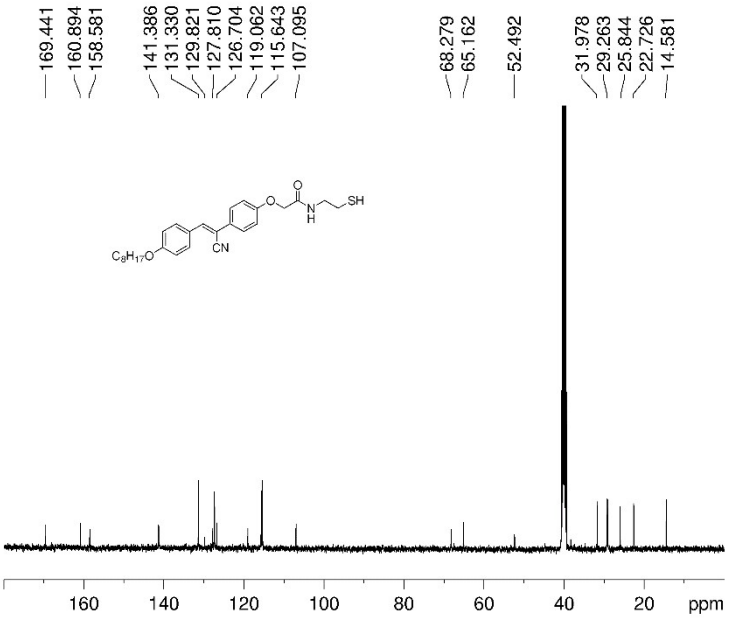

Figure S3 ^{13}C NMR of **VI-a** (100 MHz, DMSO-d_6)

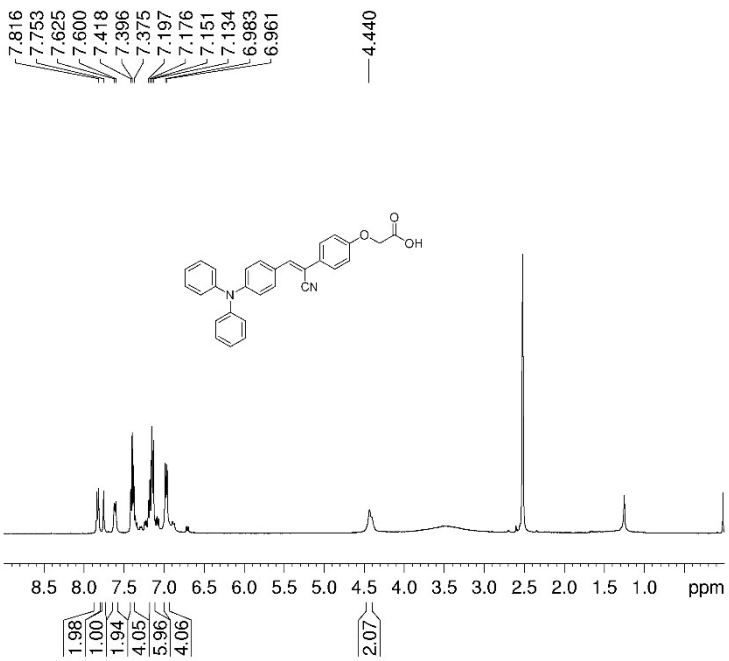

Figure S4 ^{1}H NMR (400 MHz, DMSO-d_6)

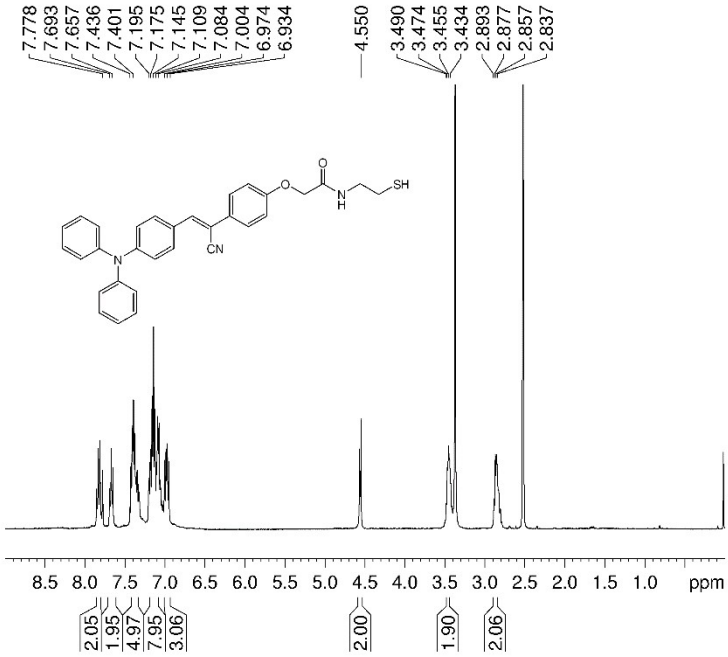

Figure S5 ^{1}H NMR of **VI-b** (400 MHz, DMSO-d_6)

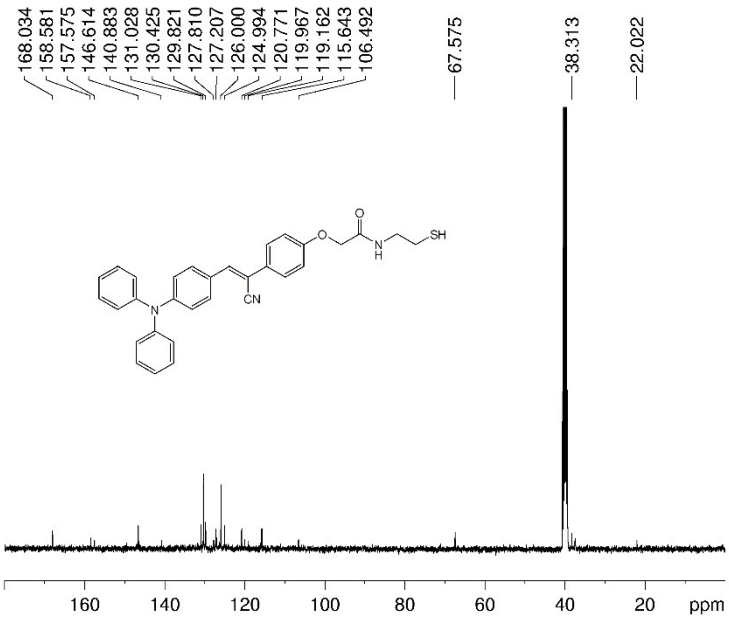

Figure S6 ^{13}C NMR of **VI-b** (100 MHz, DMSO-d_6)

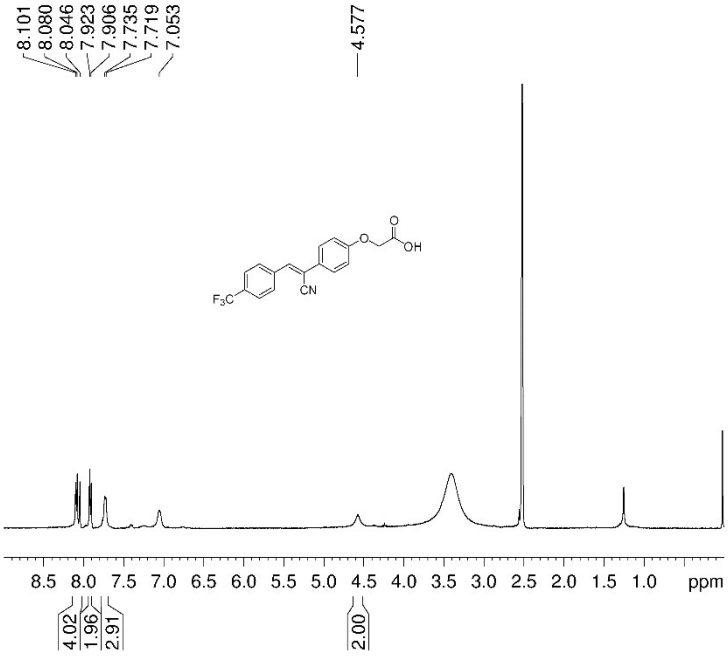

Figure S7 ^{1}H NMR (400 MHz, DMSO-d_6)

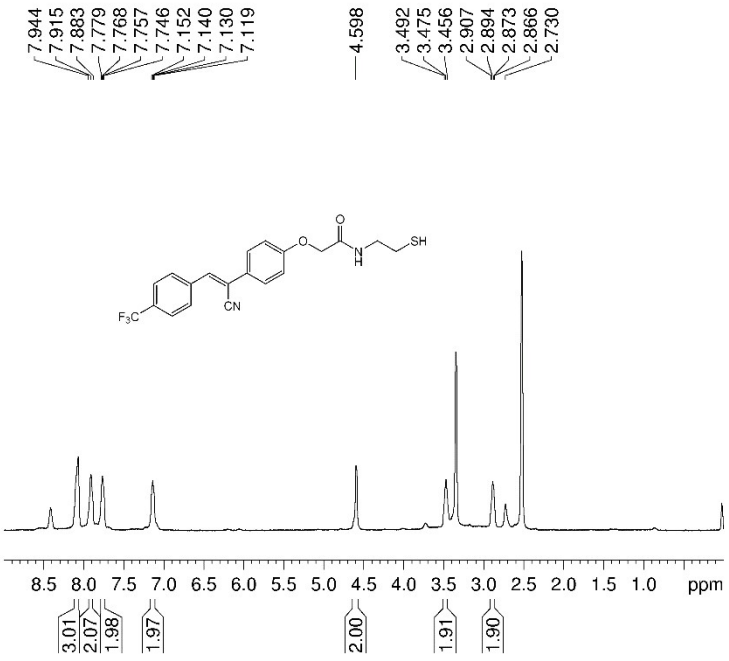

Figure S8 ^{1}H NMR of **VI-c** (400 MHz, DMSO-d_6)

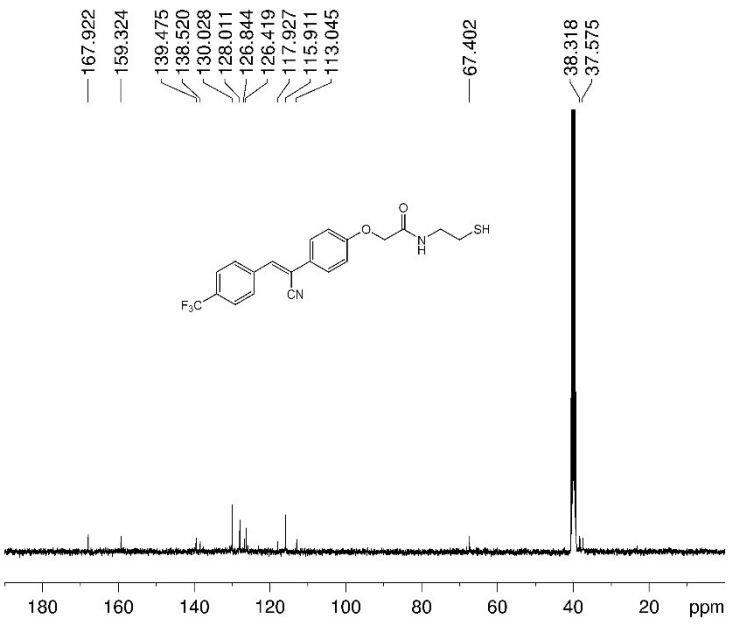

Figure S9 ^{13}C NMR of **VI-c** (100 MHz, DMSO-d_6)

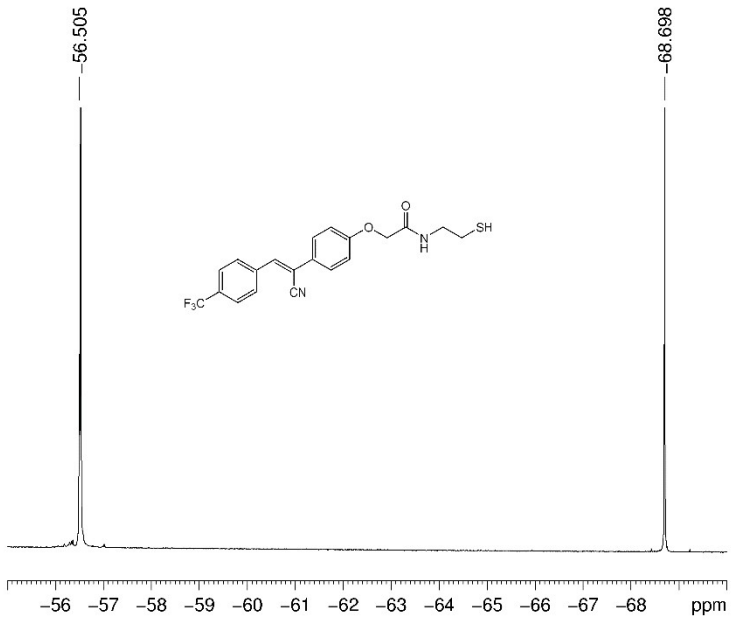

Figure S10 ^{19}F NMR of **VI-c** (376 MHz, DMSO-d_6)

Probes' characterization

Compound **VI-X** (X=a-c, 5 mM) and TCEP (6 mM) were mixed in 1 mL of THF/H_2O (9:1) and the reaction was stirred for 0.5 h. Then, evaporate THF and add 20 ml of water to the solution. Extract with dichloromethane (20 mL×3), combine the organic phases, add anhydrous sodium sulphate to the organic phases, filter and evaporate dichloromethane to obtain the crude product.

Purify the crude products by column chromatography (eluent: dichloromethane/methanol, 98:2 (v/v)) to give two pale yellow solids (probes **1** and **3**) and a light yellow solid **2**. The purified probes 1-3 were obtained and subsequently characterized by NMR and HRMS. It should be noted that to avoid oxidation of the SH groups of the probes **1-3**, the assay was performed directly with a mixed THF/H_2O solution of the probes **1-3** and TCEP without any purification.

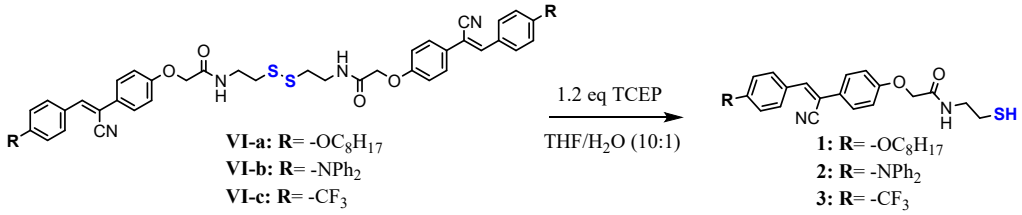

Scheme S2 The reduction procedures of probes **1-3**.

Compound 1:

^{1}H NMR (400 MHz, $CDCl_3$) δ (ppm): 7.85-7.83 (d, 2H, J = 8 Hz), 7.59-7.57 (d, 2H, J = 8 Hz), 7.35 (s, 1H), 6.97-6.94 (d, 4H, J = 12 Hz), 4.68 (s, 2H), 4.03-3.99 (t, 2 H, J = 8 Hz), 3.82 (s, 3H), 1.84-1.76 (m, 2H), 1.49-1.26 (m, 12H), 0.91-0.88 (t, 3H, J =8 Hz). ^{13}C NMR (100 MHz, $CDCl_3$) δ (ppm): 169.09, 161.13, 160.60, 158.16, 143.50, 140.54, 131.62, 130.98, 130.45, 128.86, 127.27, 126.42, 125.99, 121.00, 118.78, 115.17, 114.64, 68.25, 65.28, 52.33, 31.74, 29.19, 25.90, 22.82, 14.44. HRMS: calculated for $C_{27}H_{35}N_2O_3S$, 467.2368, found 467.2370 $[M+H]^+$.

Compound 2:

^{1}H NMR (400 MHz, $CDCl_3$) δ (ppm): 7.76-7.74 (d, 2H, J = 8 Hz), 7.62-7.59 (d, 2H, J = 8 Hz), 7.33-7.29 (m, 6H), 7.16-7.14 (m, 4H), 7.06-7.03 (m, 2H), 6.99-6.97 (m, 3H),4.55 (s, 2H), 3.58-3.53 (m 2 H), 2.75-2.69 (m, 2H). ^{13}C NMR (100 MHz, $CDCl_3$) δ (ppm): 168.03, 157.68, 150.03, 146.72, 141.08, 131.33, 130.638, 129.42, 127.61, 126.70, 126.00, 124.49, 121.07, 120.47, 118.86, 116.14, 107.20, 67.58, 52.33, 42.13, 24.64. HRMS: calculated for $C_{31}H_{28}N_3O_2S$, 506.1897, found 506.1895 $[M+H]^+$.

Compound 3:

^{1}H NMR (400 MHz, $CDCl_3$) δ (ppm): 7.97-7.95 (d, 2H, J = 8 Hz), 7.73-7.67 (dd, 2H, J = 8 Hz), 7.48 (s, 1H), 7.04-7.02 (d, 2H, J = 8 Hz), 4.57 (s, 2H), 3.59-3.54 (q, 2 H, J_1 = 8 Hz, J_2 = 16 Hz), 2.76-2.70 (q, 2 H, J_1 = 8 Hz, J_2 = 16 Hz). ^{13}C NMR (100 MHz, $CDCl_3$) δ (ppm): 167.72, 158.31, 139.07, 136.90, 129.23, 128.21, 125.90, 117.79, 115.62, 113.45, 67.29, 41.82, 24.60. ^{19}F NMR (376 MHz, $CDCl_3$) δ (ppm): -62.86. HRMS: calculated for $C_{20}H_{18}F_3N_2O_2S$, 407.1040, found 407.1044 $[M+H]^+$.

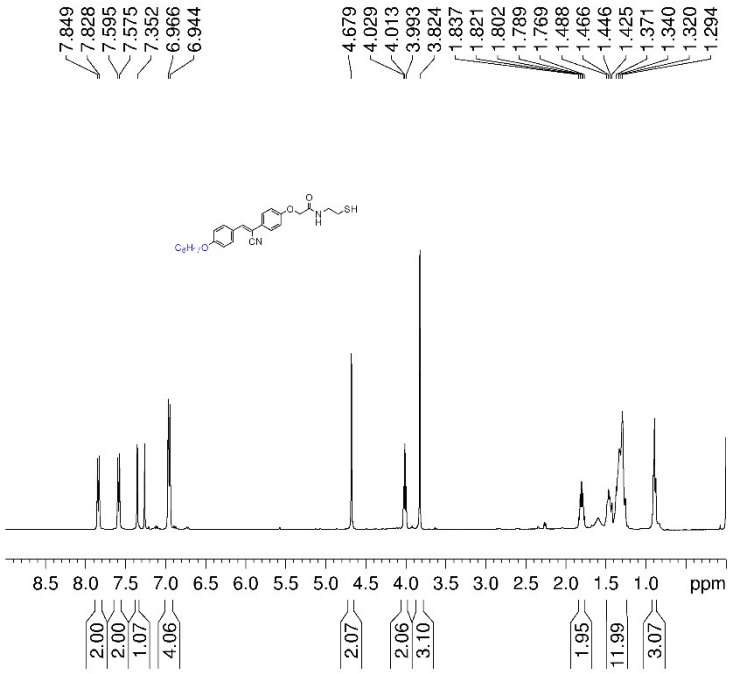

Figure S11 ^{1}H NMR (400 MHz, $CDCl_3$) of probe **1**.

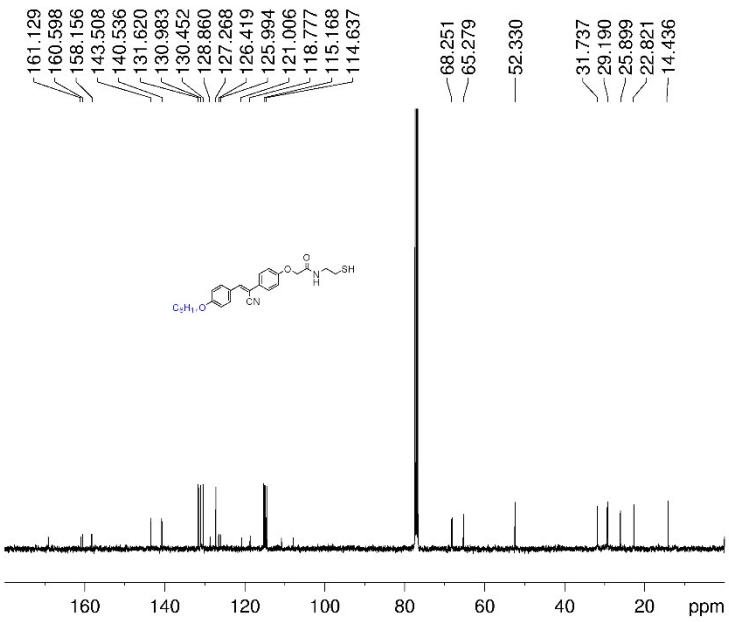

Figure S12 ^{13}C NMR (400 MHz, $CDCl_3$) of probe **1**.

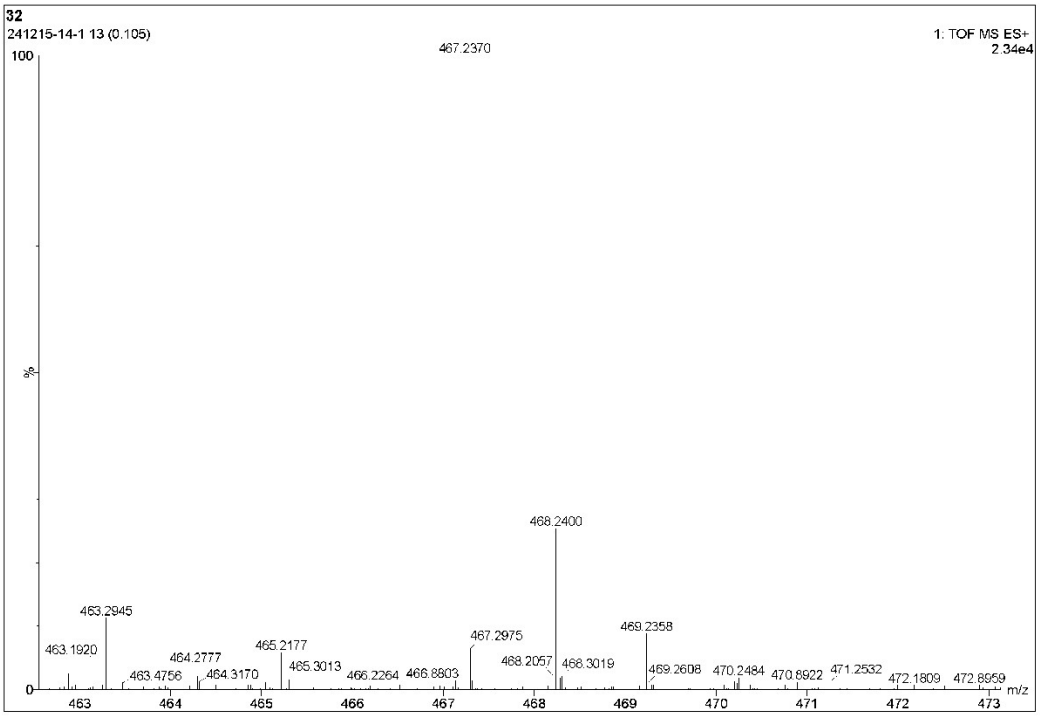

Figure S13 HRMS of probe **1**.

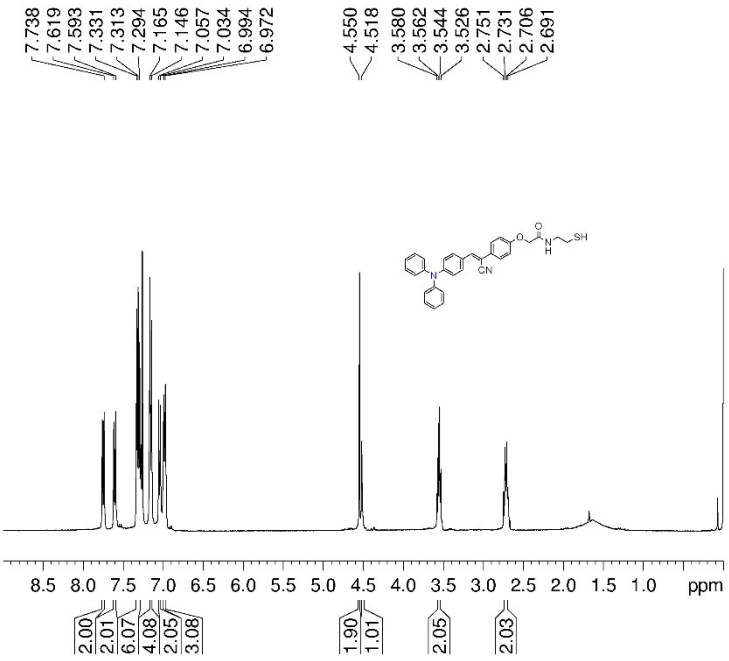

Figure S14 ^{1}H NMR (400 MHz, $CDCl_3$) of probe **2**.

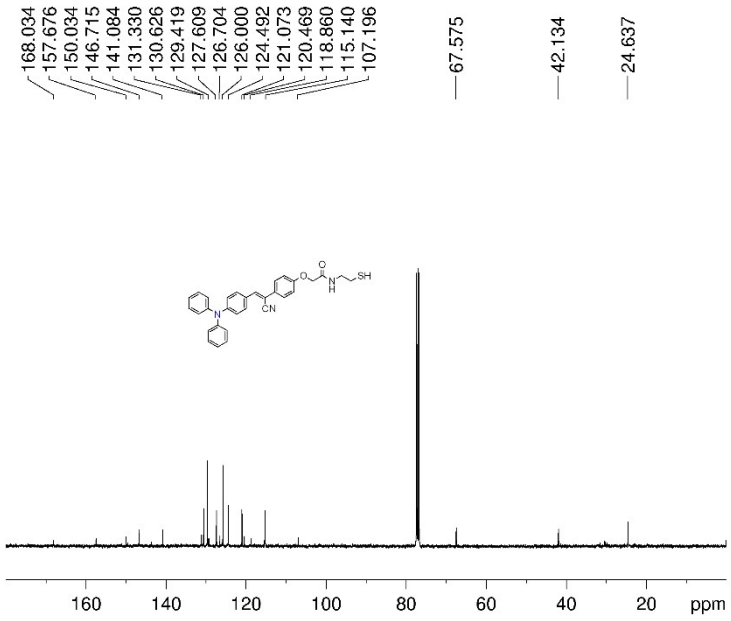

Figure S15 ^{13}C NMR (400 MHz, $CDCl_3$) of probe **2**.

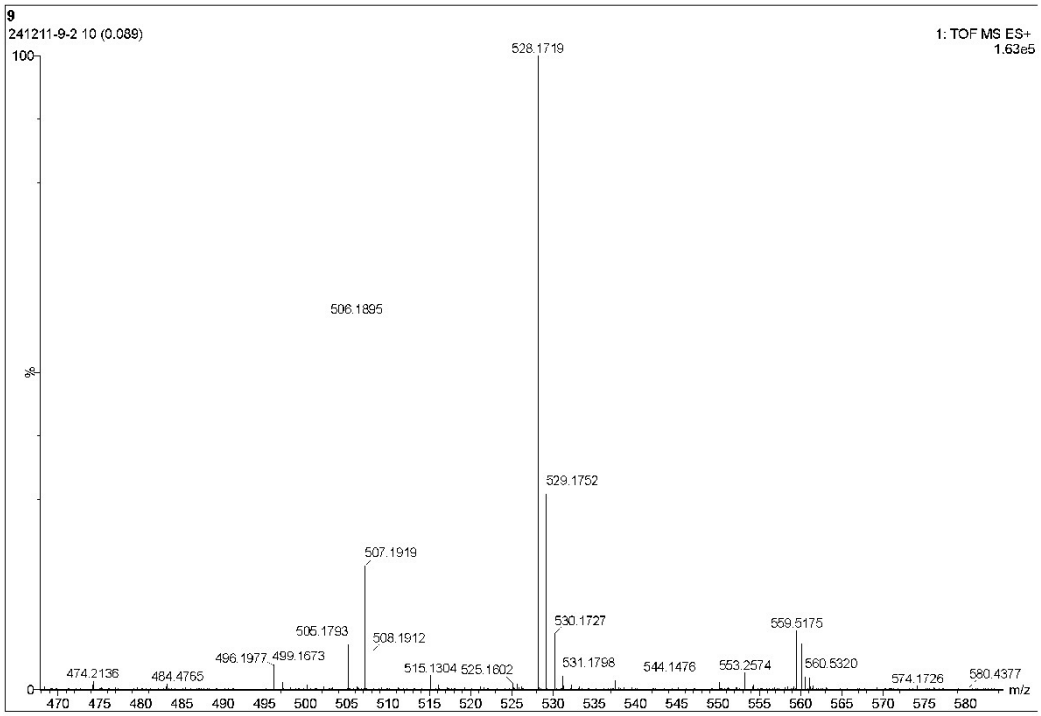

Figure S16 HRMS of probe **2**.

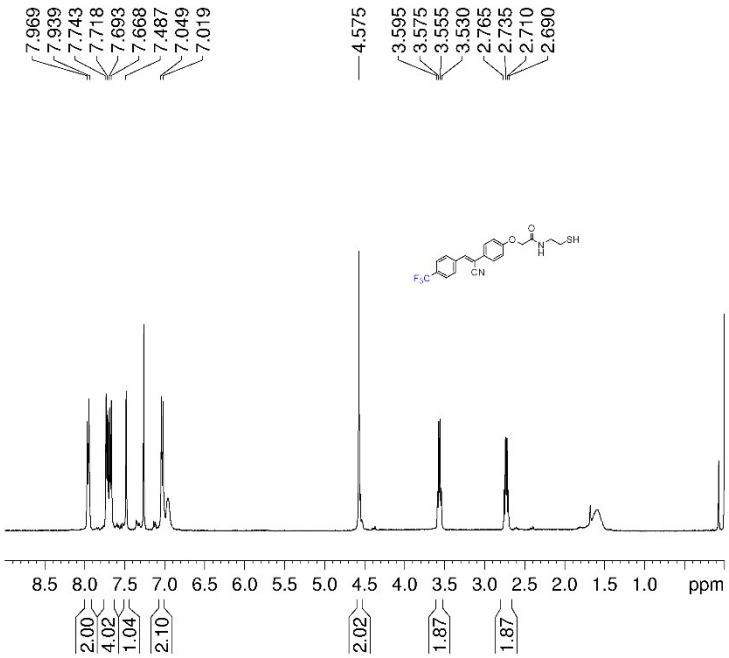

Figure S17 ^{1}H NMR (400 MHz, $CDCl_3$) of probe **3**.

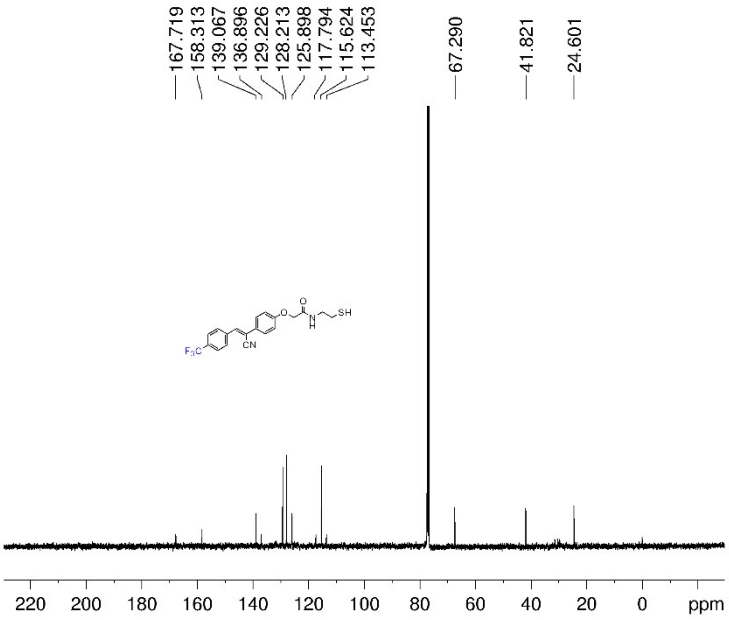

Figure S18 ^{13}C NMR (400 MHz, $CDCl_3$) of probe **3**.

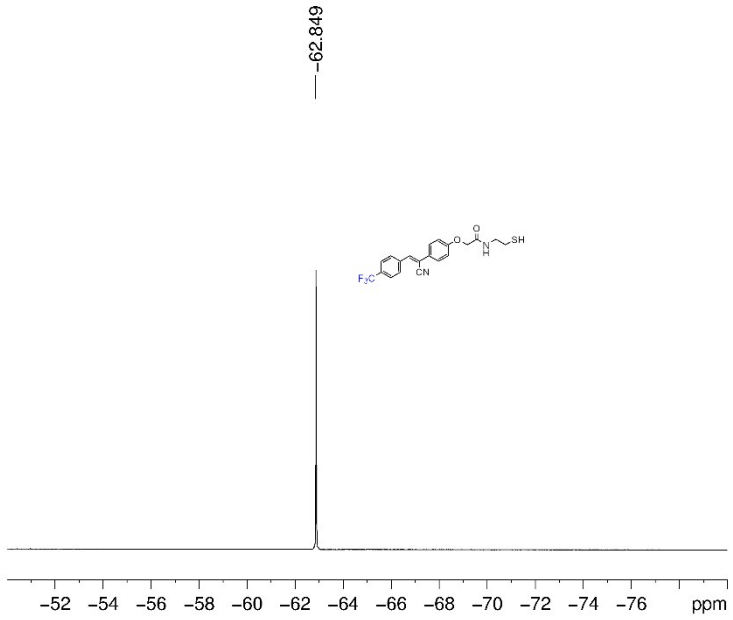

Figure S19 ^{19}F NMR (376 MHz, $CDCl_3$)

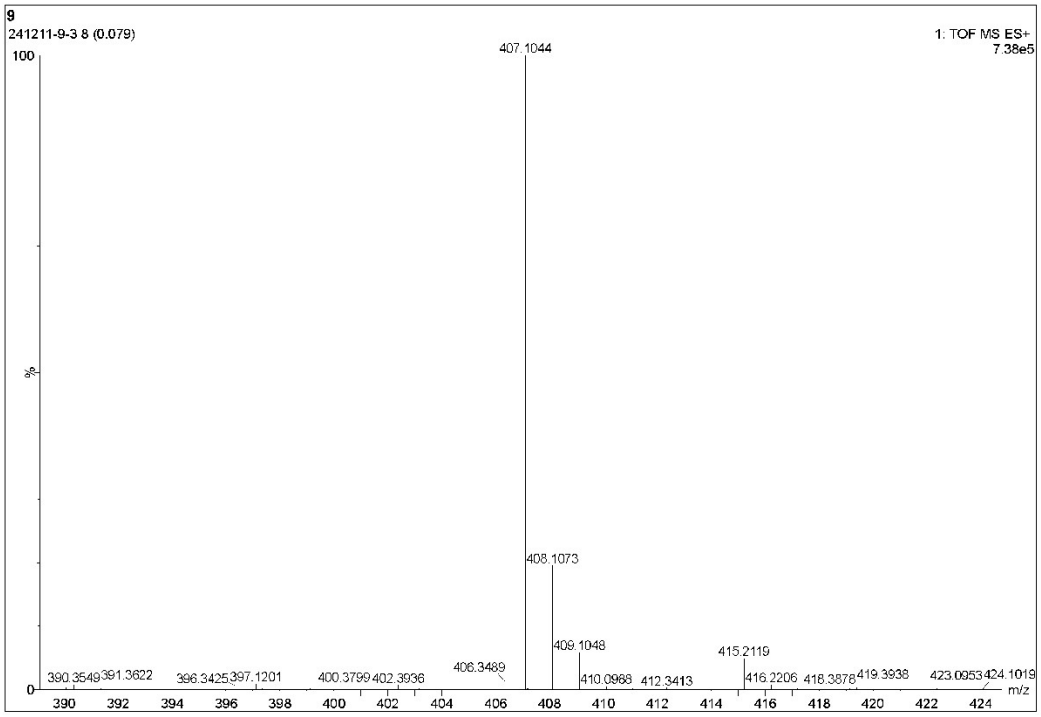

Figure 20 HRMS of probe **3**.

Photophysical properties of probes 1-3

It was well known that diphenylacrylonitrile was a simple and typical AIE molecule with strong emission at aggregated state.[2-4] The photophysical properties of the synthesized probes were firstly investigated. The UV-*vis* absorption and emission spectra of probes **1-3** were recorded in ACN solution at a fixed concentration (1×10^{-5} M). Two main absorption bands appear at 230 and

340 nm in **Figure S11**. The high energy absorption at 230 nm can be attributed to the π-π* electronic transitions of the diphenyl moiety, and the low energy absorption band at 340 nm of the long wavelength region can be regarded as the extended conjugated structure between diphenyl and cyano units. As shown in **Figure S12**, almost no fluorescence emission of probe **1** could be detected only in pure ACN solution. Upon addition of poor solvent water, almost no change can be observed until water fraction (f_w) at 50%. As the further increase of H_2O fraction up to 80%, blue fluorescence emission appears at 436 nm with 171-fold enhancement, which demonstrates that probe **1** can act as excellent AIE-active emitter in the aggregate state. Meanwhile, we also measured the fluorescent emission of probe **2** and **3**, when H_2O fraction up to 80% their emission intensity is increased by around 11-fold and 1.22-fold, respectively. The PL data thus prove that sensors **2** and **3** behave just like their parent form of α-cyanostilbene analogues, that is, they are also AIE active. [2-4]

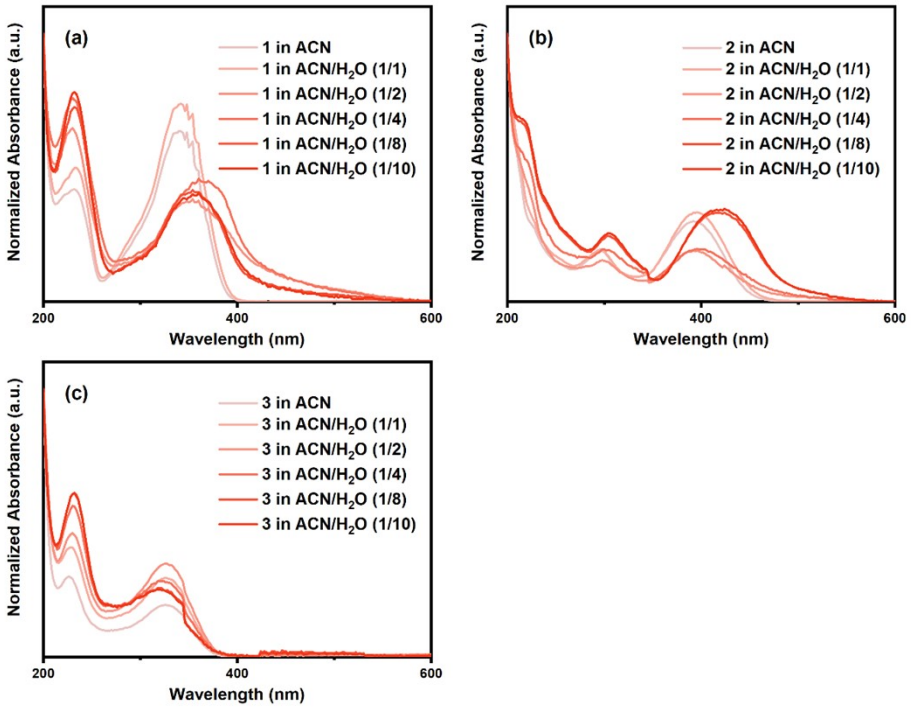

Figure S21 The UV-*vis* absorbance spectra of the probes **1-3** in mixed ACN-water solutions (v/v, water fraction (f_w) =0-91%; concentration: 1.0×10^{-5} M).

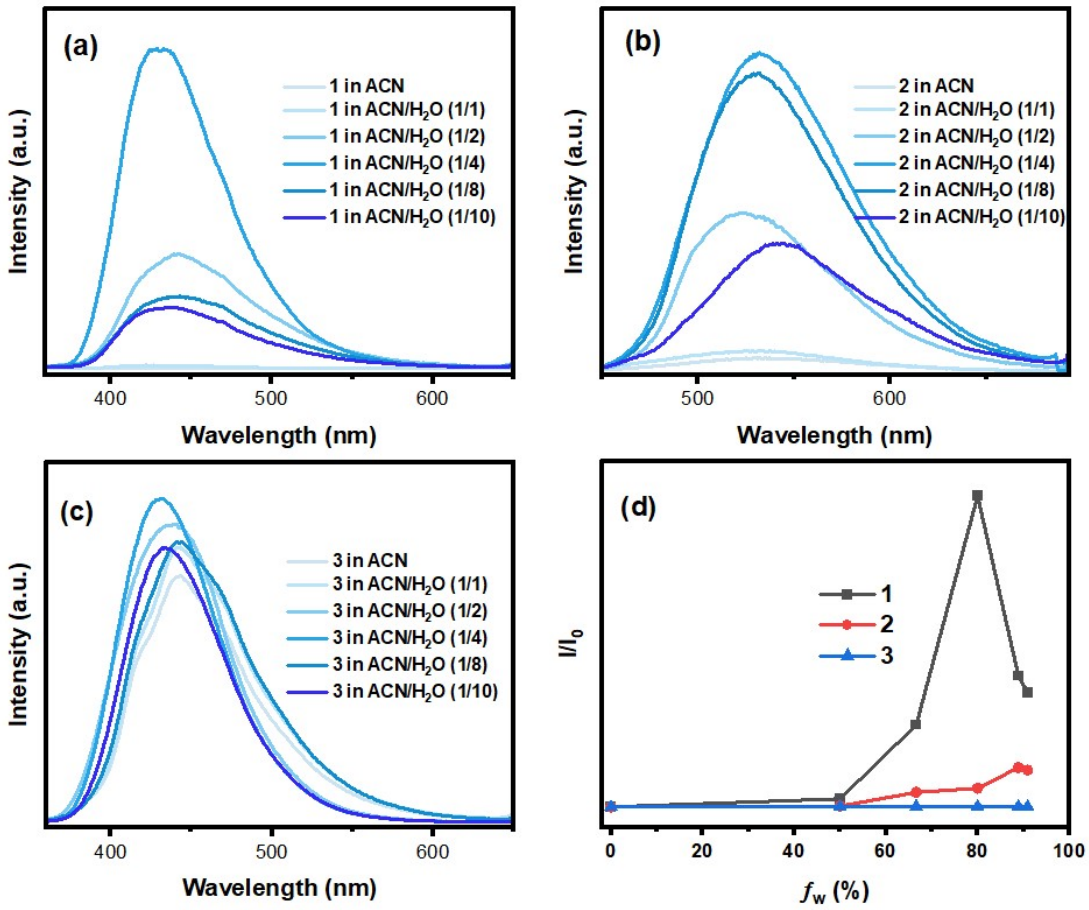

Figure S22 The fluorescence spectra of the probes **1-3** in mixed ACN-water solutions (v/v, water fraction (f_w) =0-91%; concentration: 1.0 × 10^{-5} M).

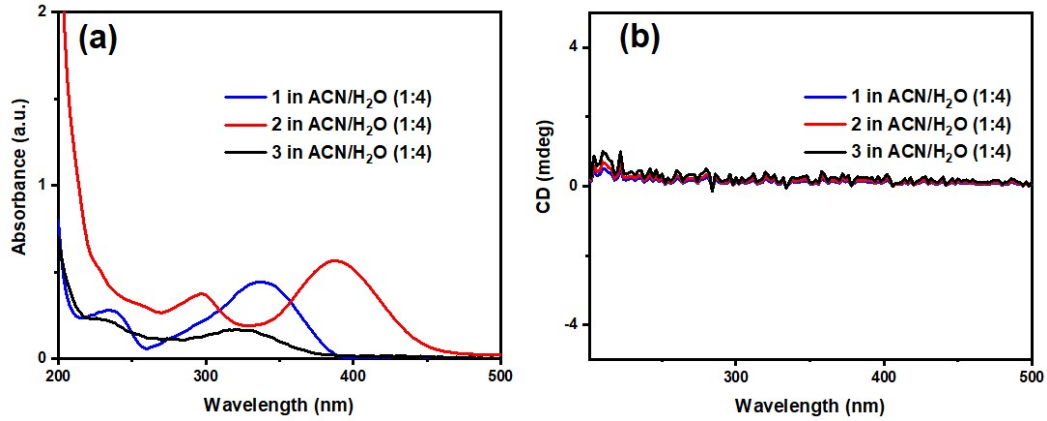

Figure S23 The UV and CD spectra of the probes **1-3** in mixed ACN-water solutions (v/v, water fraction (f_w) =80%; concentration: 1.0 × 10^{-5} M)

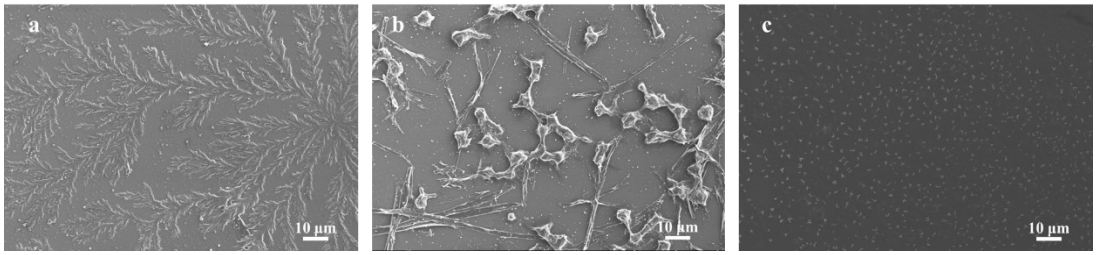

Figure. S24. SEM images of probes **1-3** in mixed ACN-water solutions (concentration: 1.0×10^{-5} M)) (a (probe **1**), b (probe **2**) and c (probe **3**)).

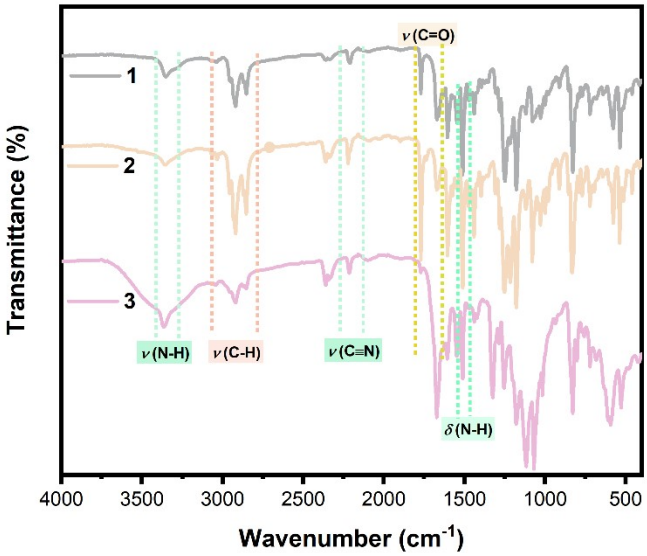

Figure. S25. FT-IR spectrum of probes **1-3**.

Structural elucidation and optimization of sensing conditions

Sensor screening

Reactions with arginine (Arg) using sensors **1**, **2** and **3** were performed as described below to identify a probe with superior chiroptical properties. (*D*/*L*)-arginine ((*D*/*L*)-Arg) (1 mM), NaOH (1.2 mM) and sensors **1**, **2**, or **3** (1 mM) were mixed in 1 mL of ACN and the reaction was shaken for 1 min. A 125.0 µL aliquot of the solution was diluted to 0.313 mM with 2.0 mL of ACN/H_2O mixture (1:4), allowed to stand for 15 min and then subjected to CD analysis using a quartz cuvette (0.1 cm path length). Sensor **1** yielded the strongest CD signal. Further optimization was therefore carried out with **1**.

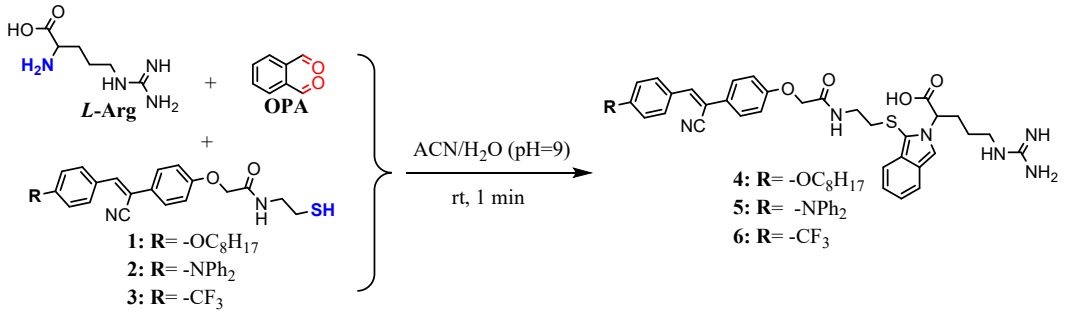

Scheme S3. Chiroptical sensing of (*L*)-Arginine with sensors **1-3**.

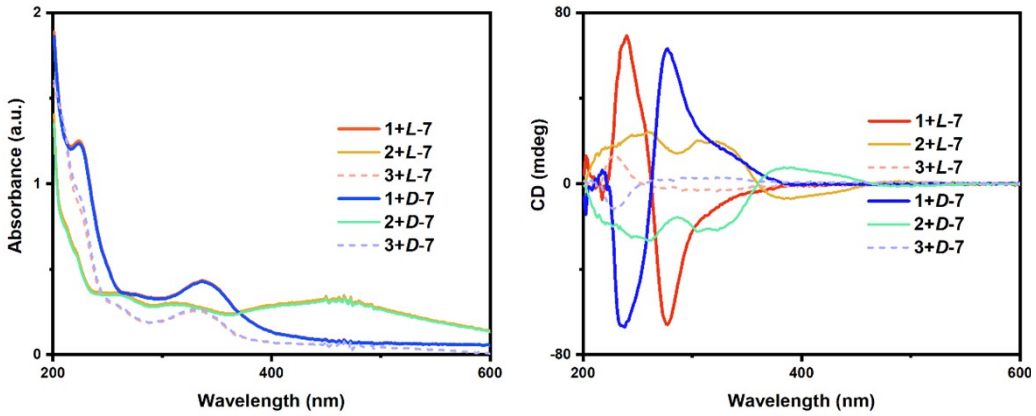

Figure S26. Chiroptical sensing of (*D*/*L*)-**7** (arginine) with probes **1-3** (UV-*vis* and CD measurements were taken at 0.313 mM with a quartz cuvette (0.1 cm path length)).

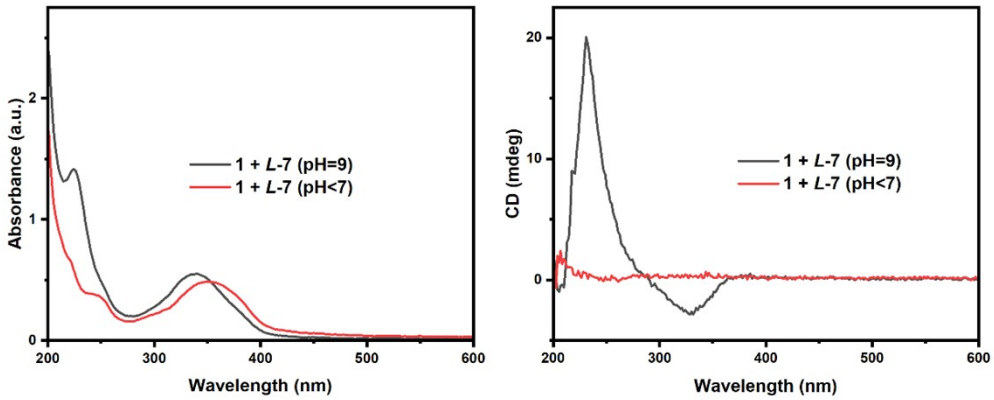

Figure S27. CD signals obtained from probe **1** sensing with *L*-**7** at different pH (0.0625 mM)

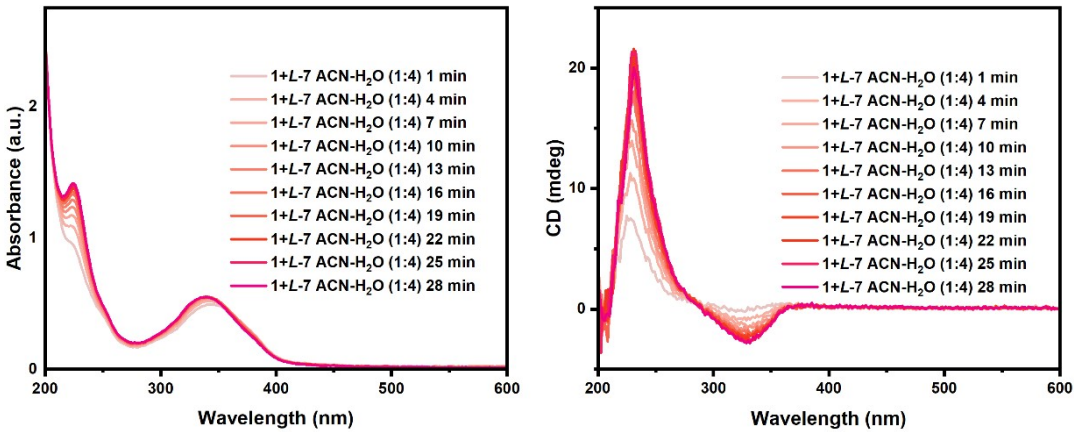

Figure S28. UV and CD spectra of probe **1** sensing with *L*-**7** at different reaction times (0.0625 mM).

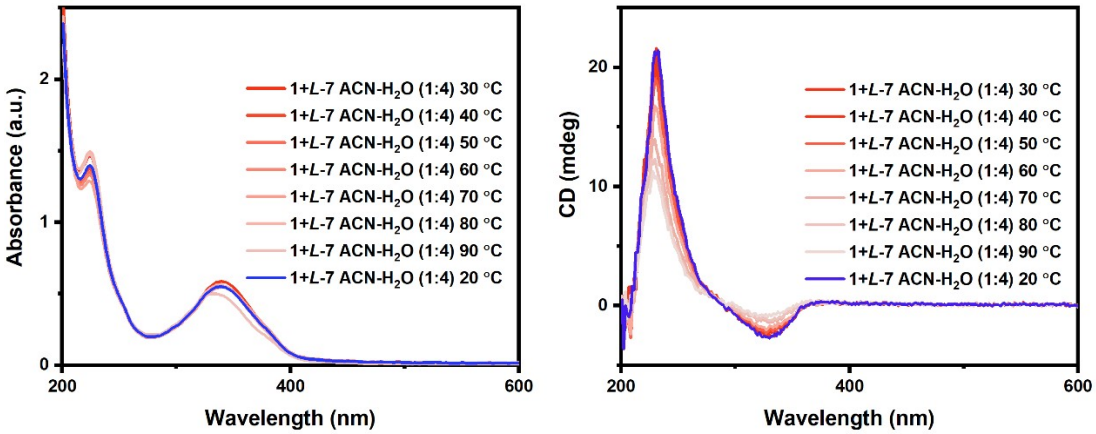

Figure S29. Temperature-variable CD spectra during heating and cooling process of probe **1** sensing with *L*-**7** in ACN/H_2O (0.0625 mM).

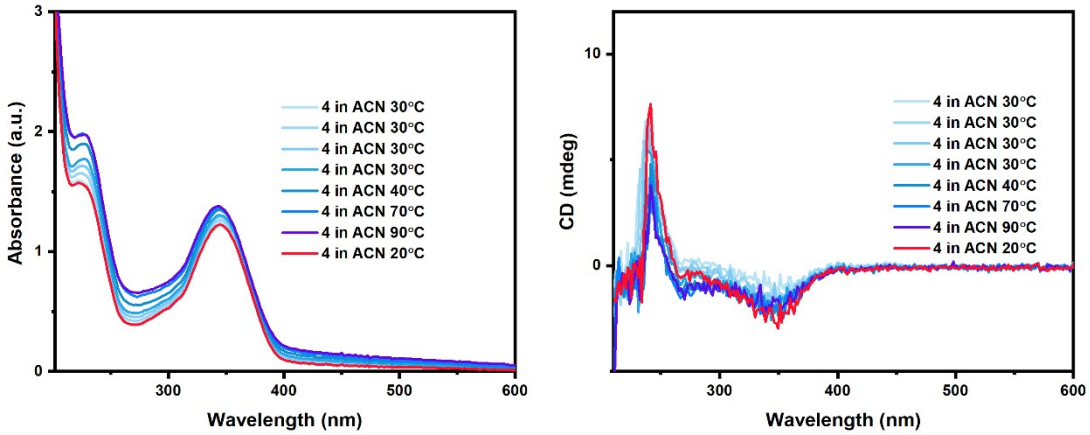

Figure S30. Temperature-variable CD spectra during heating and cooling process of pure chiroptical sensing product **4** in ACN (0.0625 mM).

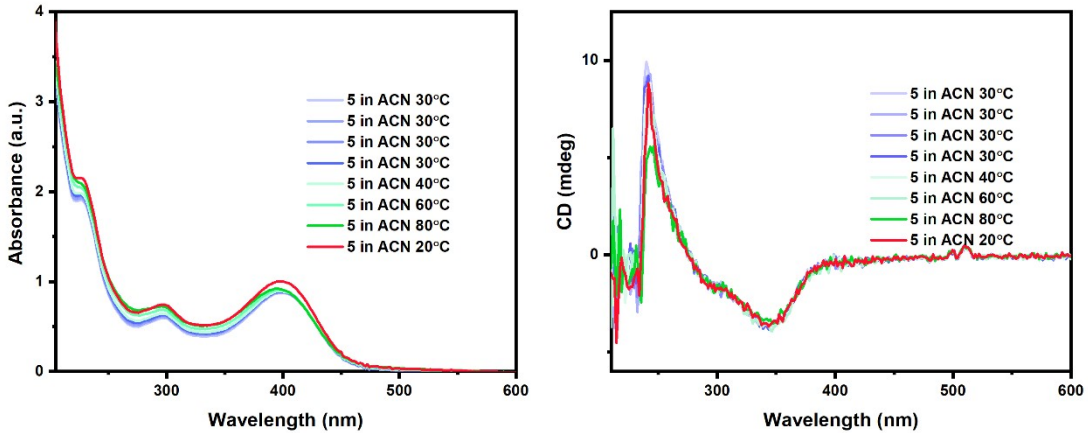

Figure S31**.** Temperature-variable CD spectra during heating and cooling process of pure chiroptical sensing product **5** in ACN (0.0625 mM).

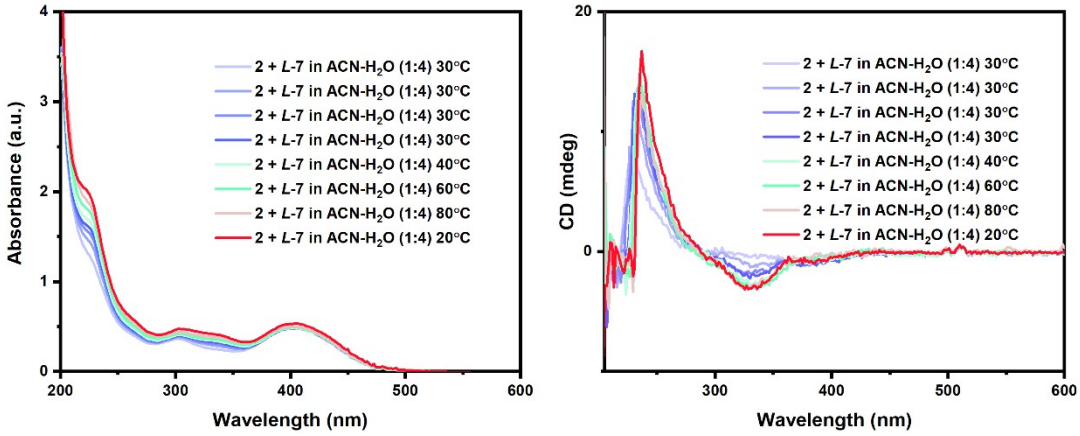

Figure S32. Temperature-variable CD spectra during heating and cooling process of probe **2** sensing with *L*-**7** in ACN/H_2O (0.0625 mM).

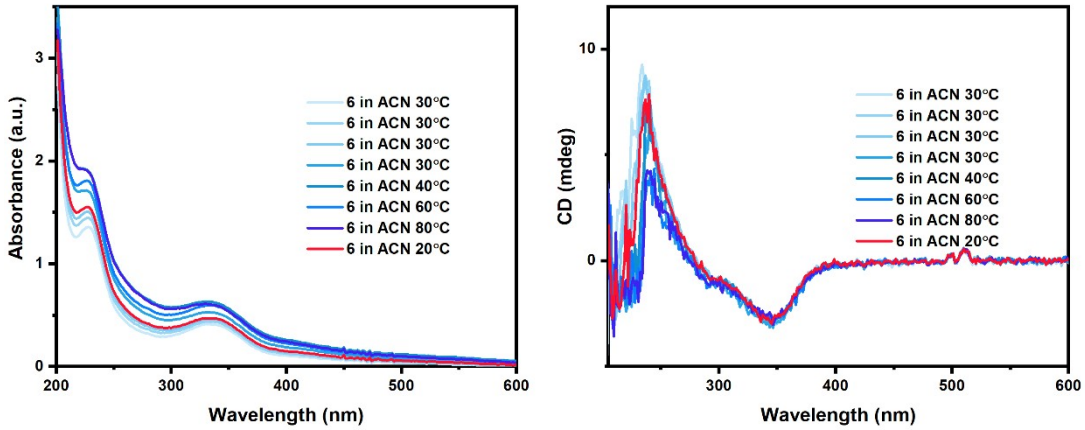

Figure S33. Temperature-variable CD spectra during heating and cooling process of pure chiroptical sensing product **6** in ACN (0.0625 mM).

Optimization of sensing procedure

Base optimization

Comparison of the CD signals of *D*/*L*-**7** using different bases at 1 mM, diluted to 0.0625 mM for measurement with a quartz cuvette (0.1 cm path length). After screening the bases, it was found that strong bases speed up the chemical reaction of the sensing process.

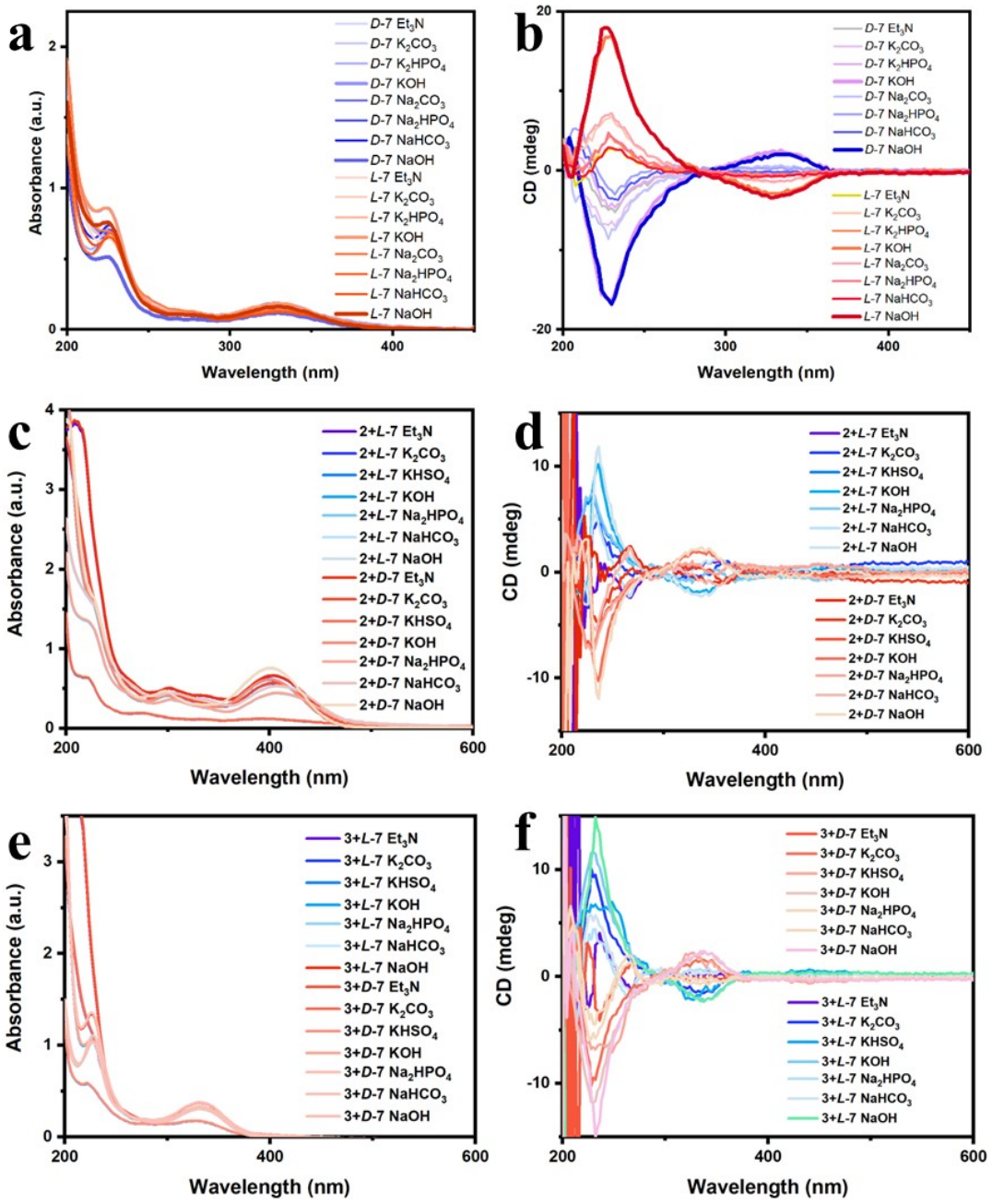

Figure S34. Chiroptical sensing of (*D*/*L*)-**7** with probes **1** (a, b), **2** (c, d) and **3** (e, f) at different bases (UV-*vis* and CD measurements were taken at 0.0625 mM with a quartz cuvette (0.1 cm path length)).

Solvent optimization

Comparison of CD and UV signals of (*D*/*L*)-**7** in ACN at 1 mM, diluted with ACN/H_2O (1:4) to 0.313 mM for testing. Mixed solvents gave the better results in CD and UV signals, so we chose ACN (ACN= acetonitrile): H_2O = 1:(0-10) (v/v) as the optimal solvent. As the isoindole products formed by different amino acids may differ in solubility, the ratio of ACN and H_2O was adjusted to guarantee the three-component reaction to proceed well.

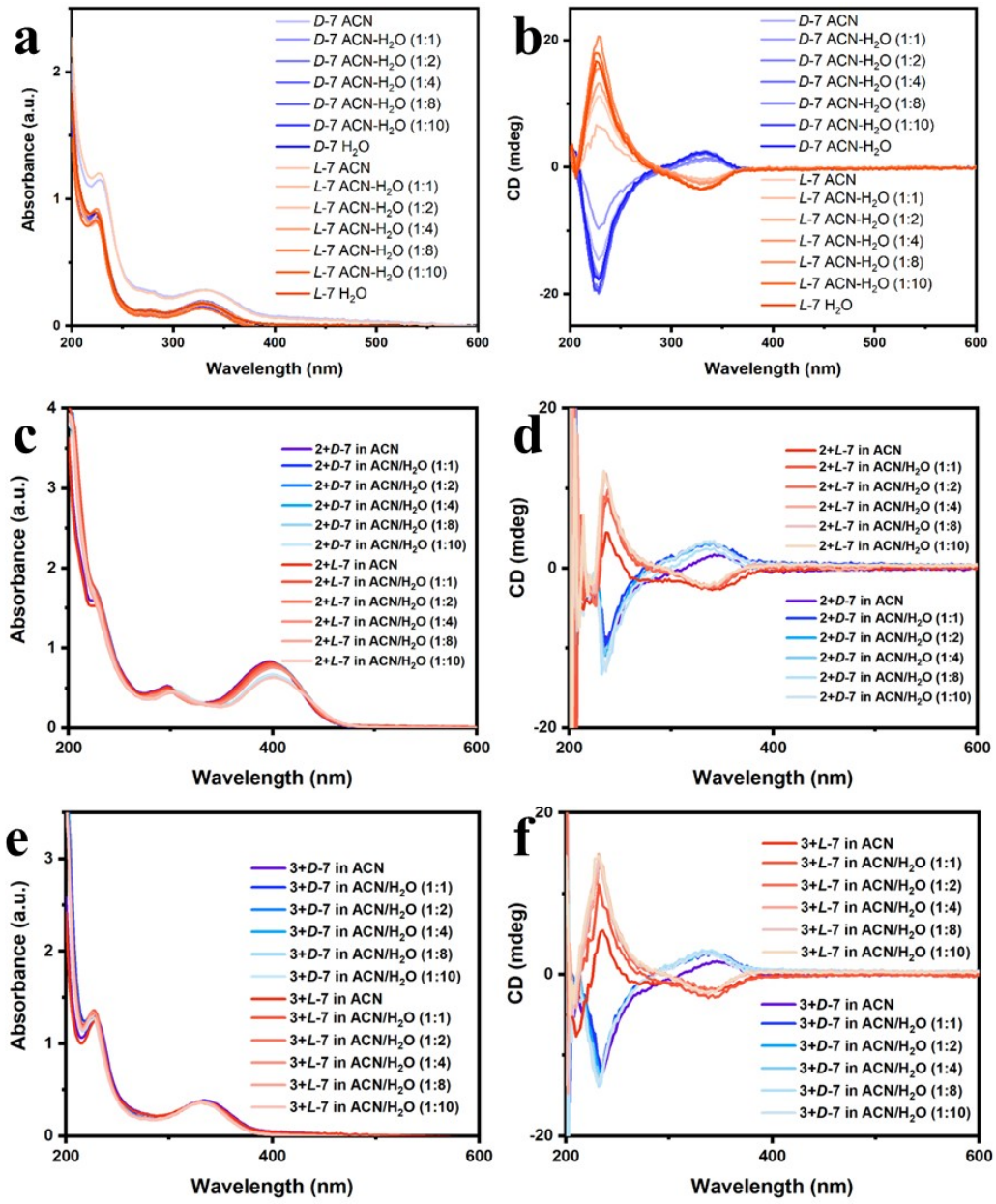

Figure S35. Chiroptical sensing of (*D*/*L*)-**7** with probes **1** (a, b), **2** (c, d) and **3** (e, f) at different mixtures (UV-*vis* and CD measurements were taken at 0.0625 mM with a quartz cuvette (0.1 cm path length)).

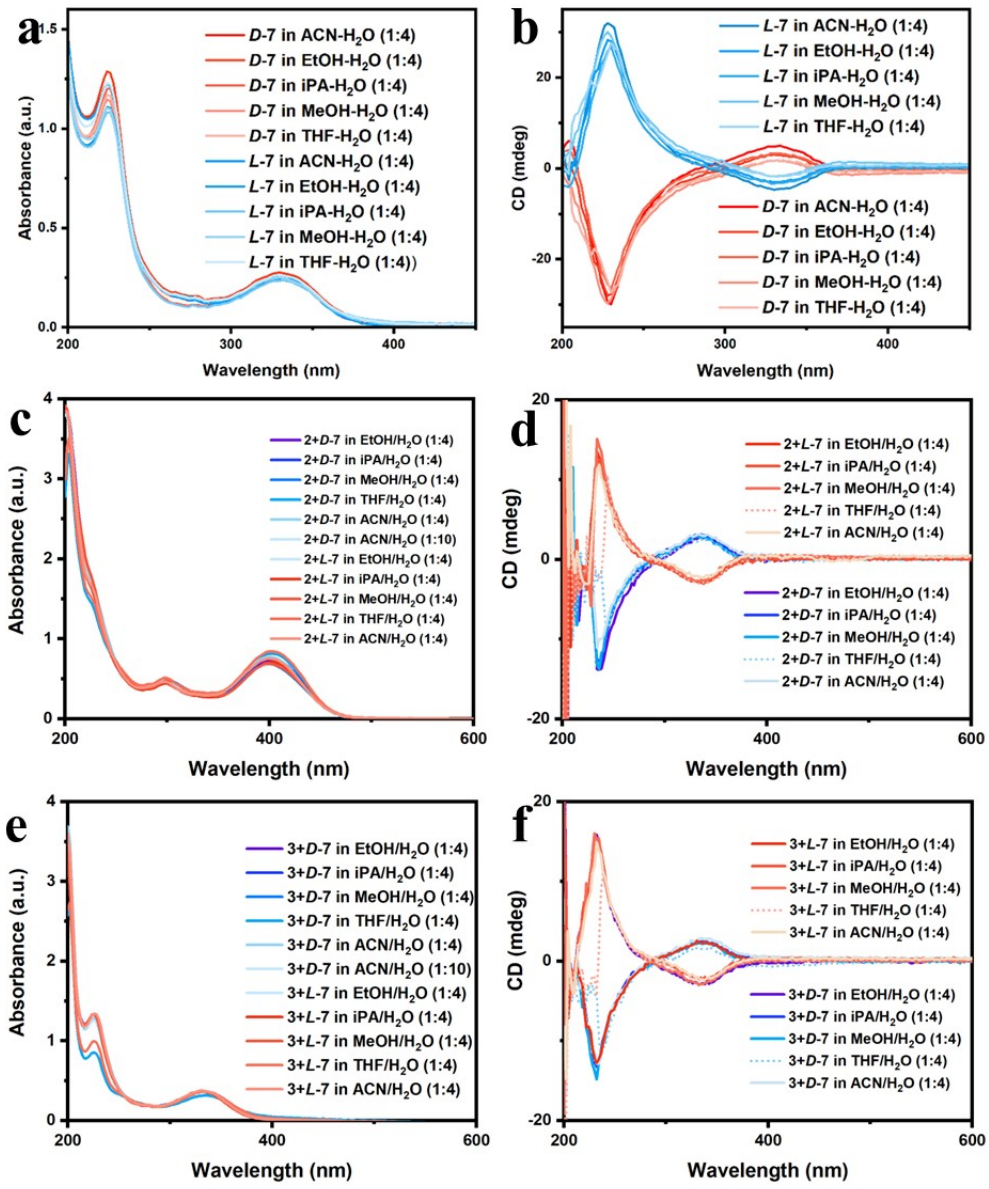

Figure S36. Chiroptical sensing of (*D*/*L*)-**7** with probes **1** (a, b), **2** (c, d) and **3** (e, f) in different reaction solvents (UV-*vis* and CD measurements were taken at 0.0625 mM with a quartz cuvette (0.1 cm path length)).

As shown in Figure S36, the UV and CD spectra of **4**, **5**, and **6** were only slightly affected by the reaction solvents. In these assays it was found that the reaction solvents have a negligible effect on the measurement procedure and give almost identical results. Differences in the CD signal between dilution solvents were negligible. Strong CD spectra were obtained when ACN/H_2O (4:1) and ACN/H_2O (1:4) were used as the reaction and the dilution solvent, respectively. All subsequent reactions were therefore carried out using ACN/H_2O (4:1) and ACN/H_2O (1:4) as reaction and dilution solvent, unless otherwise stated.

Stability test

The reaction was performed in ACN/H_2O (4:1) at 1 mM, diluted with ACN/H_2O (1:4) to 0.0625 mM for CD and UV-*vis* testing. The reaction was completed 3-15 minutes under these conditions.

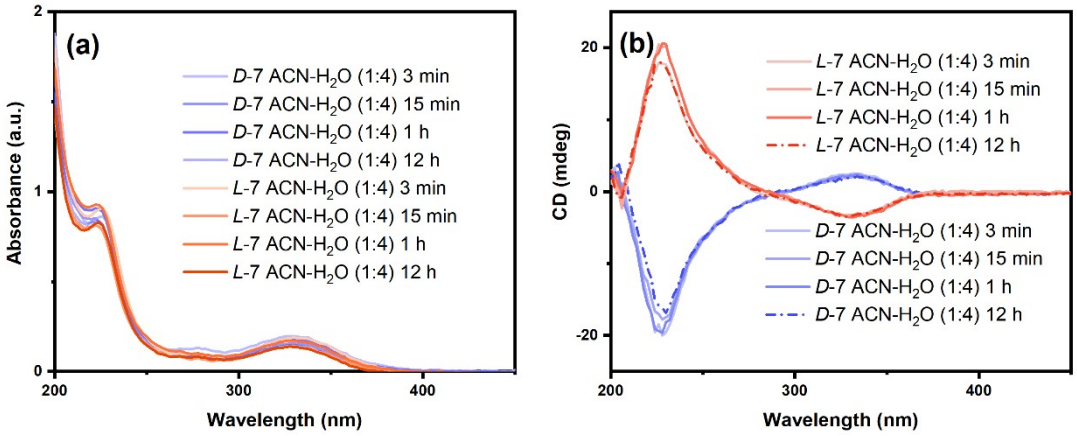

Figure S37. UV-*vis* and CD spectra of (*D*/*L*)-**7** reacting with **OPA** and **1** over time.

Structural elucidation

A solution of sensors **1**, **2**, and **3** (2 mM), OPA (2 mM), and *L*-Arg (2 mM) in 5 mL of acetonitrile. The 5 M NaOH solution was then added, and the pH of the mixed system was adjusted to 9, followed by stirring for 15 min. The reaction mixture was then extracted directly with ethyl acetate 3 times. The organic phase was collected and dried with anhydrous Na_2SO_4, then the solvent was removed by rotary evaporator to give the crude product. The resulting yellow crude solid was loaded onto a silica gel column with DCM/MeOH (98:2, v/v), and eluted with the same solvent system (96:4, v/v). The pure fractions were collected, then the solvent was removed under reduced pressure to give three pure pale-yellow solids. (Compounds **4**, **5** and **6** are partially degrade during long-term storage in organic solvents without avoiding light and air (THF, ACN, MeOH, EtOH, CH_2Cl_2， etc.) due to their poor self-assembly.).The reaction products were collected for ^{1}H NMR test.

Compound **4** (0.68 g, 93%)**:** ^{1}H NMR (400 MHz, $CDCl_3$) δ (ppm): 7.88-7.86 (d, 2H, *J*=8 Hz), 7.64-7.62 (d, 2H, *J* = 8 Hz), 7.48 (s, 1H), 7.38-7.30 (m, 3H), 7.02-6.97 (m, 6H), 4.58-4.56 (m, 2H), 4.06-4.02(m, 2H), 3.74-3.70 (m, 2H), 2.94-2.91 (m, 2H), 1.86-1.82 (m, 4H), 1.52-1.47 (m, 15H), 0.95-0.92 (t, 3H, *J*=8 Hz). ^{13}C NMR (100 MHz, $CDCl_3$) δ (ppm): 168.34, 161.30, 157.48, 143.60, 140.88, 131.53, 131.03, 127.31, 126.40, 118.36, 115.44, 114.94, 68.28, 67.48, 58.63, 53.50, 37.61, 31.88, 29.36, 27.25, 26.04, 22.83, 18.40, 14.38.

Compound **5** (0.69 g, 89%)**:** ^{1}H NMR (400 MHz, $CDCl_3$) δ (ppm): 7.79-7.76 (d, 1H, *J*=12 Hz), 7.64-7.62 (d, 1H, *J* = 8 Hz), 7.43-7.41 (d, 1H, *J* = 8 Hz), 7.36-7.32 (m, 4H), 7.20-7.02 (m, 17H), 6.85-6.82 (d, 1H, *J*=12 Hz), 4.56-4.54 (m, 2H), 3.74-3.71 (m, 2H), 2.92-2.88 (m, 2H), 1.35-1.30 (m,

7H). ^{13}C NMR (100 MHz, $CDCl_3$) δ (ppm): 174.08, 146.59, 144.80, 143.46, 131.40, 130.50, 129.61, 125.81, 124.36, 121.01, 120.34, 115.53, 53.41, 37.54, 30.62, 29.27, 18.32.

Compound **6** (0.59 g, 88%)**:** ^{1}H NMR (400 MHz, $CDCl_3$) δ (ppm): 7.88-7.86 (d, 2H, J=8 Hz), 7.64-7.62 (d, 2H, J = 8 Hz), 7.48 (s, 1H), 7.38-7.30 (m, 3H), 7.02-6.97 (m, 6H), 4.58-4.56 (m, 2H), 4.56-4.54 (m, 2H), 3.74-3.71 (m, 2H), 2.92-2.88 (m, 2H), 1.35-1.30 (m, 7H). ^{13}C NMR (100 MHz, $CDCl_3$) δ (ppm): 169.74, 157.88, 157.27, 153.96, 130.73, 129.82, 116.05, 113.24, 64.26, 58.53, 53.50, 36.00, 31.98, 29.36, 27.25, 25.74, 22.83, 18.40, 13.98.

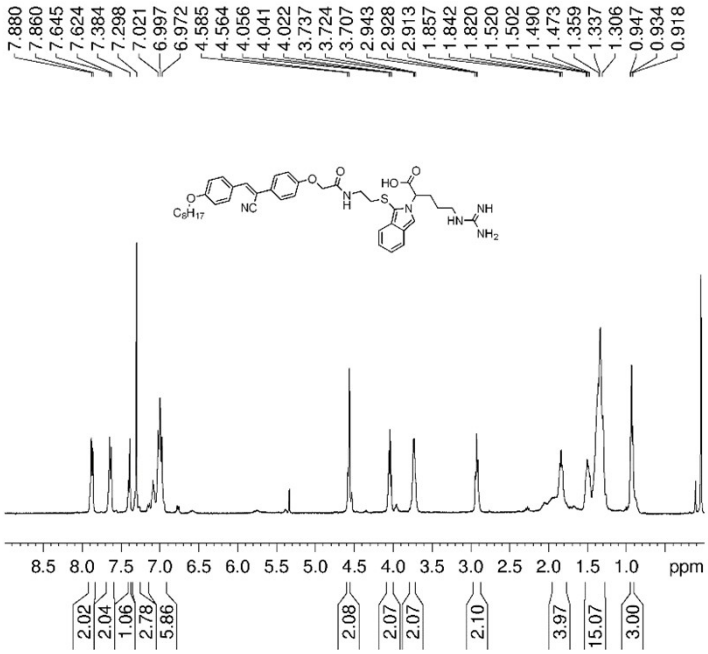

Figure S38 ^{1}H NMR (400 MHz, $CDCl_3$)

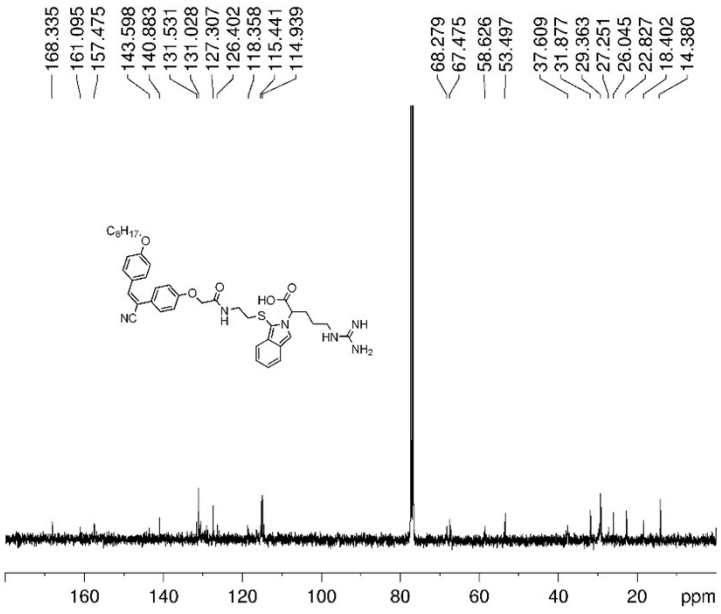

Figure S39 ^{13}C NMR (100 MHz, $CDCl_3$)

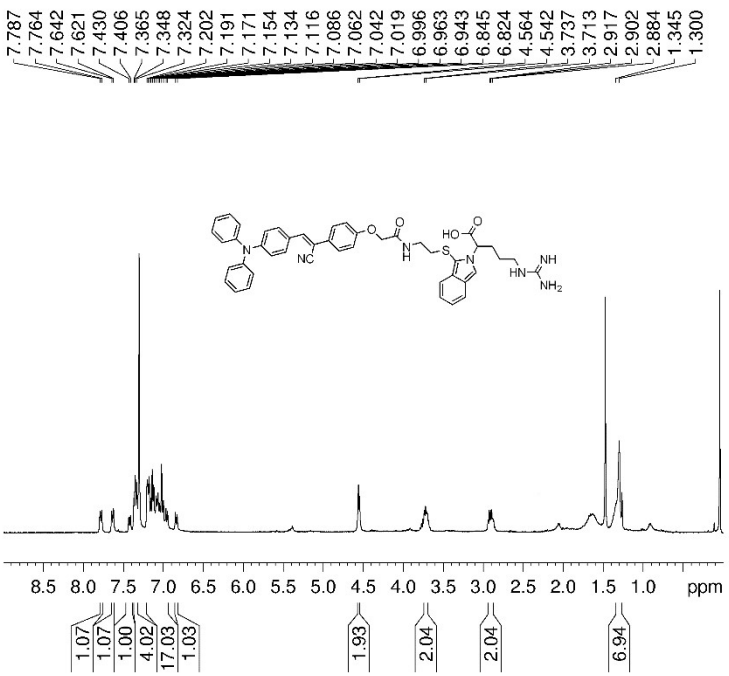

Figure S40 ^{1}H NMR (400 MHz, $CDCl_3$)

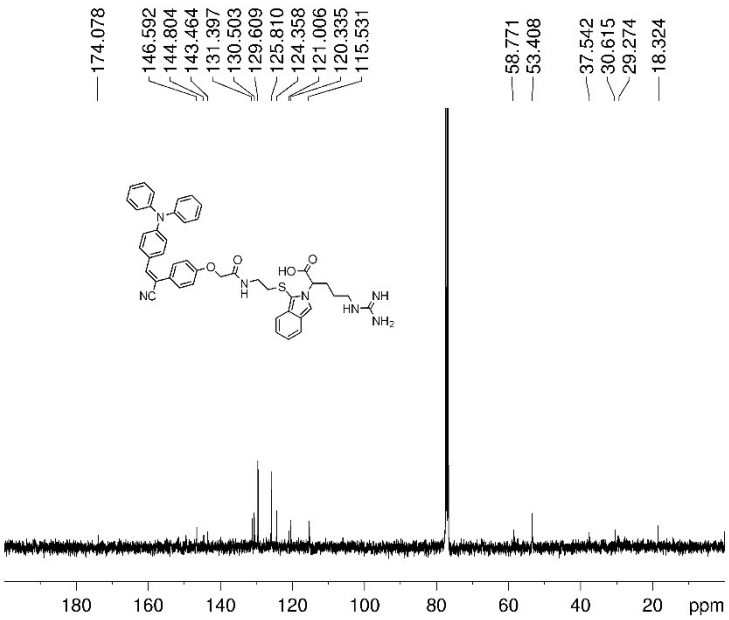

Figure S41 ^{13}C NMR (100 MHz, $CDCl_3$)

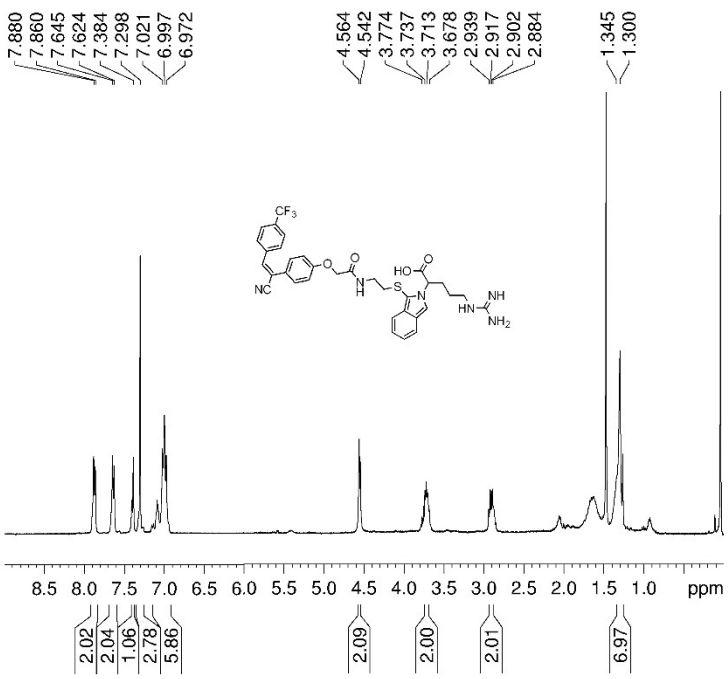

Figure S42 ^{1}H NMR (400 MHz, $CDCl_3$)

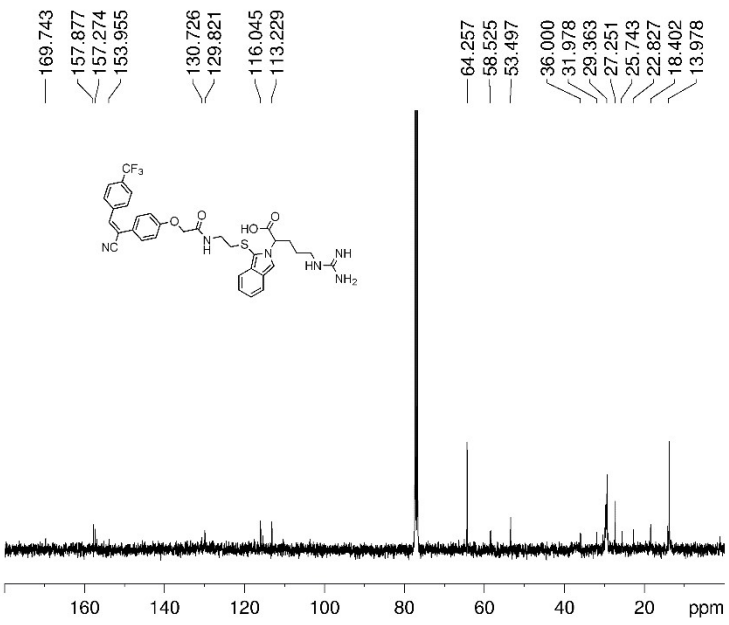

Figure S43 ^{13}C NMR (100 MHz, $CDCl_3$)

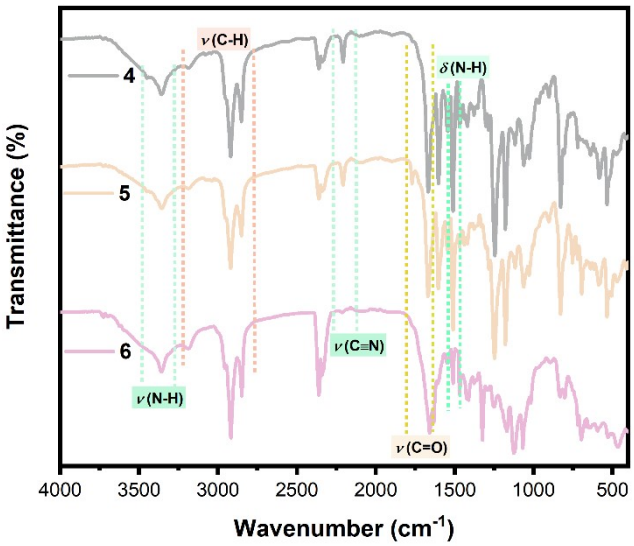

Figure. S44. FT-IR spectrum of products **4-6**.

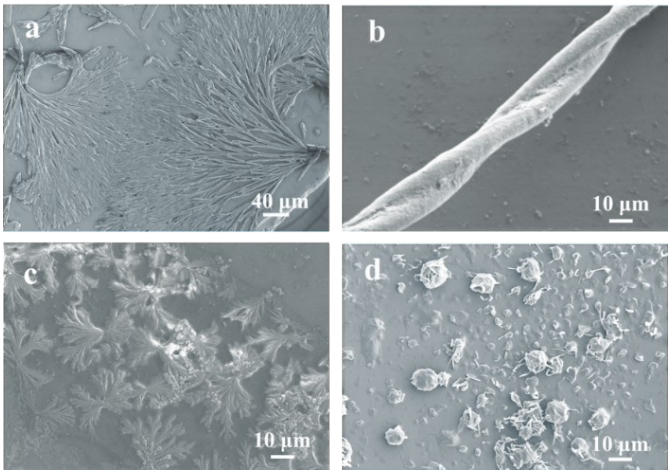

Figure S45. SEM images of probes **1-3** reaction with OPA and *L*-Arginine ((a) probe **1** (at 0.313 mM); (b) probe **1** (at 0.0313 mM); (c) probe **2** (at 0.313 mM); (d) probe **3** (at 0.313 mM)).

Computational Methods

Geometries were optimized and characterized by frequency calculations to be energy minima (zero imaginary frequencies) or transition states (only one imaginary frequency) at the B3LYP/6-31G(d) level in the gas phase. The energy was then refined by B3LYP/6-311++G(d,p)-SMD single-point energy calculations in water solution using the SMD[5] solvation model. All calculations were performed with Gaussian 16 [6].

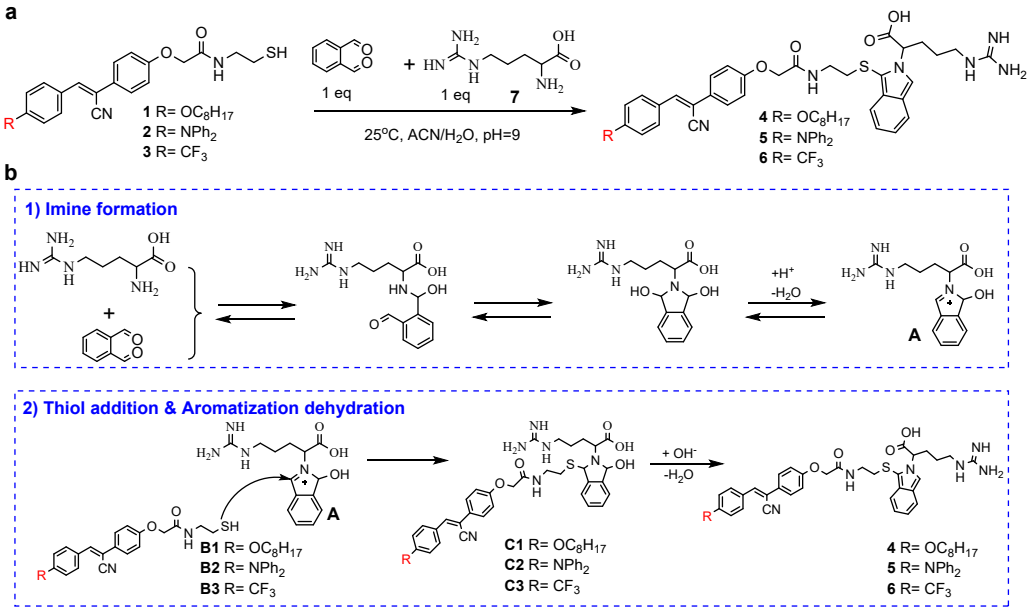

Scheme S4. Stepwise and concerted mechanism for the sensors **1-3** reaction with **7** and OPA.

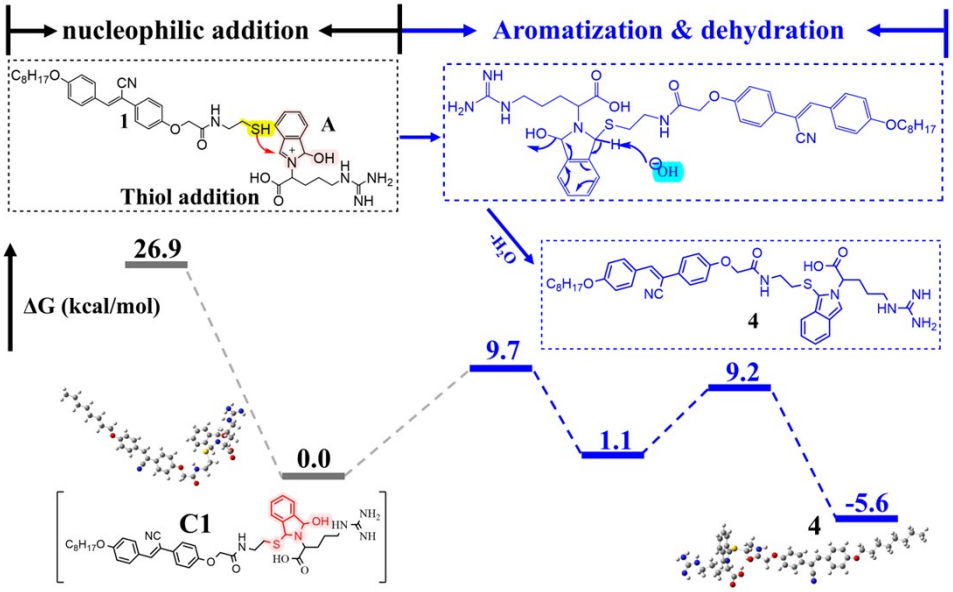

Figure S46. Stepwise, concerted mechanism and free energy surface for the probe **1** reaction with ***L*-7**.

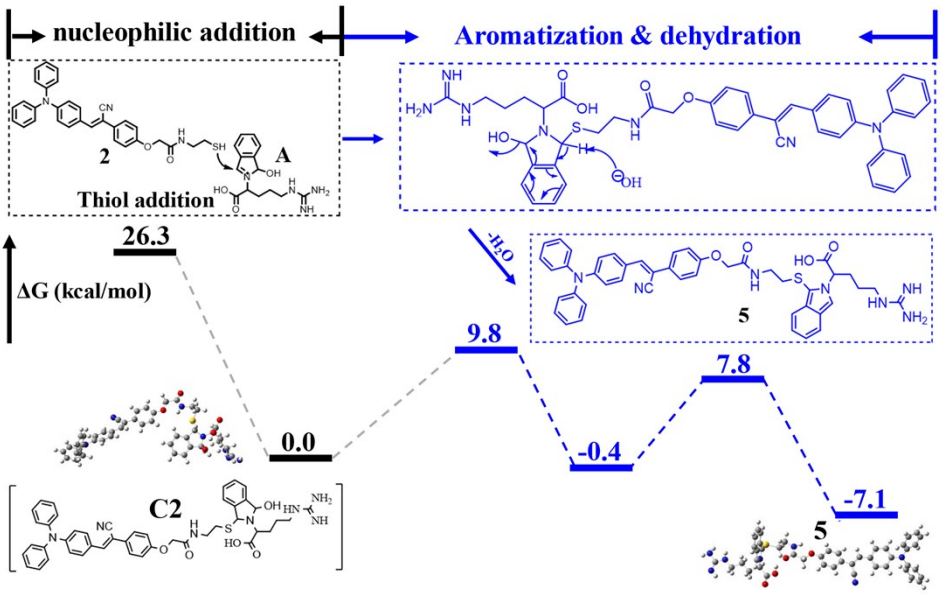

Figure S47. Stepwise, concerted mechanism and free energy surface for the probe **2** reaction with *L*-**7**.

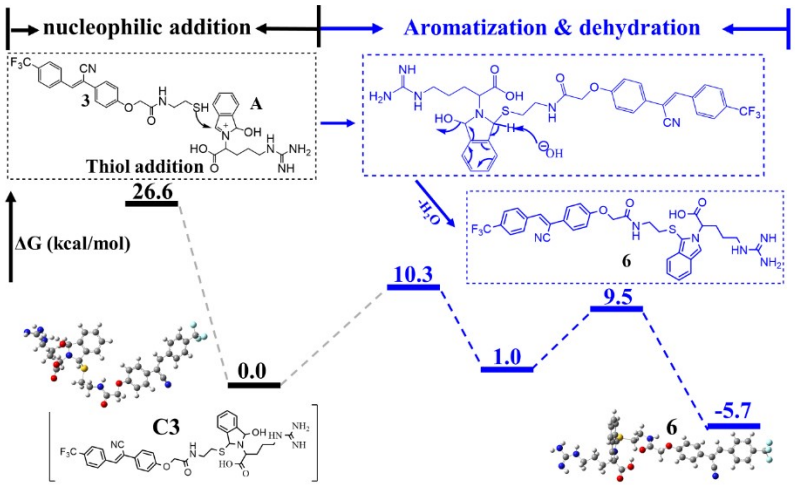

Figure. S48 Stepwise, concerted mechanism and free energy surface for the probe **3** reaction with *L*-**7**.

Molecular dynamics simulations

All molecular dynamics simulations were carried out using Gromacs 2018.8 program[5] with general Amber force fields (GAFF).[6] In this work, all molecules were optimized by Gaussian 16 program using M06-2X hybrid functional with 6-31g* basis set.[7] Multiwfn was used to construct RESP charges.[8] 15 molecules of various products (**4**, **5** and **6**), 1000 Acetonitrile molecule and 4000 water molecules were put into a cubic box with a side length of 8 nm using packmol software.[9] The cut-off for neighbor list of Verlet method and that for short-range interactions is 1.2 nm in all calculations with periodic boundary conditions in all three directions. After the energy minimization, the systems were equilibrated in NPT ensemble. In this simulation, the system was

simulated for 200 ps using Berendsen thermostat at 298.15K with a coupling constant of 0.1 ps.[10] The time step of each simulation was taken as 2 fs. Then, all systems were finally run in NVT ensemble for 20 ns at 298.15K. The time step of each simulation was 2 fs.

Interaction energy analysis ($E_{intermolecular\text{-}nonbonding\text{-}interaction}$) was calculated with the summary of Short-range Coulomb interactions ($E_{Coul\text{-}SR}$) and Long-range van der Waals interactions ($E_{LJ\text{-}SR}$), $E_{intermolecular\text{-}nonbonding\text{-}interaction} = E_{Coul\text{-}SR} + E_{LJ\text{-}SR}$.

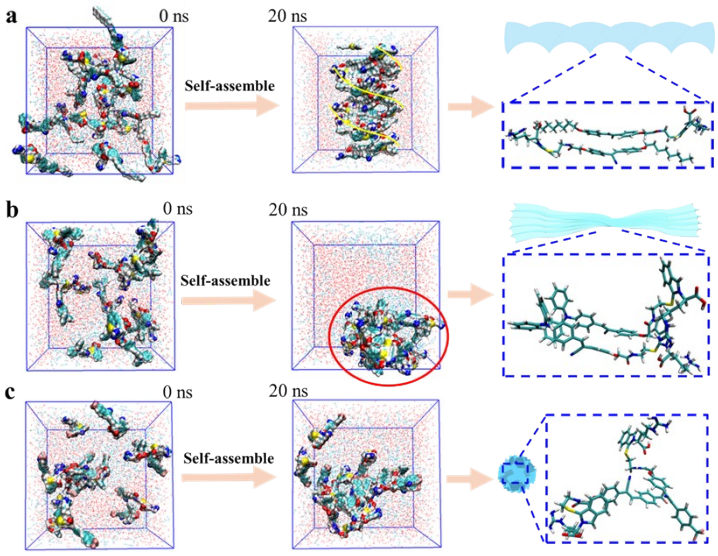

Figure S49 MD simulation results (20 ns) of (a) **4**, (b) **5**, (c) **6**, and their detailed intermolecular interactions.

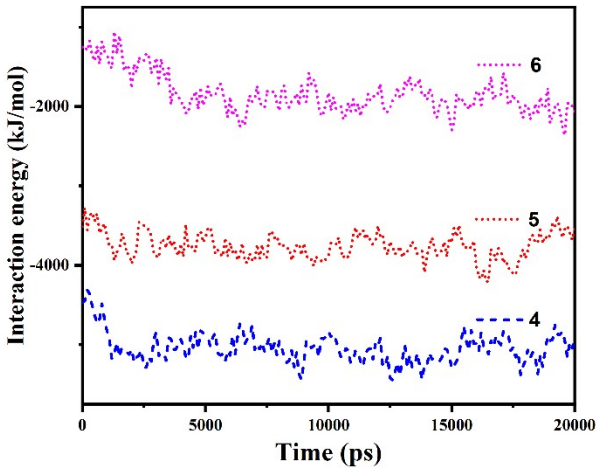

Figure S50**.** The energy change curves of probes **4**, **5**, and **6** systems over time during 20 ns MD process.

By testing the interactions of the different types of probes after assembly, it was found that their intermolecular interaction energies were -5041.25 kJ/mol for compound **4**, -3755.51 kJ/mol for compound **5** and -1838.22 kJ/mol for compound **6**. The higher the value of the intermolecular interaction energy, the stronger the intermolecular binding ability. Combined with the above MD

analysis, it was found that the order of the assembly ability of the three types of probes was as follows: **4**>**5**>**6**.

Sensing scope: amino acids, polypeptides, amines and amino alcohols

General Information

The utility of probe **1** was tested with all chiral amino acids, polypeptides, amines and amino alcohols. The CD spectra of the diluted solutions were collected with a quartz cuvette (0.1 cm path length). Chiral analyte (5 mM), NaOH (6 mM) and probe **1** (5 mM) were mixed in 1 mL of ACN/H_2O mixture (4/1) and the reaction was shaken for 1 min (the pH was adjusted to 9 by NaOH). A 125.0 μL aliquot of the solution was diluted to 0.313 mM with 2.0 mL ACN/H_2O mixture (1/4), allowed to stand for 15 min and then subjected to CD or CPL analysis using a quartz cuvette (0.1 and 1 cm path length for CD and CPL analysis, respectively). All subsequent reactions were carried out using the above procedure, unless otherwise stated.

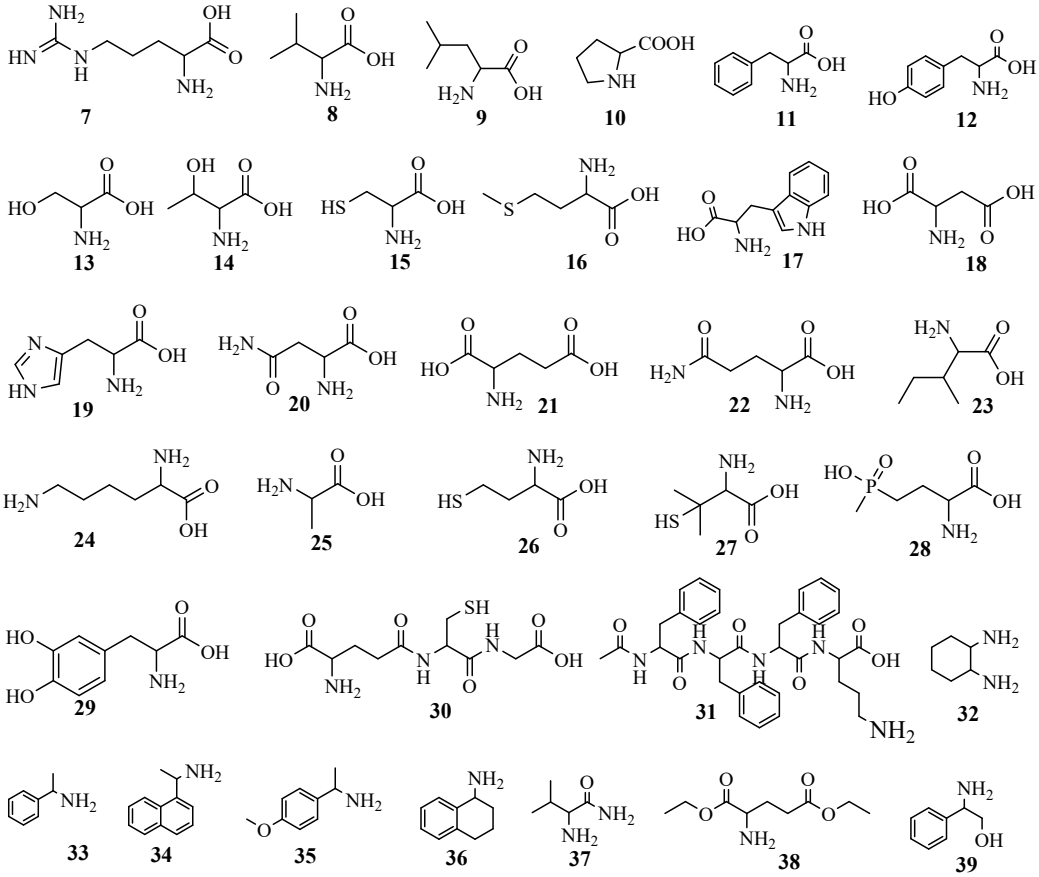

Scheme S5. Substrate scope of probe **1**.

The CD spectra of successful analytes

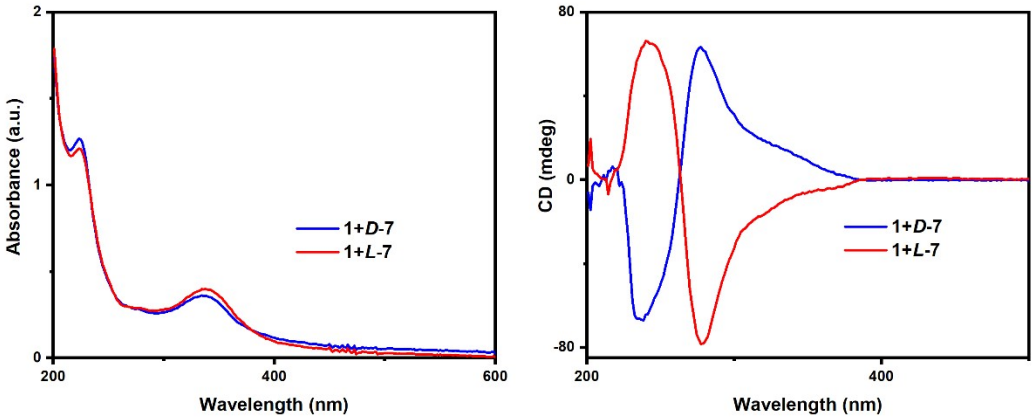

Figure S51. UV-*vis* and CD spectra of (*D*/*L*)-**7** reacting with OPA and **1**

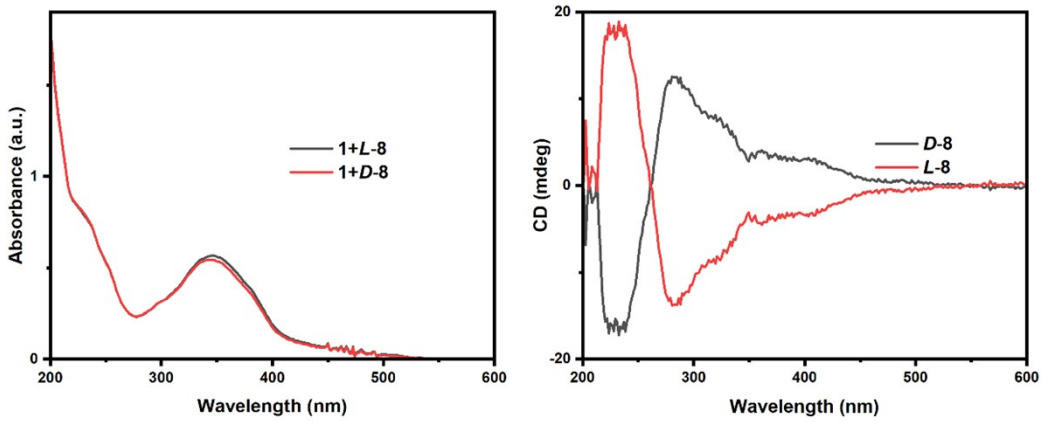

Figure S52. UV-*vis* and CD spectra of (*D*/*L*)-**8** reacting with OPA and **1**

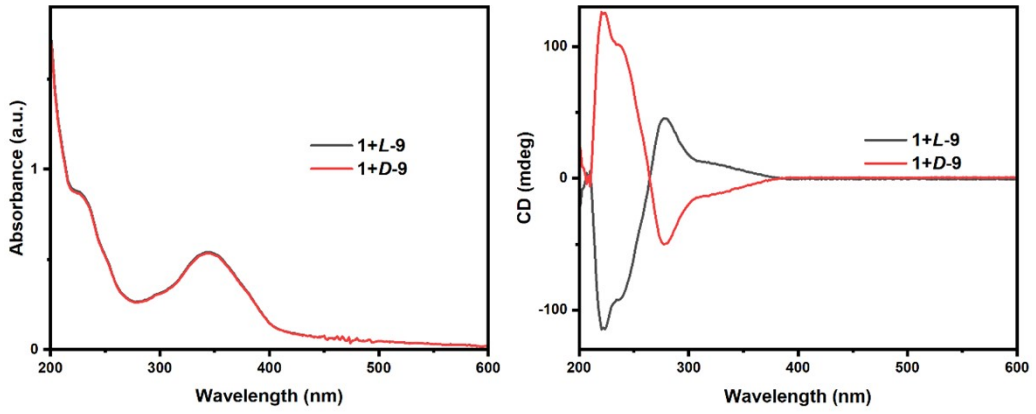

Figure S53. UV-vis and CD spectra of (*D*/*L*)-**9** reacting with OPA and **1**.

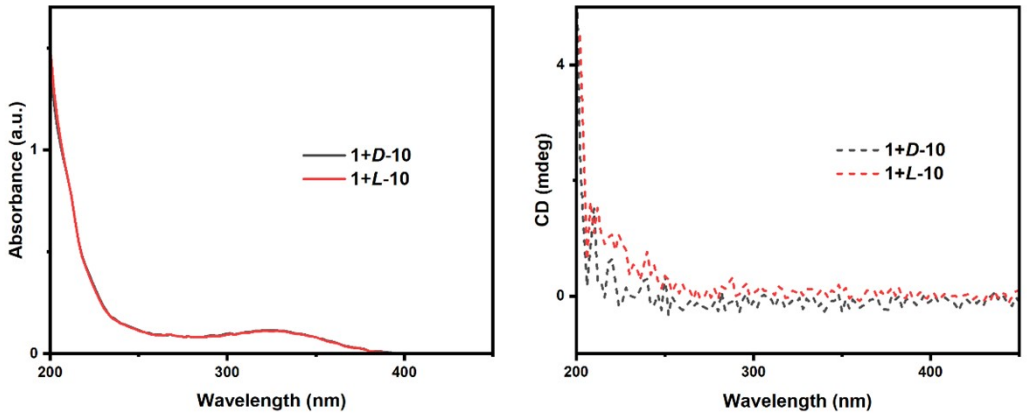

Figure S54. UV-vis and CD spectra of (*D*/*L*)-**10** reacting with OPA and **1**

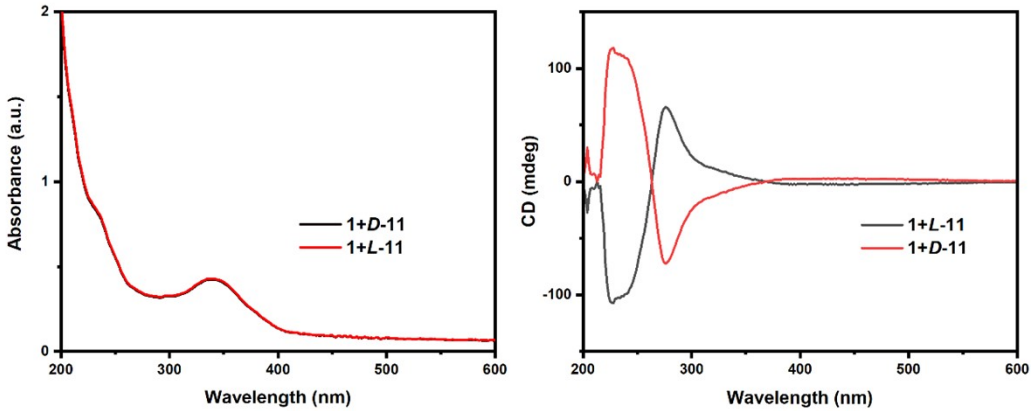

Figure S55. UV-*vis* and CD spectra of (*D*/*L*)-**11** reacting with OPA and **1**

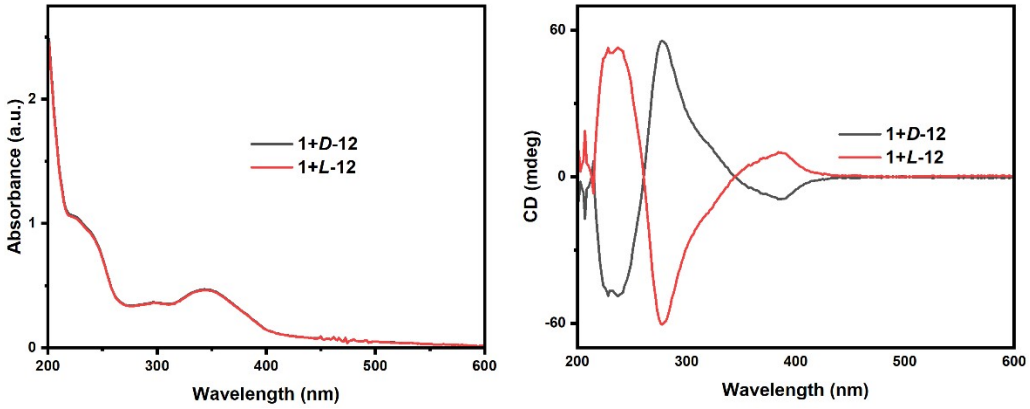

Figure S56. UV-*vis* and CD spectra of (*D*/*L*)-**12** reacting with OPA and **1**

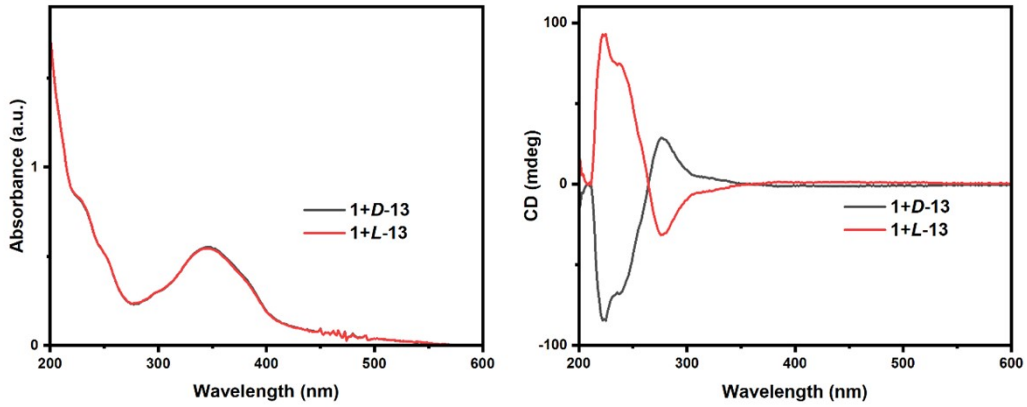

Figure S57. UV-*vis* and CD spectra of (*D*/*L*)-**13** reacting with OPA and **1**

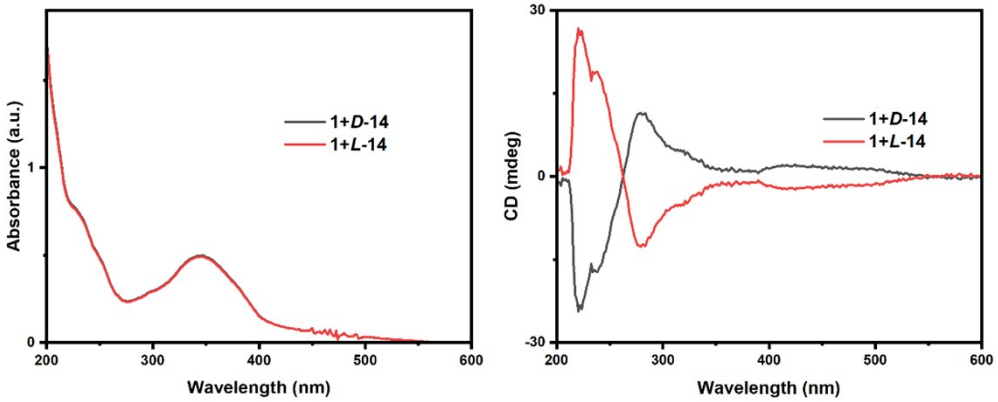

Figure S58. UV-*vis* and CD spectra of (*D*/*L*)-**14** reacting with OPA and **1**.

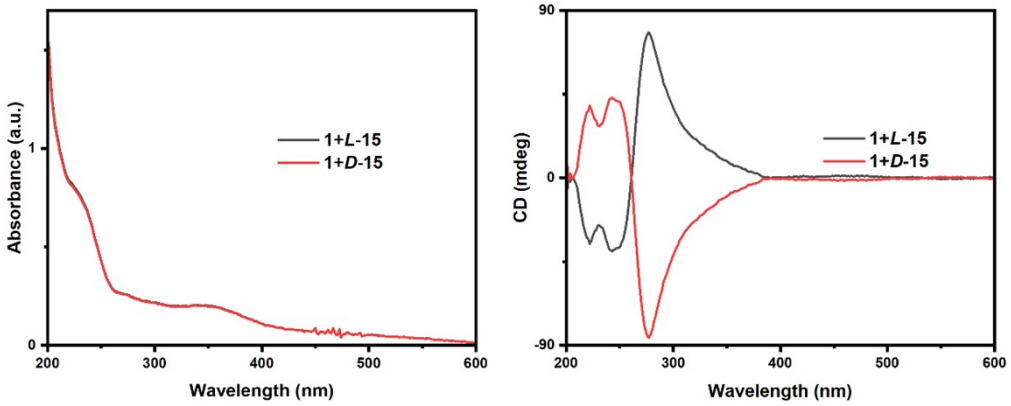

Figure S59. UV-*vis* and CD spectra of (*D*/*L*)-**15** reacting with OPA and **1**

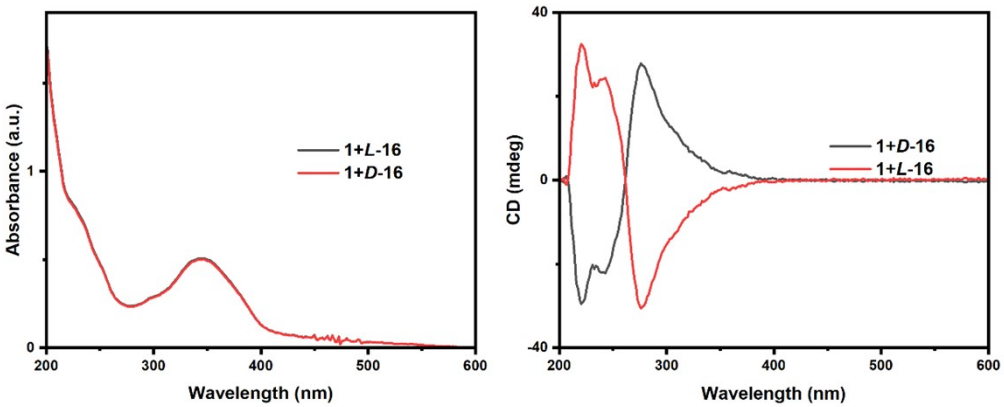

Figure S60. UV-*vis* and CD spectra of (*D*/*L*)-**16** reacting with OPA and **1**

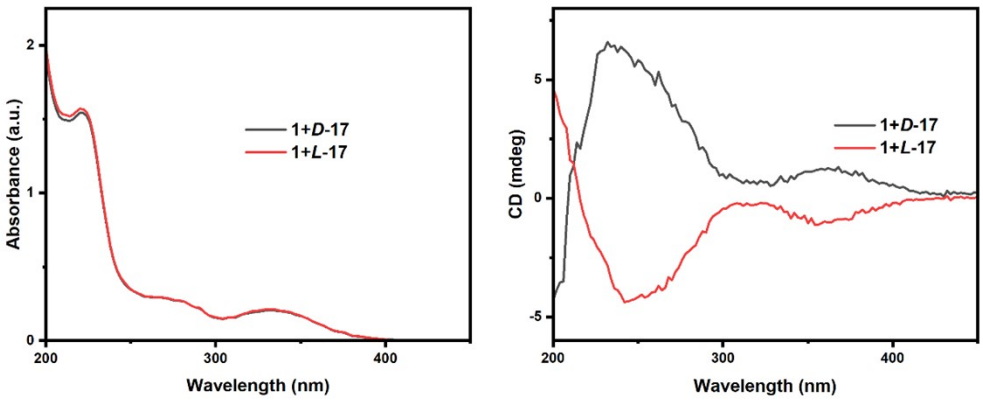

Figure S61. UV-*vis* and CD spectra of (*D*/*L*)-**17** reacting with OPA and **1**

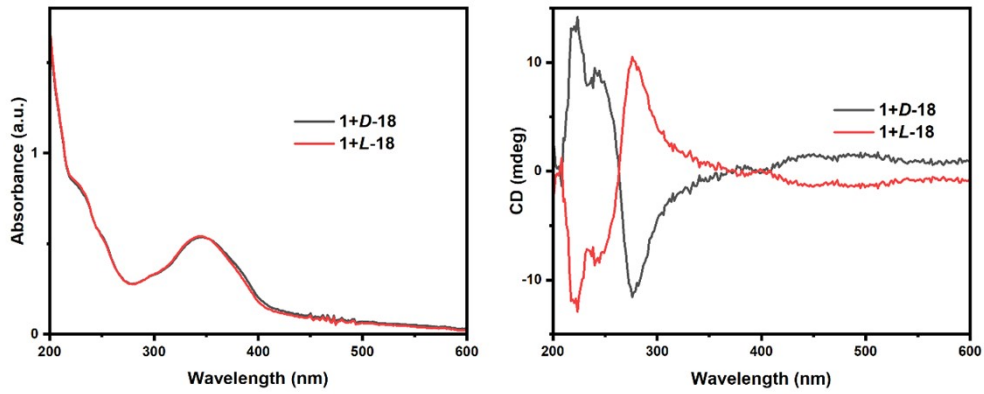

Figure S62. UV-*vis* and CD spectra of (*D*/*L*)-**18** reacting with OPA and **1**

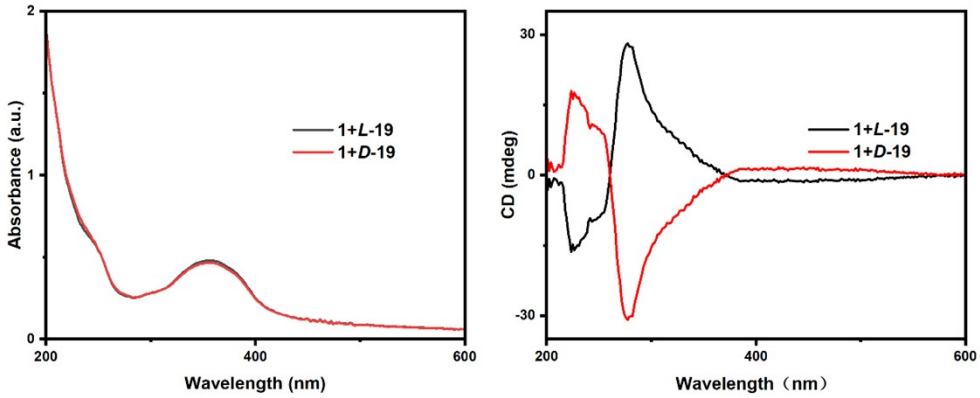

Figure S63. UV-*vis* and CD spectra of (*D*/*L*)-**19** reacting with OPA and **1**

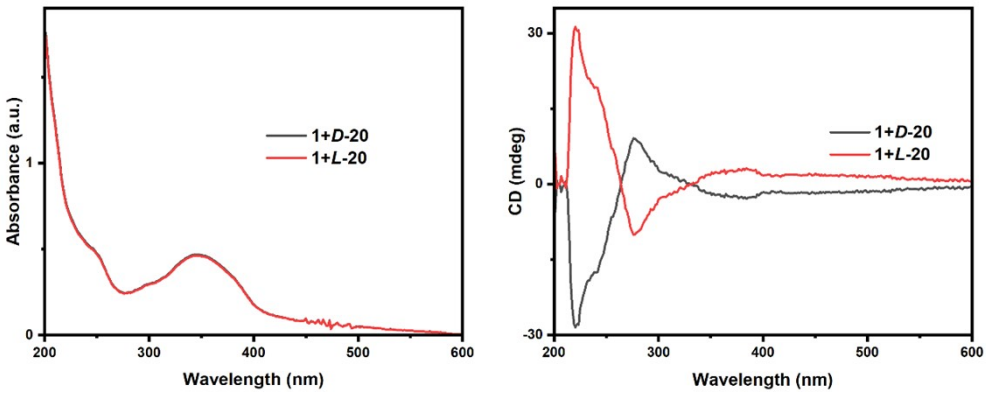

Figure S64. UV-*vis* and CD spectra of (*D*/*L*)-**20** reacting with OPA and **1**

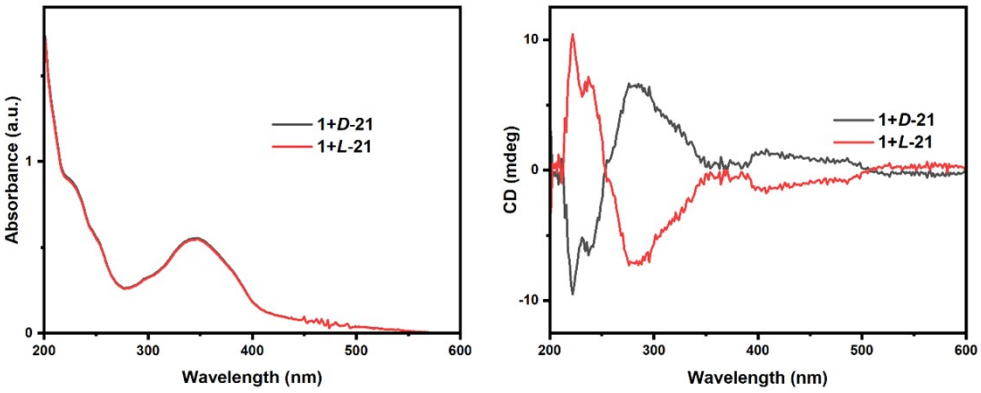

Figure S65. UV-*vis* and CD spectra of (*D*/*L*)-**21** reacting with OPA and **1**

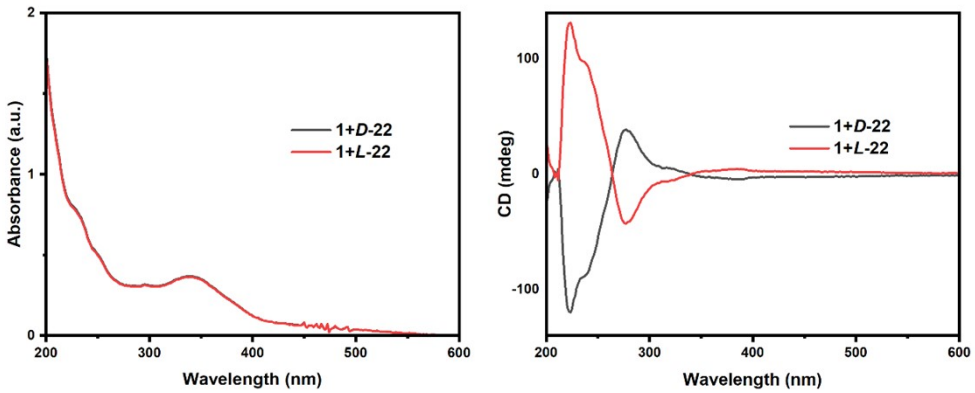

Figure S66. UV-*vis* and CD spectra of (*D*/*L*)-**22** reacting with OPA and **1**

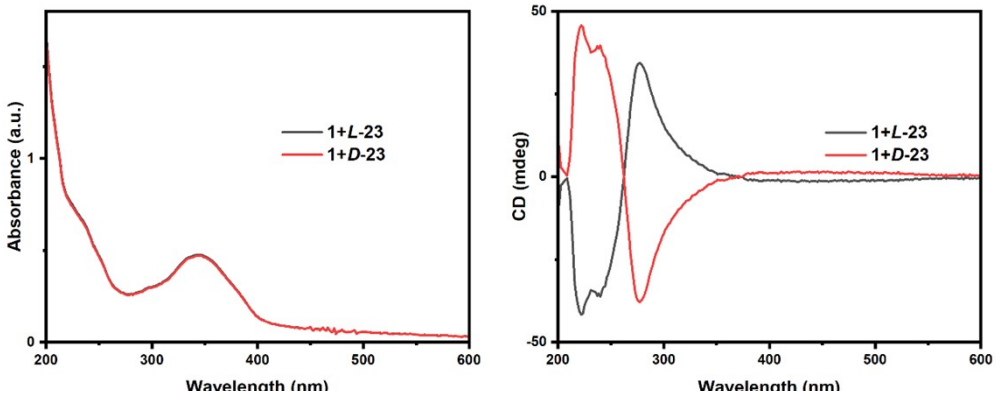

Figure S67. UV-*vis* and CD spectra of (*D*/*L*)-**23** reacting with OPA and **1**

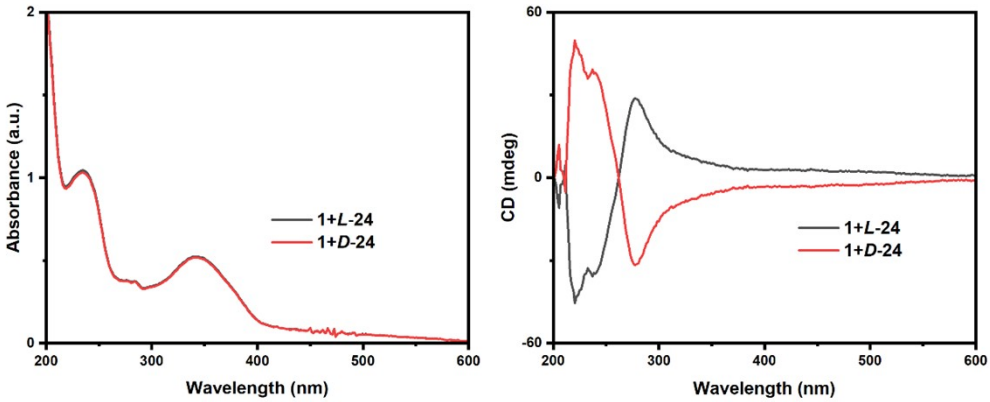

Figure S68. UV-*vis* and CD spectra of (*D*/*L*)-**24** reacting with OPA and **1**

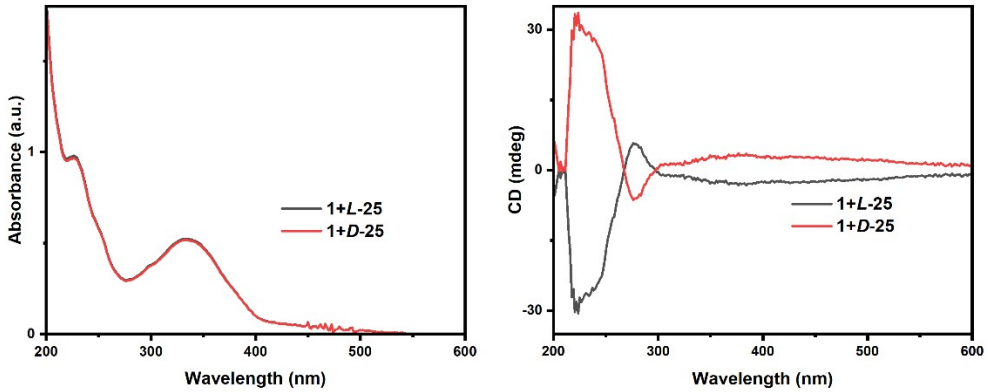

Figure S69. UV-*vis* and CD spectra of (*D*/*L*)-**25** reacting with OPA and **1**

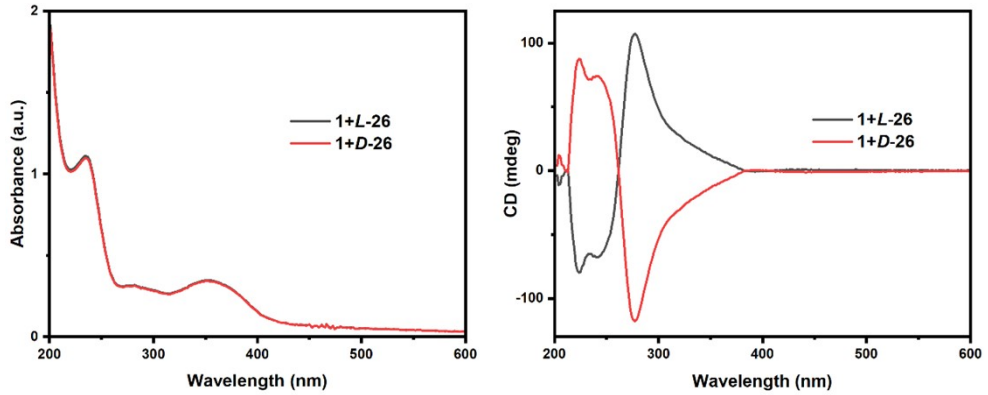

Figure S70. UV-*vis* and CD spectra of (*D*/*L*)-**26** reacting with OPA and **1**

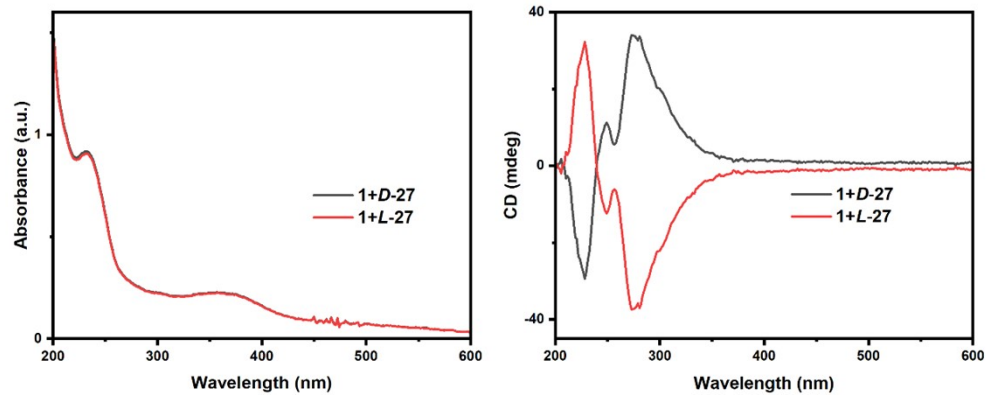

Figure S71. UV-*vis* and CD spectra of (*D*/*L*)-**27** reacting with OPA and **1**

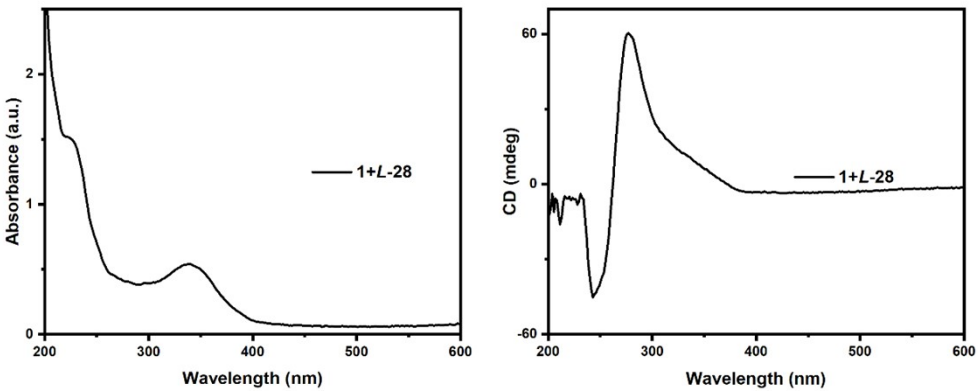

Figure S72. UV-*vis* and CD spectra of *L*-**28** reacting with OPA and **1**

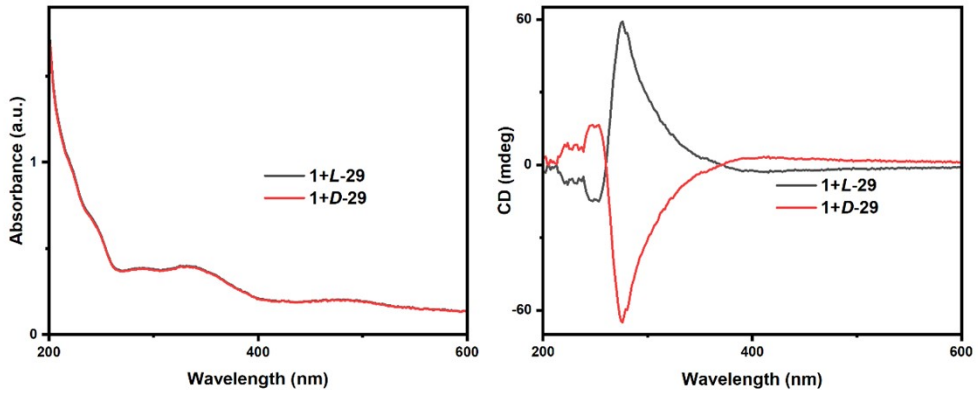

Figure S73. UV-*vis* and CD spectra of (*D*/*L*)-**29** reacting with OPA and **1**

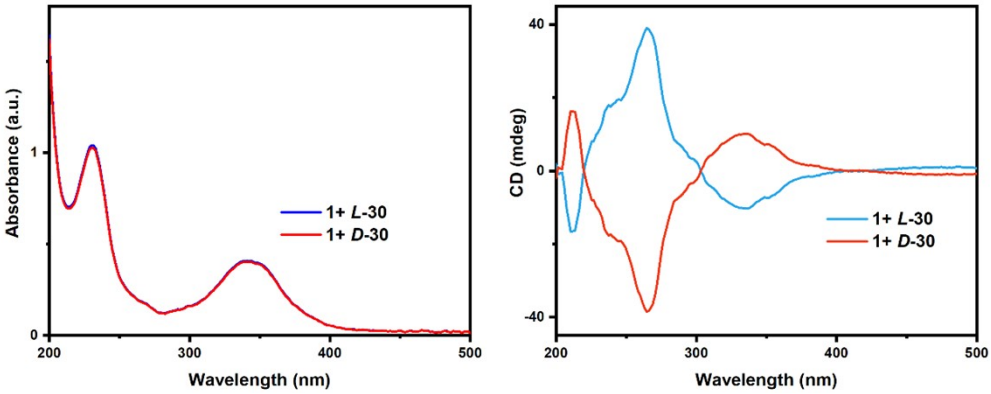

Figure S74. UV-*vis* and CD spectra of (*D*/*L*)-**30** reacting with OPA and **1**

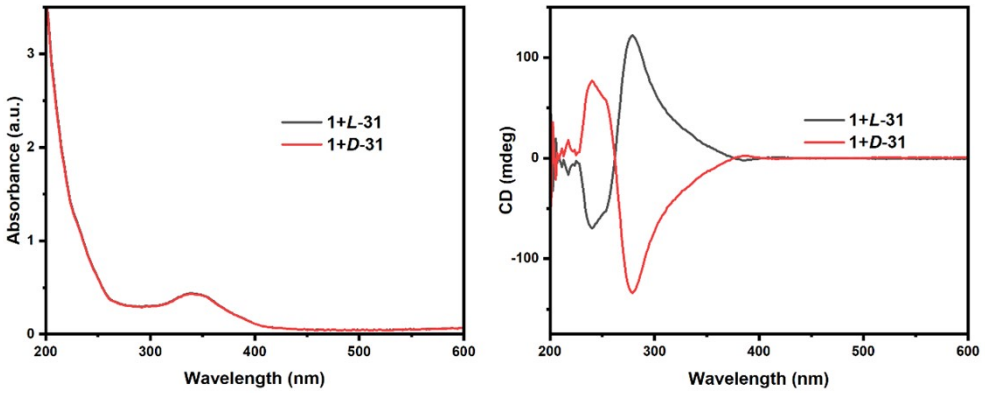

Figure S75. UV-*vis* and CD spectra of (*D*/*L*)-**31** reacting with OPA and **1**

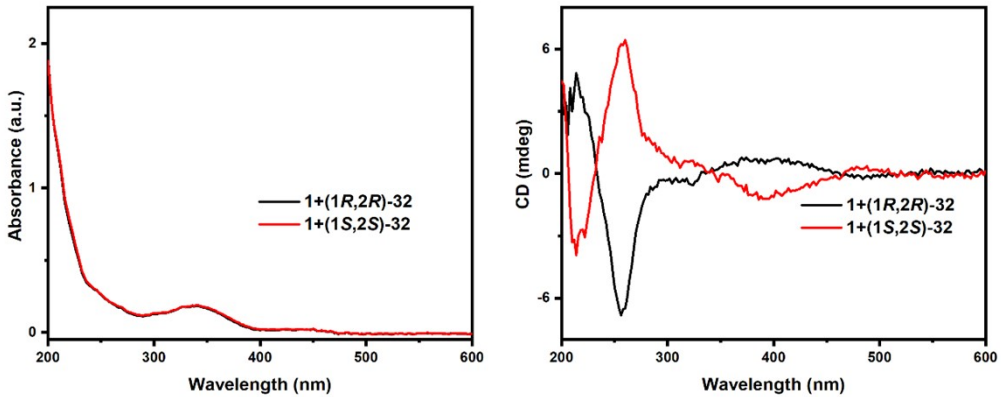

Figure S76. UV-*vis* and CD spectra of (*R*,*R*/*S*,*S*)-**32** reacting with OPA and **1**

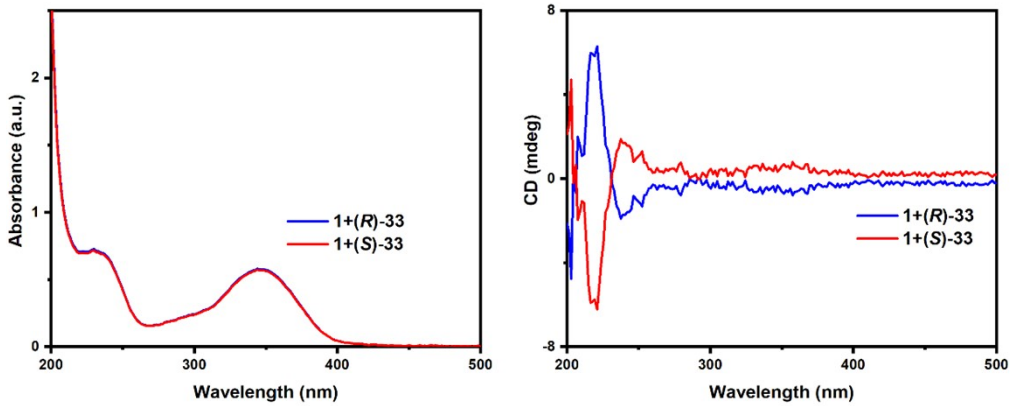

Figure S77. UV-*vis* and CD spectra of (*R*/*S*)-**33** reacting with OPA and **1**

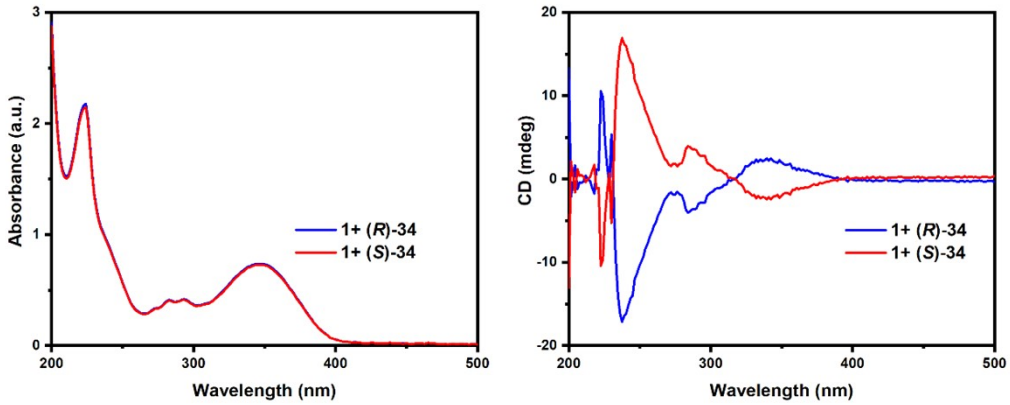

Figure S78. UV-*vis* and CD spectra of (*R*/*S*)-**34** reacting with OPA and **1**

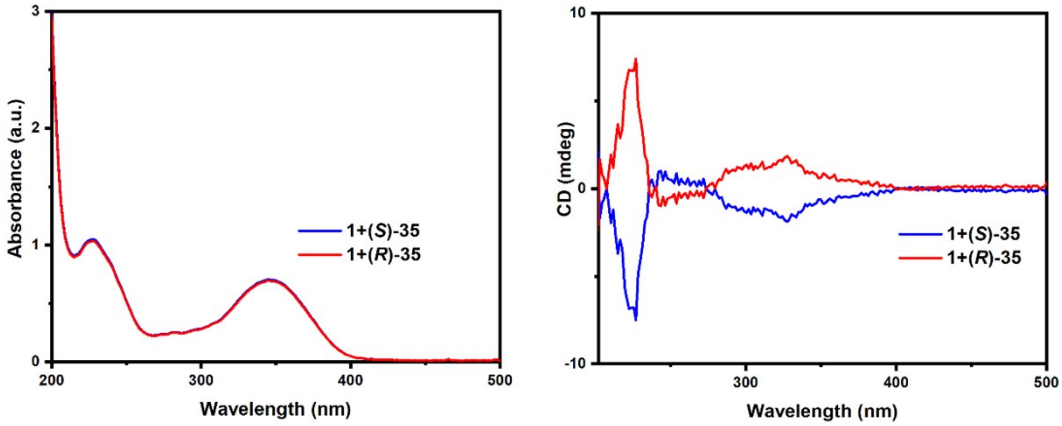

Figure S79. UV-vis and CD spectra of (*R*/*S*)-**35** reacting with OPA and **1**

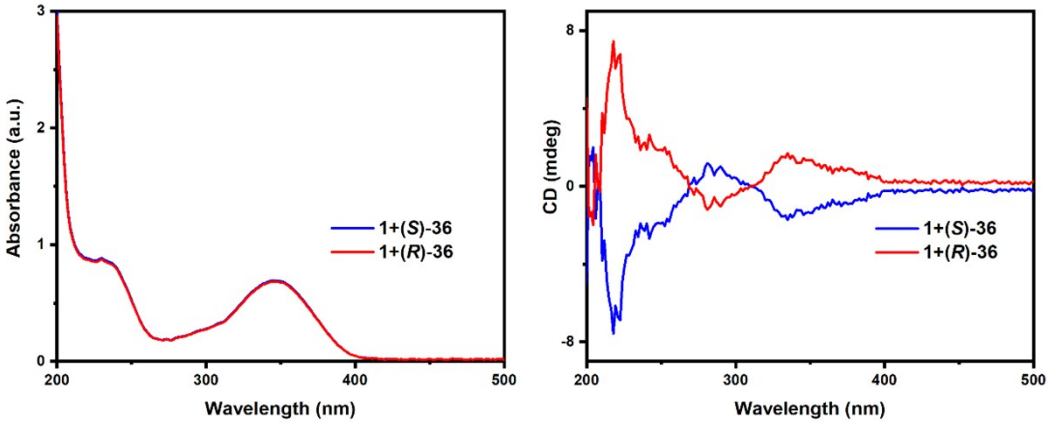

Figure S80. UV-vis and CD spectra of (*R*/*S*)-**36** reacting with OPA and **1**

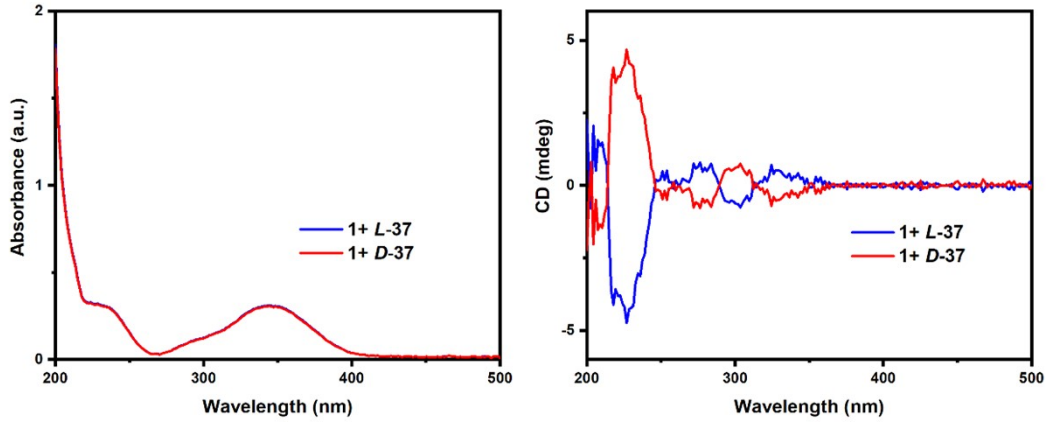

Figure S81. UV-vis and CD spectra of (*R*/*S*)-**37** reacting with OPA and **1**

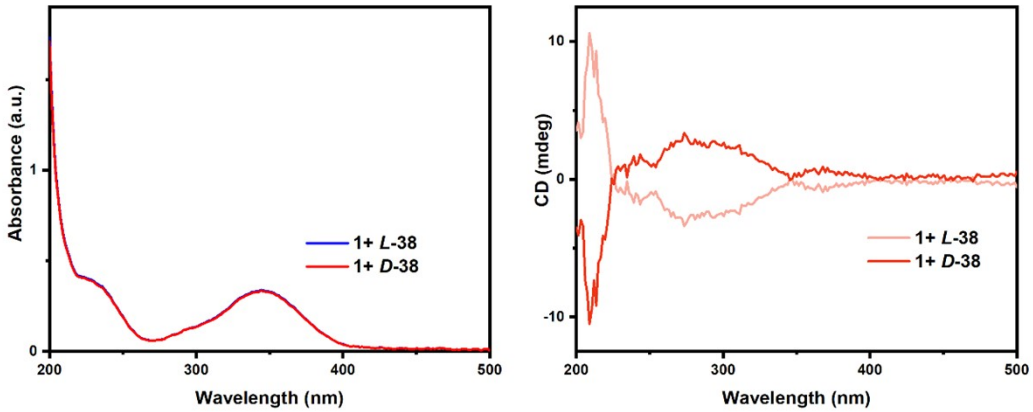

Figure S82. UV-vis and CD spectra of (*D*/*L*)-**38** reacting with OPA and **1**

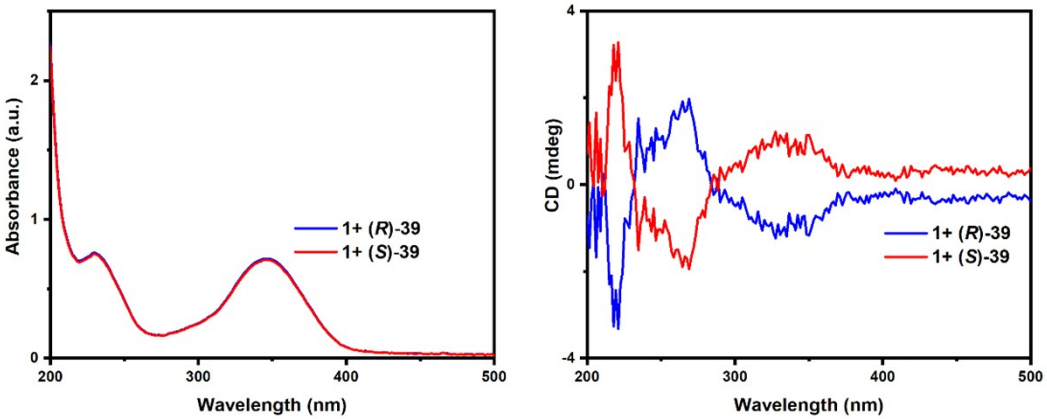

Figure S83. UV-vis and CD spectra of (*R*/*S*)-**39** reacting with OPA and **1**

The CPL spectra of successful analytes

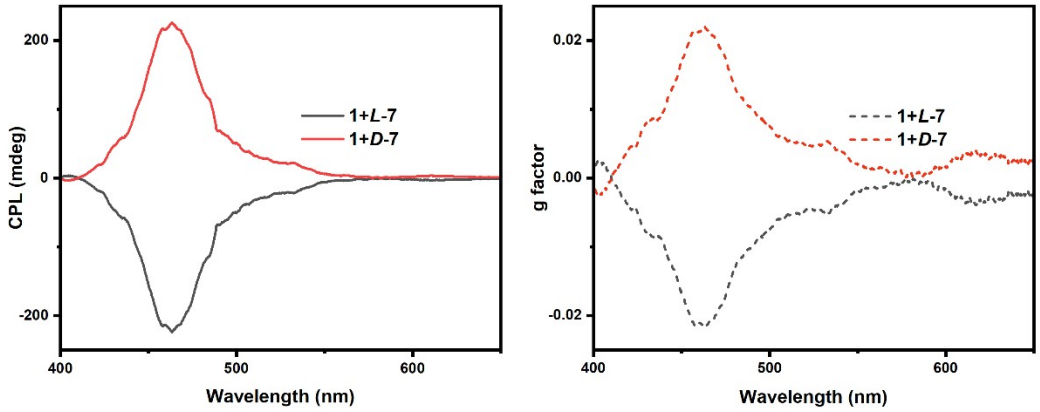

Figure S84. CPL and *g* factor spectra of (*D*/*L*)-**7** reacting with OPA and **1**

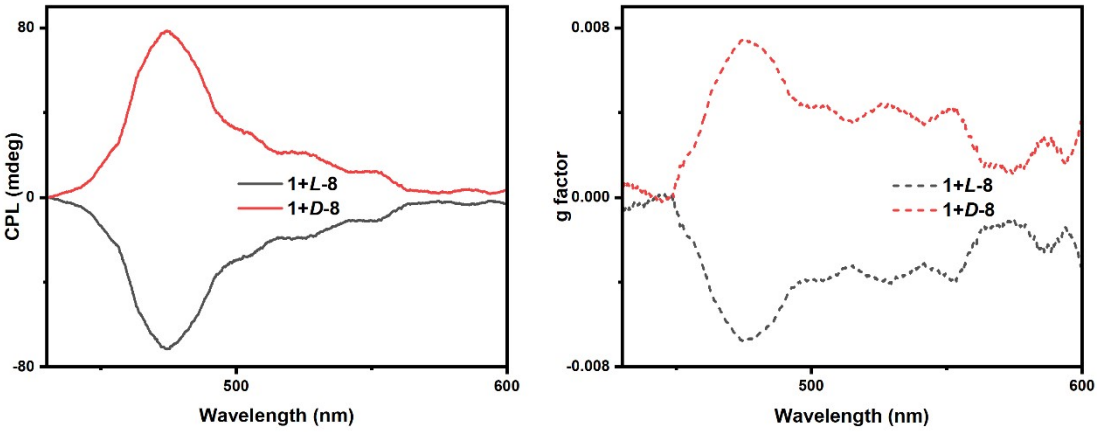

Figure S85. CPL and *g* factor spectra of (*D*/*L*)-**8** reacting with OPA and **1**

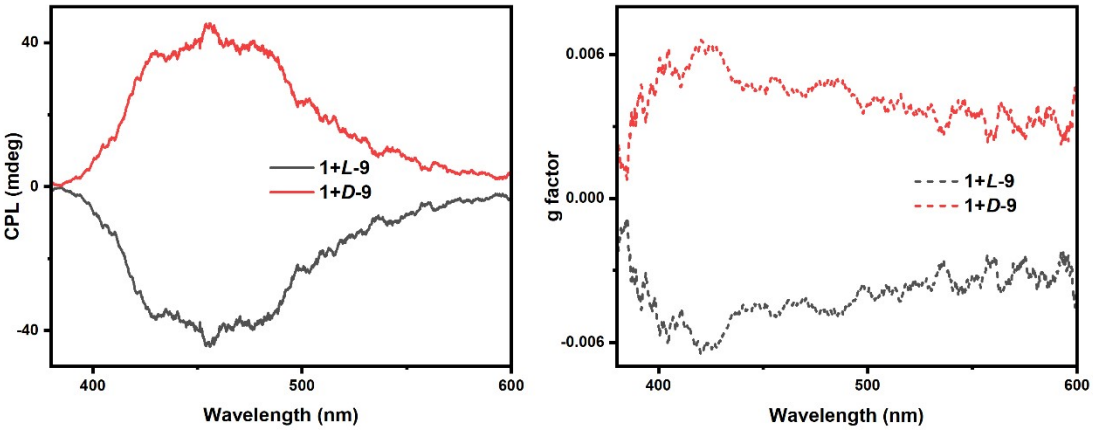

Figure S86. CPL and *g* factor spectra of (*D*/*L*)-**9** reacting with OPA and **1**

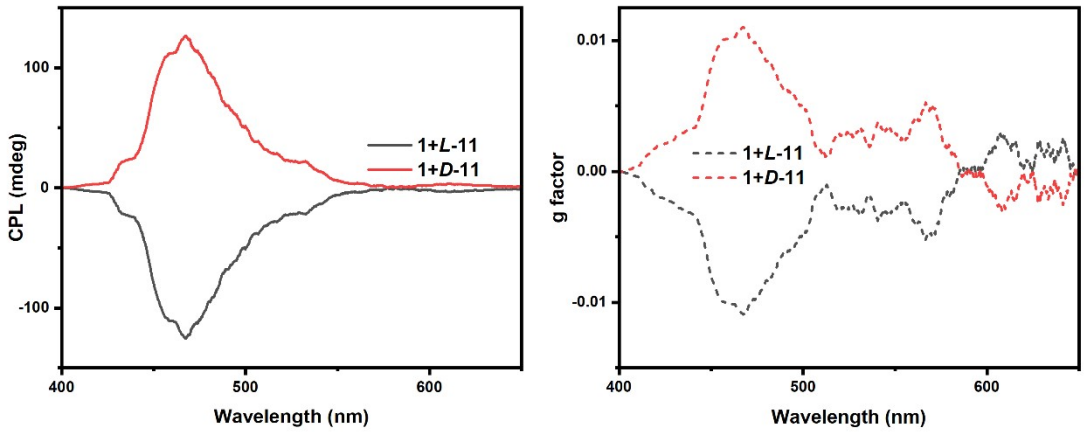

Figure S87. CPL and *g* factor spectra of (*D*/*L*)-**11** reacting with OPA and **1**

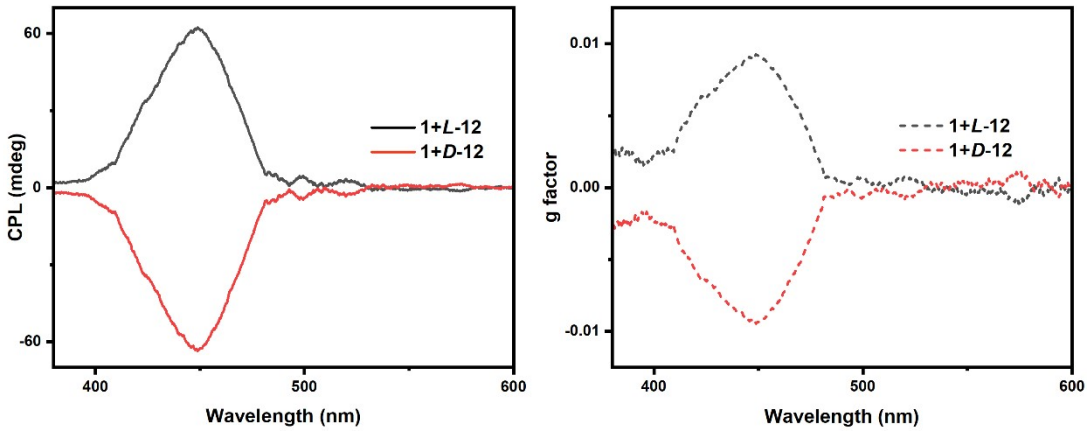

Figure S88. CPL and *g* factor spectra of (*D*/*L*)-**12** reacting with OPA and **1**

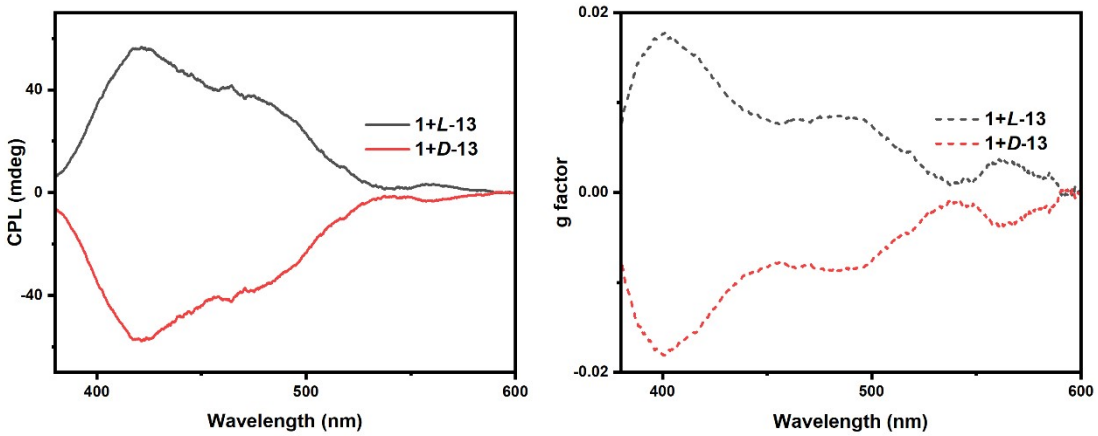

Figure S89. CPL and *g* factor spectra of (*D*/*L*)-**13** reacting with OPA and **1**

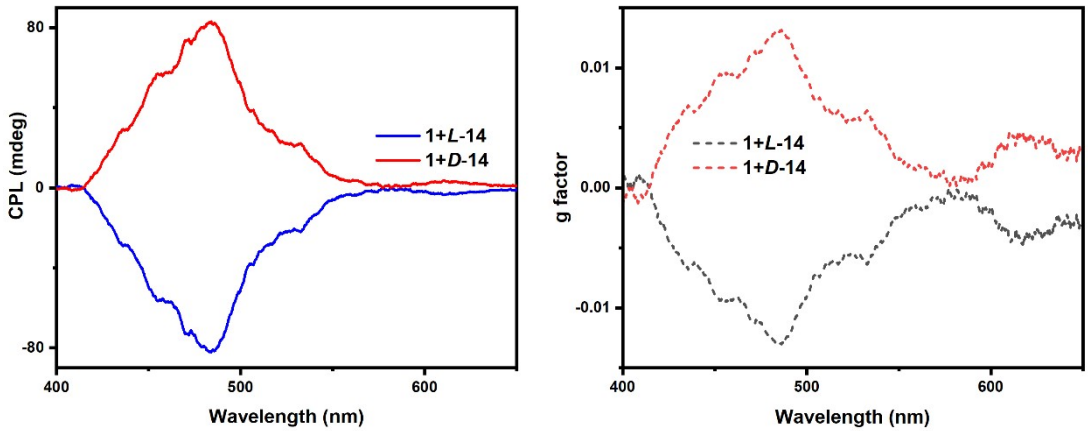

Figure S90. CPL and *g* factor spectra of (*D*/*L*)-**14** reacting with OPA and **1**

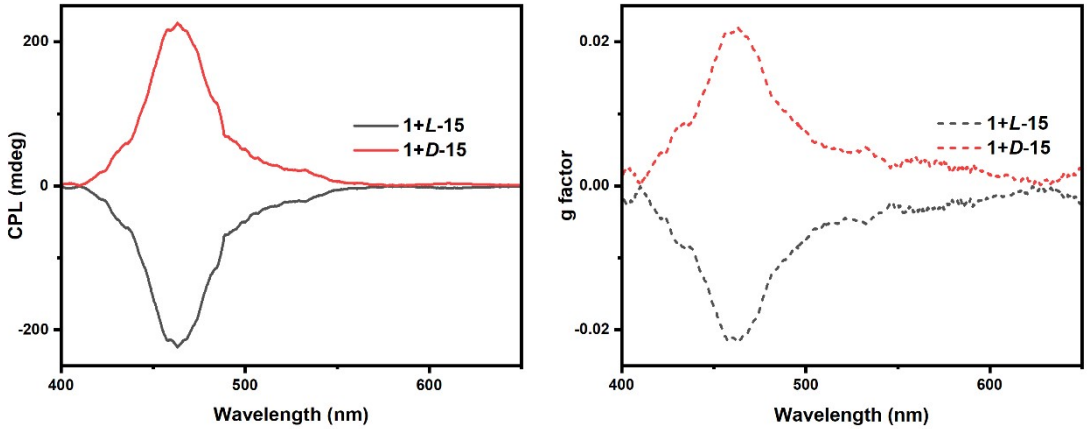

Figure S91. CPL and *g* factor spectra of (*D*/*L*)-**15** reacting with OPA and **1**

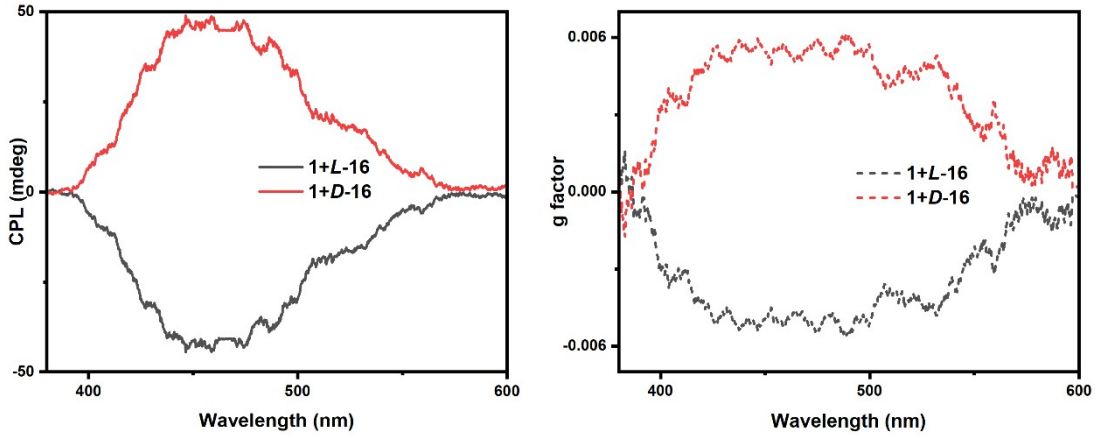

Figure S92. CPL and *g* factor spectra of (*D*/*L*)-**16** reacting with OPA and **1**

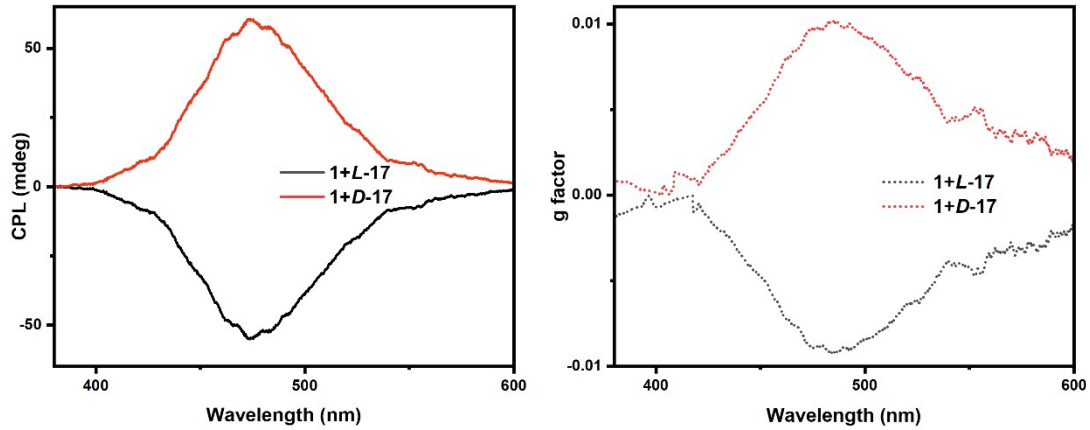

Figure S93. CPL and *g* factor spectra of (*D*/*L*)-**17** reacting with OPA and **1**

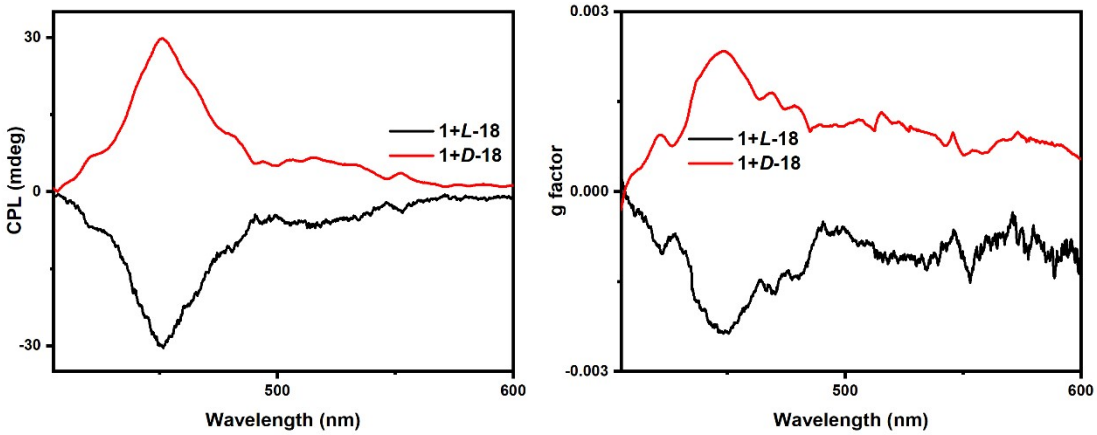

Figure S94. CPL and *g* factor spectra of (*D*/*L*)-**18** reacting with OPA and **1**

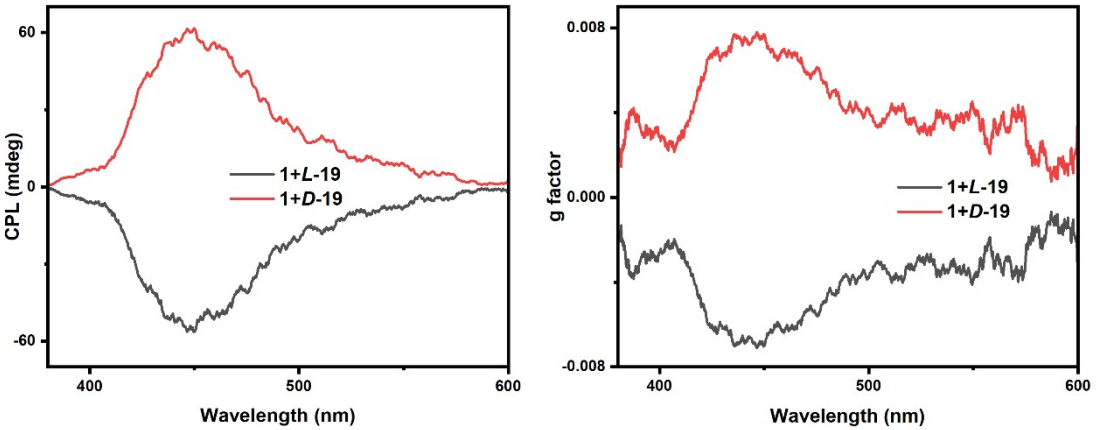

Figure S95. CPL and *g* factor spectra of (*D*/*L*)-**19** reacting with OPA and **1**

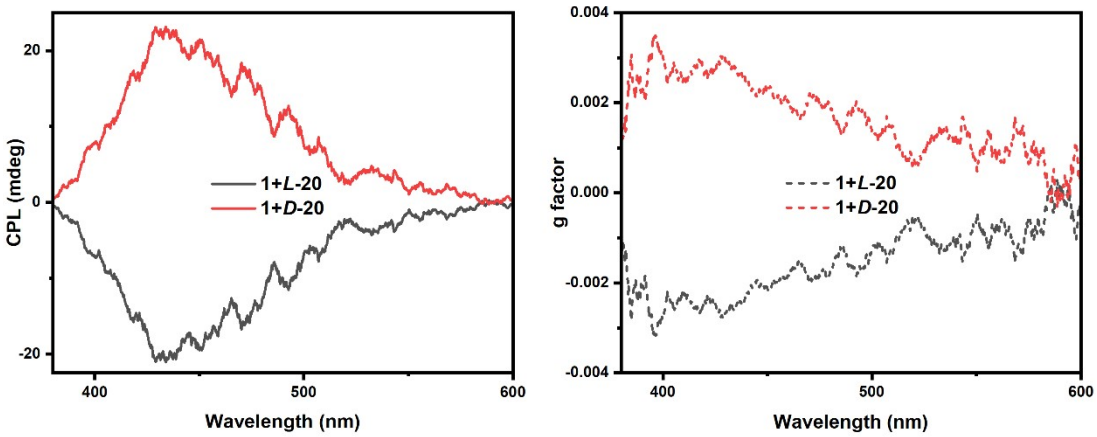

Figure S96. CPL and *g* factor spectra of (*D*/*L*)-**20** reacting with OPA and **1**

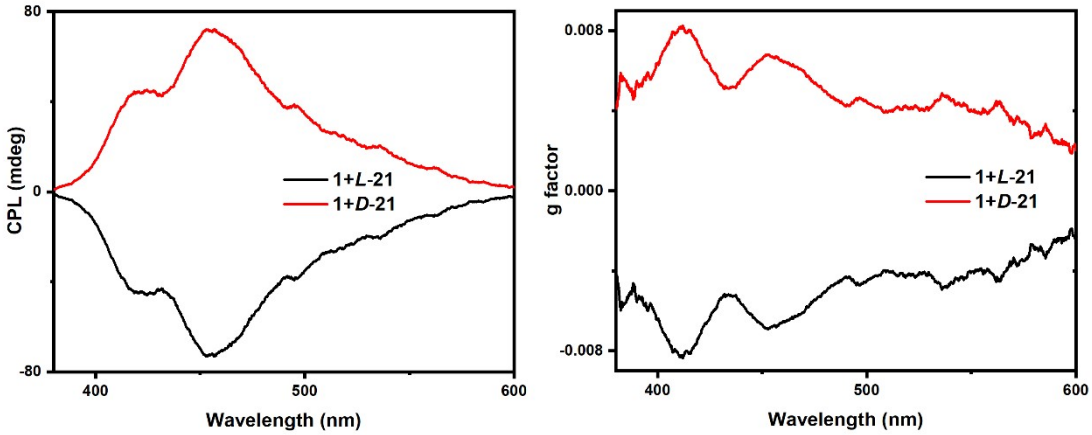

Figure S97. CPL and *g* factor spectra of (*D*/*L*)-**21** reacting with OPA and **1**

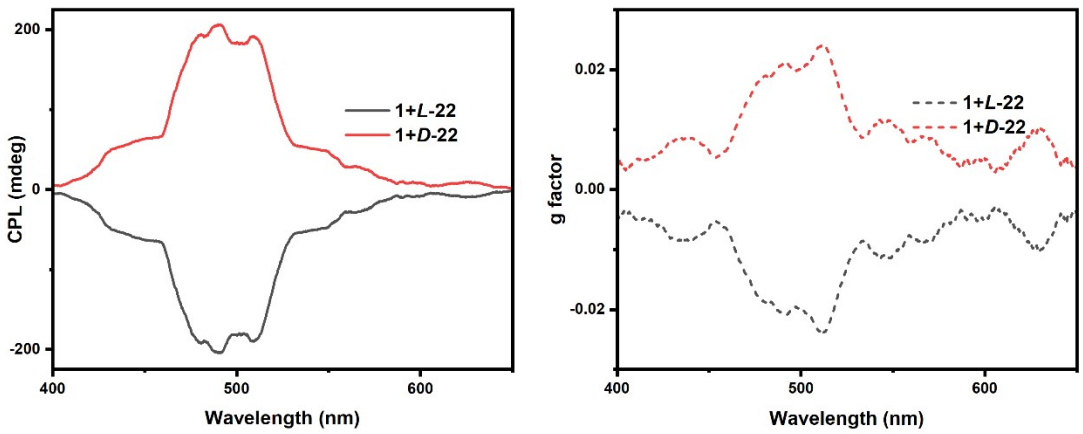

Figure S98. CPL and *g* factor spectra of (*D*/*L*)-**22** reacting with OPA and **1**

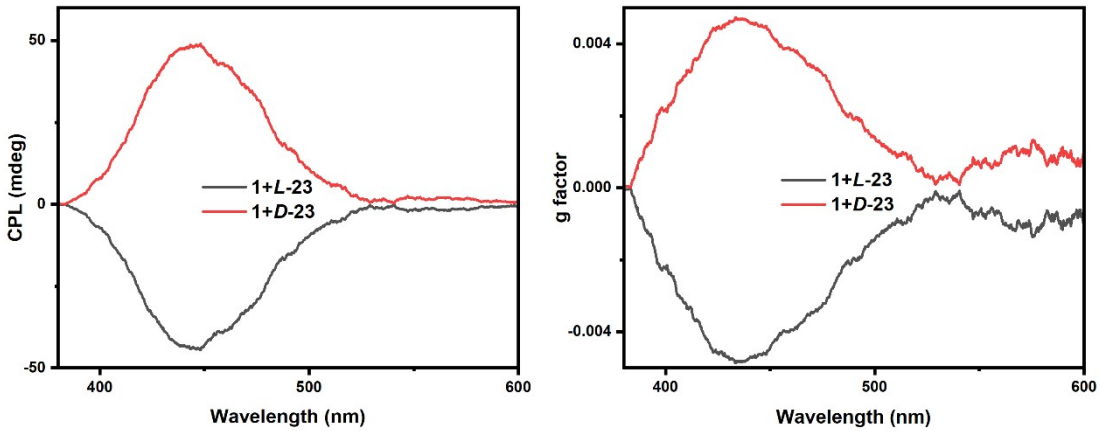

Figure S99. CPL and *g* factor spectra of (*D*/*L*)-**23** reacting with OPA and **1**

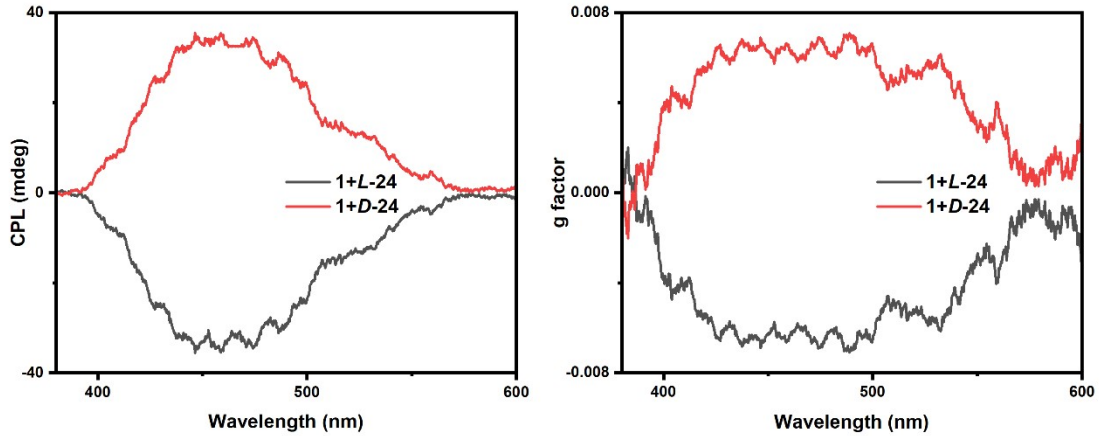

Figure S100. CPL and *g* factor spectra of (*D*/*L*)-**24** reacting with OPA and **1**

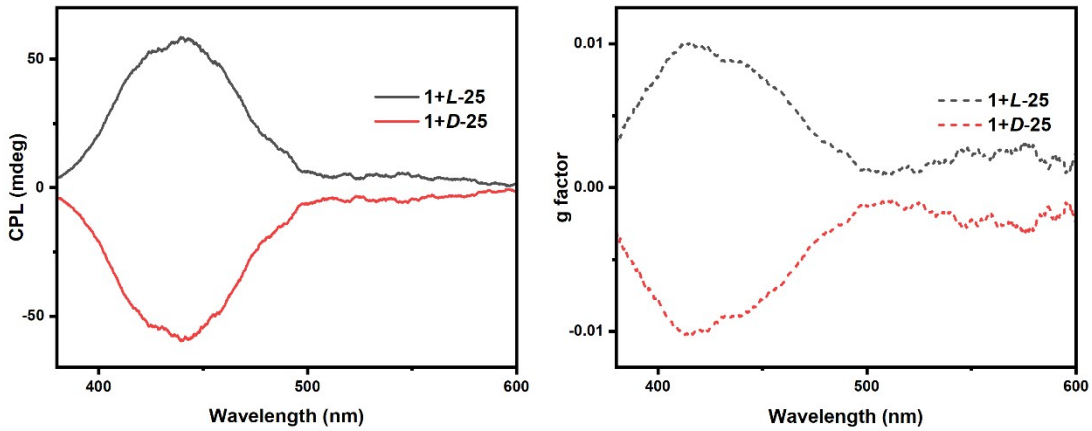

Figure S101. CPL and *g* factor spectra of (*D*/*L*)-**25** reacting with OPA and **1**

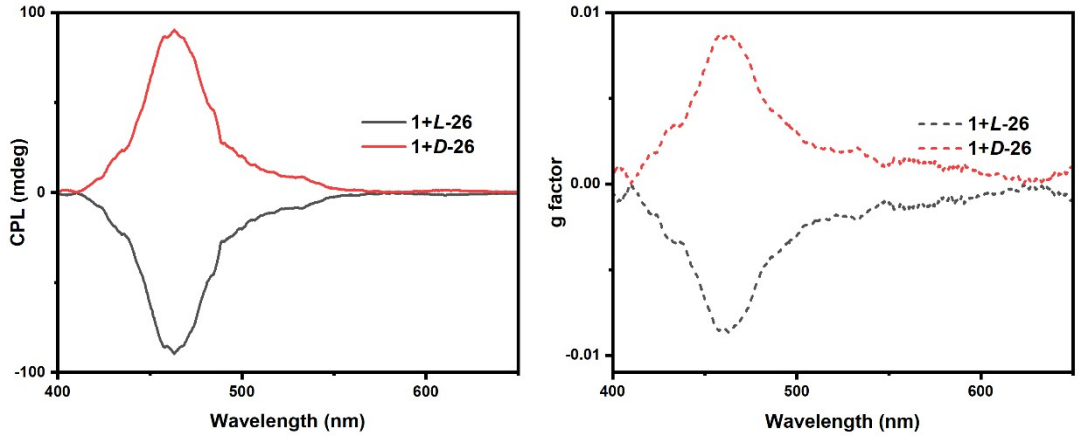

Figure S102. CPL and *g* factor spectra of (*D*/*L*)-**26** reacting with OPA and **1**

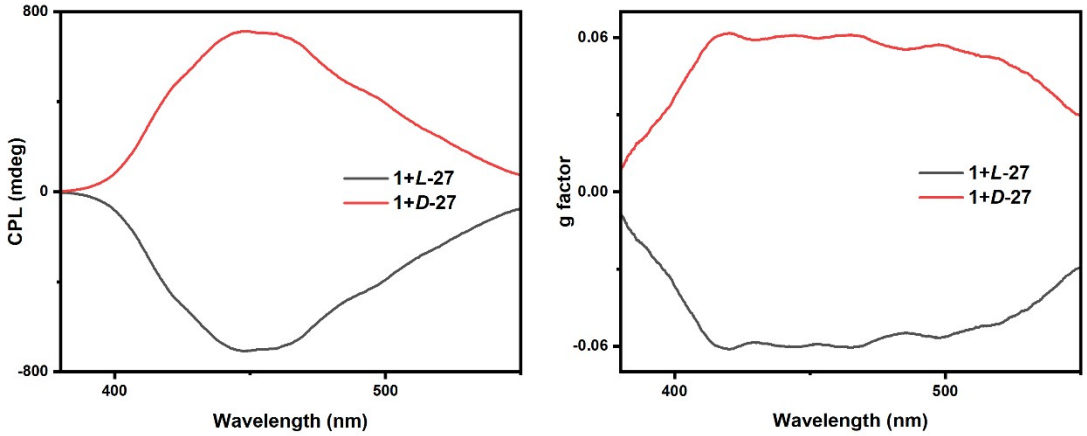

Figure S103. CPL and *g* factor spectra of (*D*/*L*)-**27** reacting with OPA and **1**

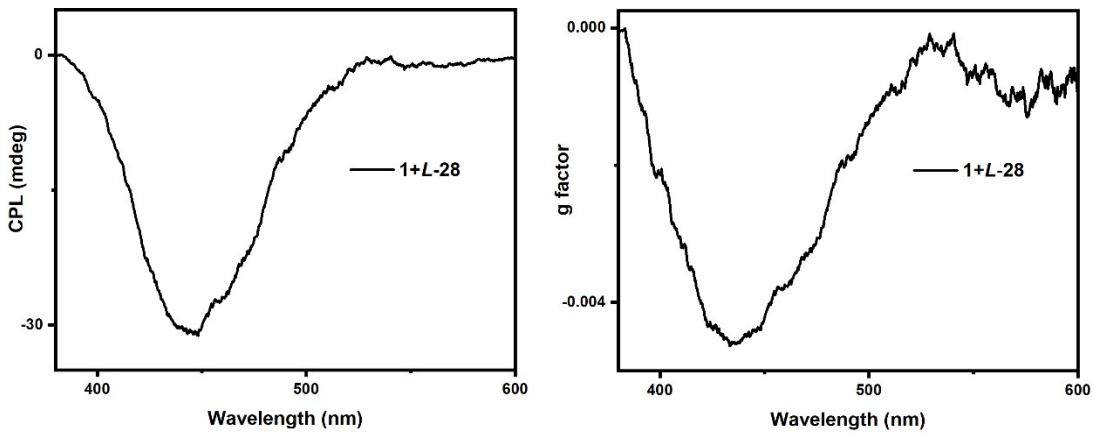

Figure S104. CPL and *g* factor spectra of *L*-**28** reacting with OPA and **1**

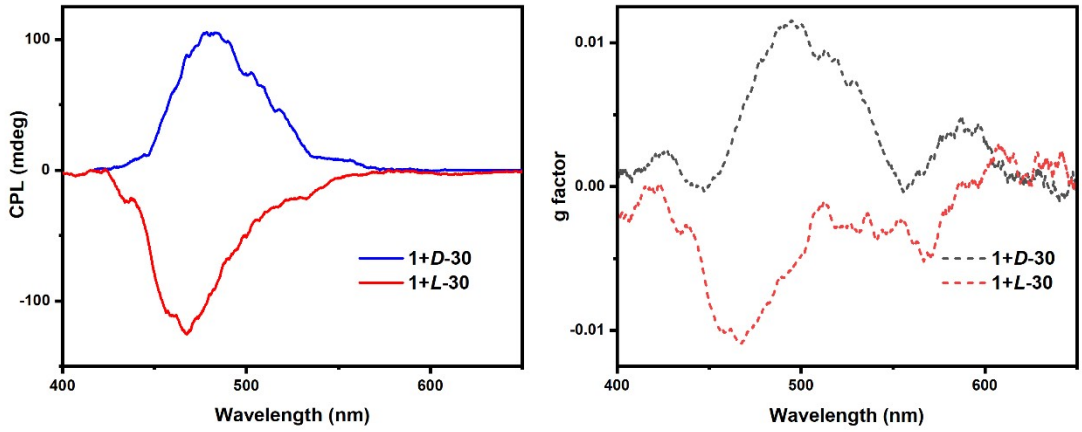

Figure S105. CPL and *g* factor spectra of (*D*/*L*)-**30** reacting with OPA and **1**

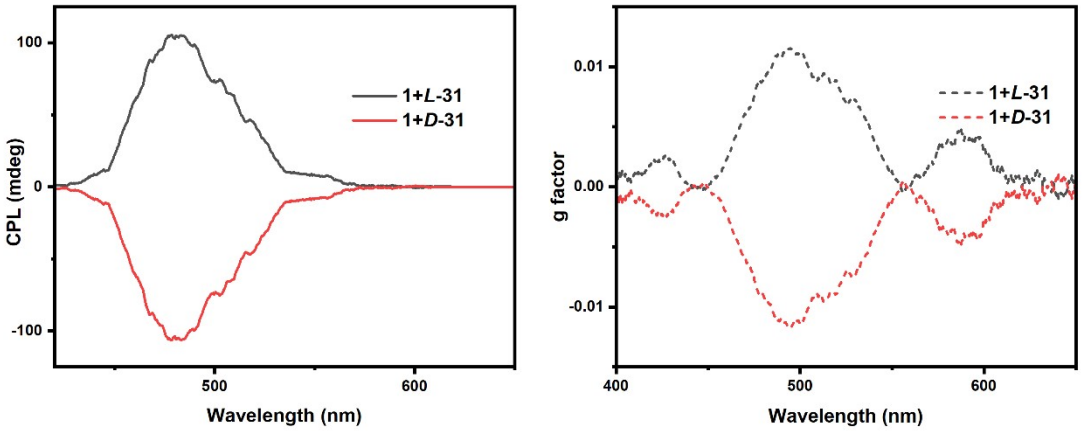

Figure S106. CPL and *g* factor spectra of (*D*/*L*)-**31** reacting with OPA and **1**

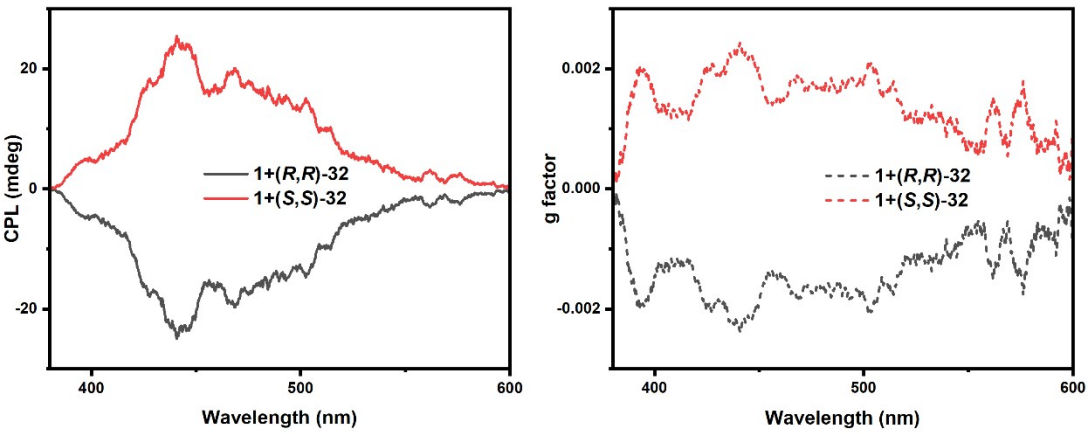

Figure S107. CPL and *g* factor spectra of (*R, R*/*S, S*)-**32** reacting with OPA and **1**

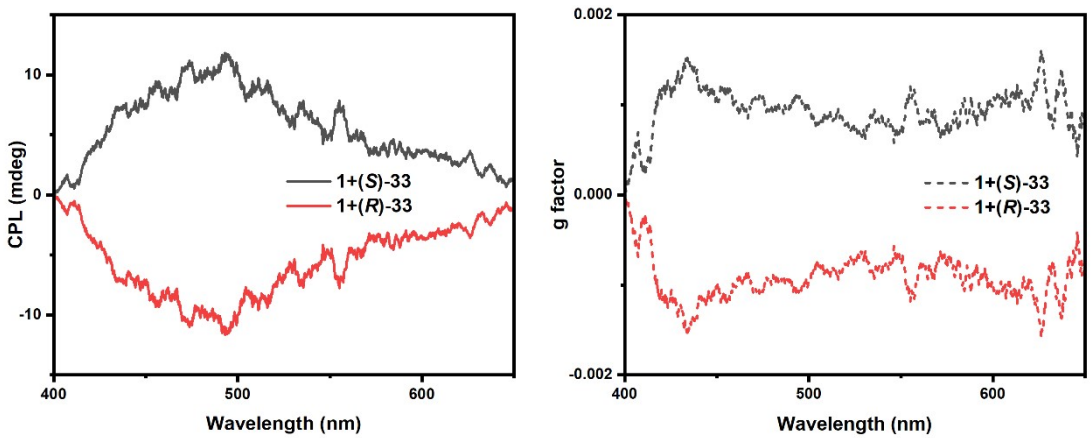

Figure S108. CPL and *g* factor spectra of (*S*/*R*)-**33** reacting with OPA and **1**

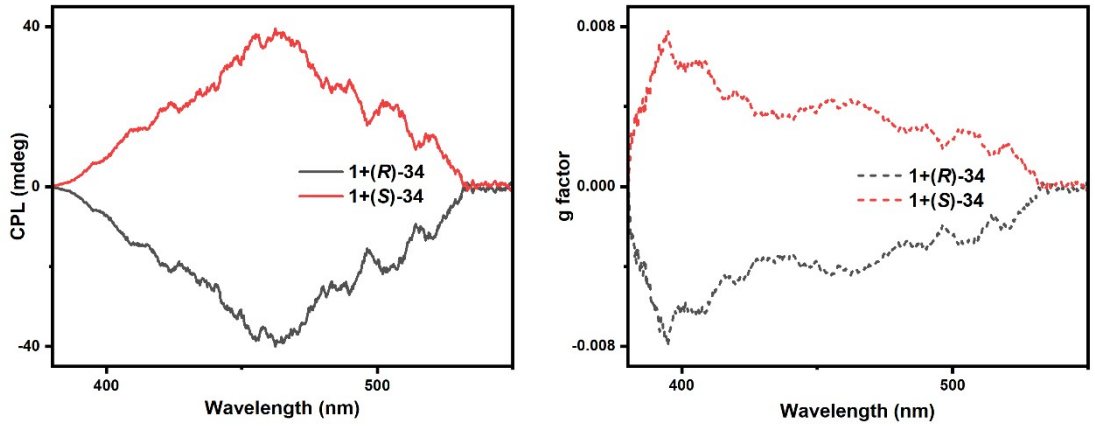

Figure S109. CPL and *g* factor spectra of (*S*/*R*)-**34** reacting with OPA and **1**

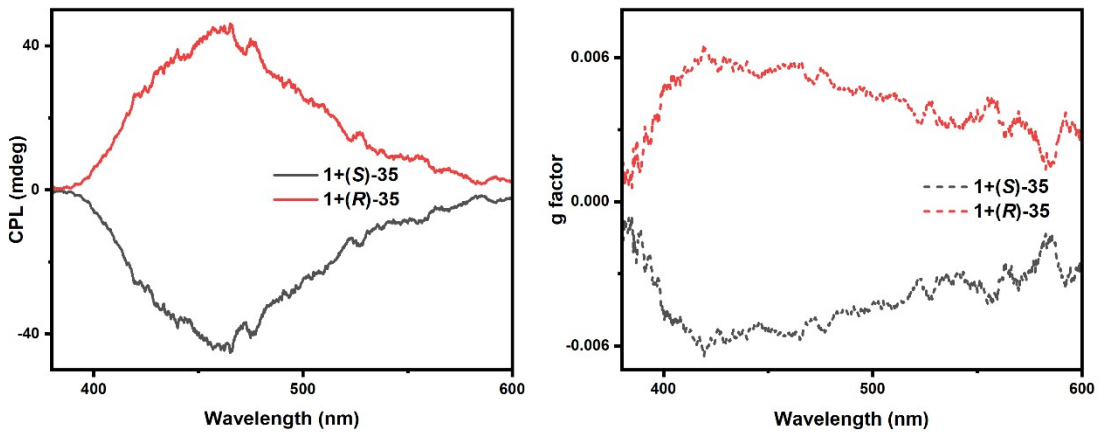

Figure S110. CPL and *g* factor spectra of (*S*/*R*)-**35** reacting with OPA and **1**

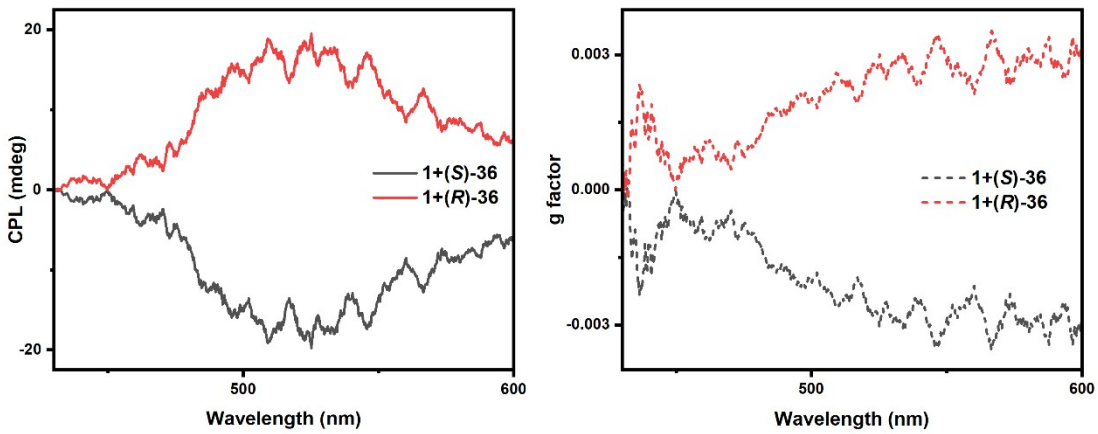

Figure S111. CPL and *g* factor spectra of (*S*/*R*)-**36** reacting with OPA and **1**

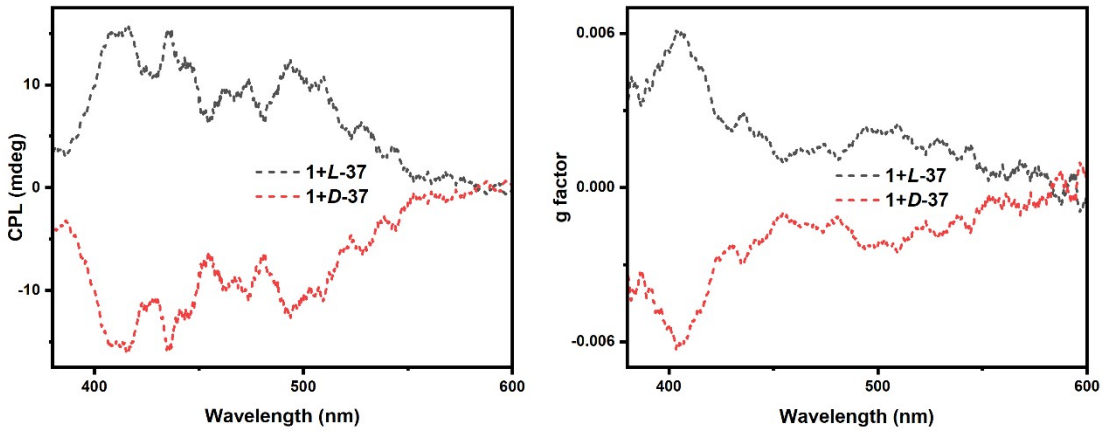

Figure S112. CPL and *g* factor spectra of (*D*/*L*)-**37** reacting with OPA and **1**

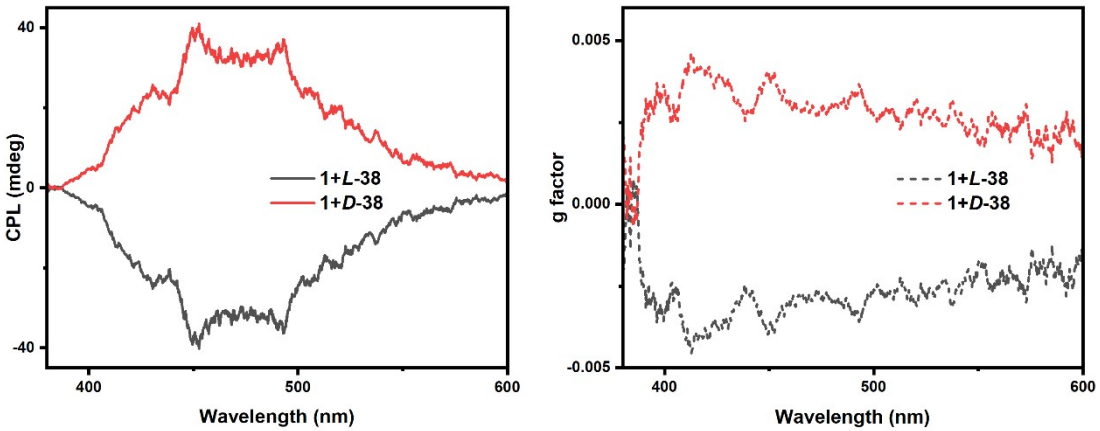

Figure S113. CPL and *g* factor spectra of (*D*/*L*)-**38** reacting with OPA and **1**

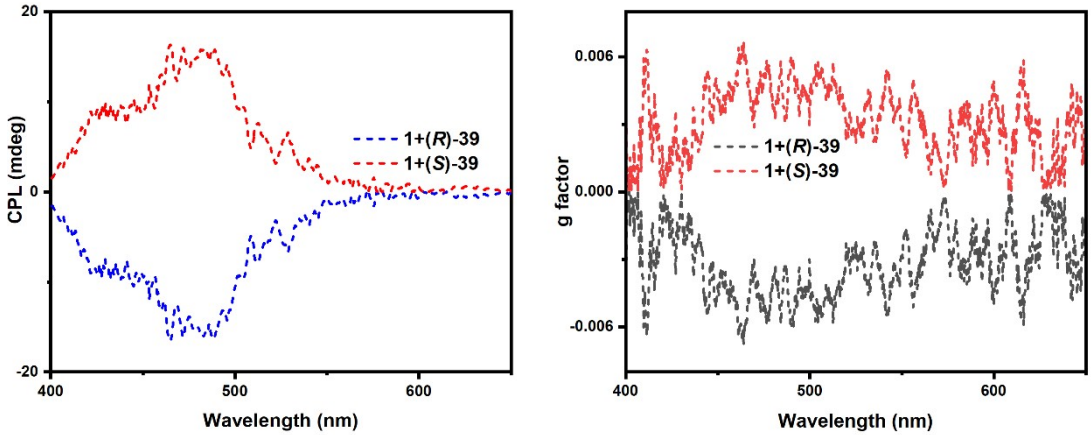

Figure S114. CPL and *g* factor spectra of (*R*/*S*)-**39** reacting with OPA and **1**.

Structural elucidation

Compound *L*-**15** (0.05 g, 87%)**:** ^{1}H NMR (400 MHz, $CDCl_3$) δ (ppm): 7.88-7.86 (d, 2H, *J*=8 Hz), 7.64-7.62 (d, 2H, *J* = 8 Hz), 7.38-7.30 (m, 2H), 7.08-6.95 (m, 8H), 4.55-4.53 (m, 2H), 4.05-4.03(m, 2H), 3.77-3.70 (m, 2H), 2.92-2.90 (m, 2H), 1.85-1.82 (m, 2H), 1.50-1.47 (m, 4H), 1.36-1.26 (m, 11H), 0.94-0.91 (t, 3H, *J*=8 Hz). ^{13}C NMR (100 MHz, $CDCl_3$) δ (ppm):185.22, 178.43, 163.68, 150.20, 147.97, 131.83, 130.88, 129.60, 127.37, 115.49, 114.74, 110.50, 58.59, 53.60, 31.95, 29.30, 22.72, 18.56, 14.12.

Compound *L*-**27** (0.06 g, 92%)**:** ^{1}H NMR (400 MHz, $CDCl_3$) δ (ppm): 7.88-7.86 (d, 2H, *J*=12 Hz), 7.64-7.62 (d, 2H, *J* = 8 Hz), 7.38-7.30 (m, 3H), 7.02-6.97 (m, 6H), 4.58-4.56 (m, 2H), 4.06-4.02 (m, 2H), 3.74-3.71 (m, 2H), 2.94-2.91 (m, 2H), 1.86-1.82 (t, 3H, *J*=8 Hz), 1.52-1.31 (m, 16H), 0.95-0.92 (t, 3H, *J*=8 Hz). ^{13}C NMR (100 MHz, $CDCl_3$) δ (ppm): 168.24, 160.59, 158.08, 143.70, 141.08, 131.73, 131.13, 130.73, 129.62, 127.31, 125.90, 118.56, 115.34, 114.84, 113.13, 107.29, 68.48, 67.48, 64.36, 58.73, 53.50, 38.21, 37.61, 31.78, 29.46, 26.05, 22.53, 18.70, 14.28, 13.68.

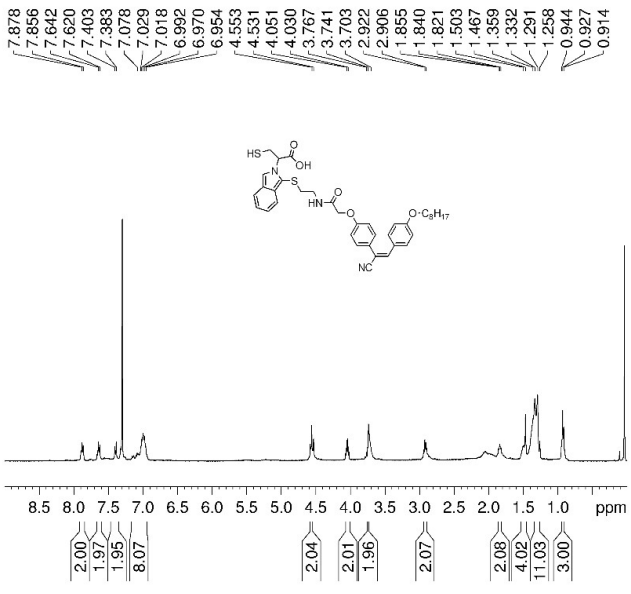

Figure S115 ^{1}H NMR of *L*-**15** (400 MHz, $CDCl_3$)

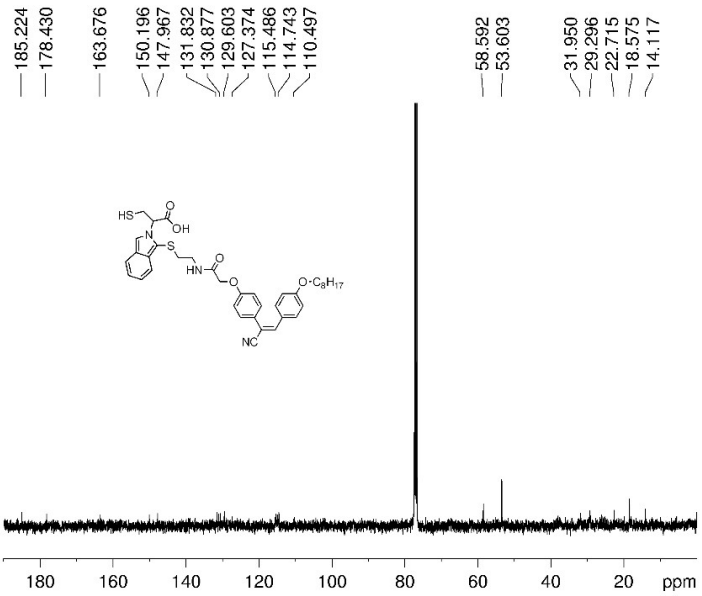

Figure S116 ^{13}C NMR of *L*-**15** (400 MHz, $CDCl_3$)

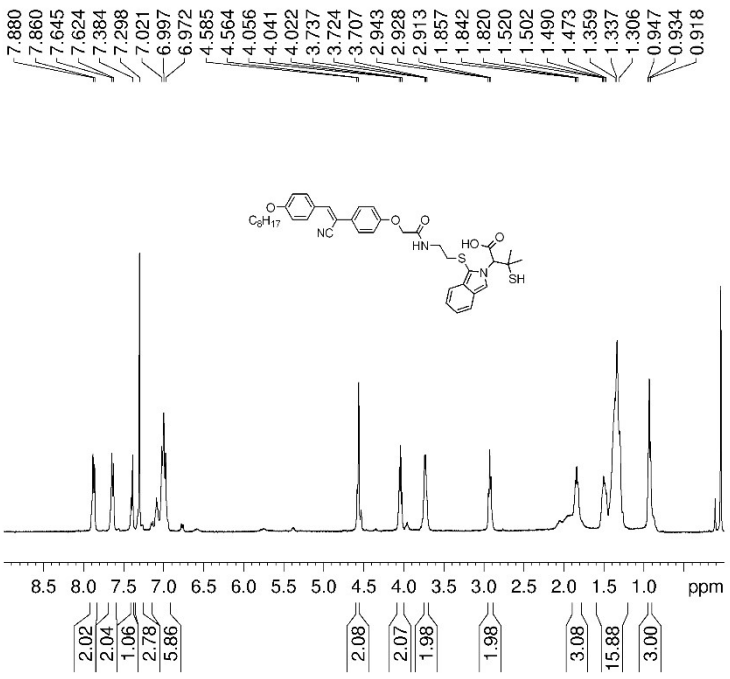

Figure S117 ^{1}H NMR of *L*-**27** (400 MHz, $CDCl_3$)

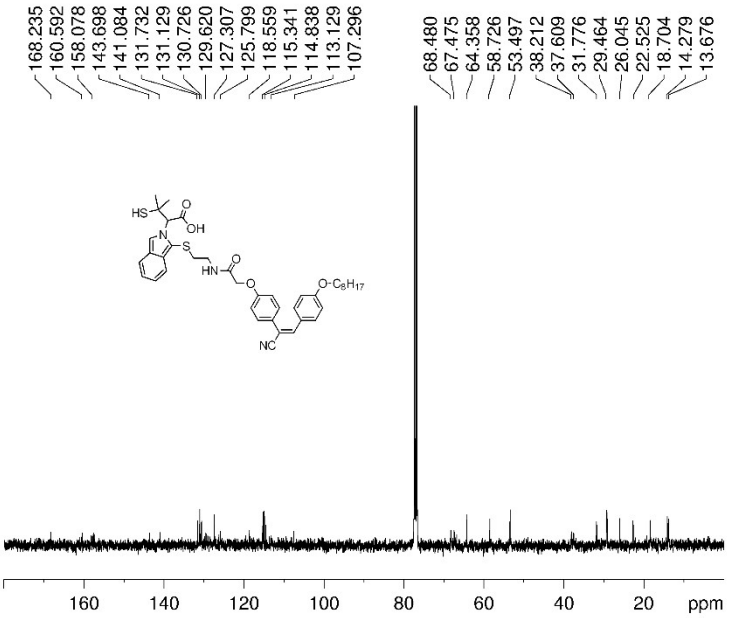

Figure S118 ^{13}C NMR of *L*-**27** (400 MHz, $CDCl_3$)

Quantitative amino acid sensing: absolute configuration, enantiomeric excess and total concentration

Calibration curve for concentration analysis of (*L*)-7 using probe 1

Arginine **7** in varying concentrations (0.625, 1.2, 2.5, 3.33, 5 mM), NaOH (6 mM) and probe **1** (5 mM) were mixed in 1 mL of ACN and the reaction was shaken for 1 min (the pH was adjusted to 9 by NaOH). A 125.0 μL aliquot of the solution was diluted with 2.0 mL of ACN/H_2O mixture (1:4) and subjected to CD analysis using a quartz cuvette (0.1 cm path length). The UV absorbance at 230 and 340 nm increased as the original concentration of (*L*)-**7** varied from 0.0 to 5.0 mM. Plotting and curve fitting of the UV absorbance change at 230 and 340 nm against the concentration (mM) of (*L*)-**7** gave a polynomial equation. (230 nm: y = 3.56287x+0.04804, R^2 = 0.9995; 340 nm: y = 1.03914x+0.05548, R^2 = 0.997).

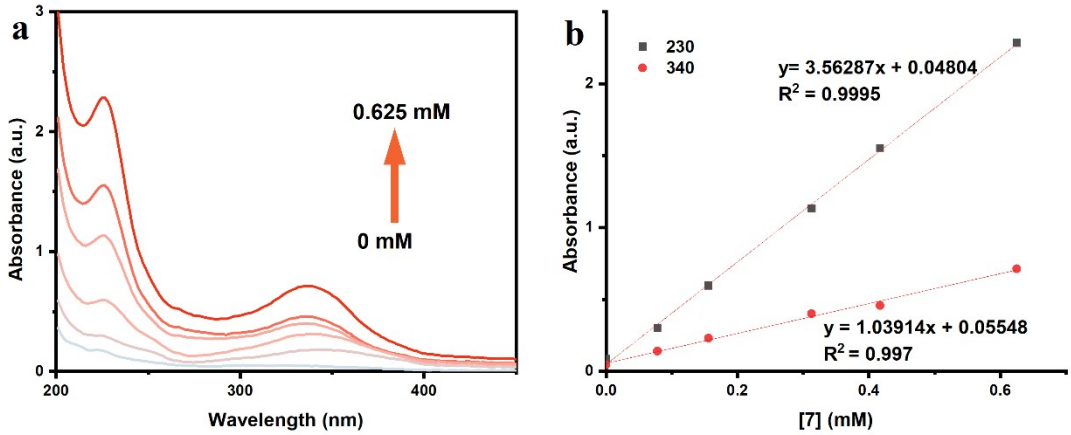

Figure S119. (a) Change in the UV absorbance upon reaction of (*L*)-**7** with probe **1**. (b) Absorbance at 230 and 340 nm of the reaction mixture plotted against the concentration of (*L*)-**7**.

Calibration curve for enantioselective analysis of arginine using probe 1

A calibration curve was constructed using samples containing aspartic acid with varying enantiomeric composition. Probe **1** (5 mM) and arginine (5.0 mM) with varying *ee*'s (+100, +80, +60, +40, +20, 0, -20, -40, -60, -80, -100%) were dissolved in 1 mL of ACN/H_2O mixture (4:1) and the reaction was shaken for 1 min (the pH was adjusted to 9 by NaOH). A 125.0 μL aliquot of the solution was diluted with 2.0 mL of ACN/H_2O mixture (1:4), allowed to stand for 15 min and then subjected to CD analysis using a quartz cuvette (0.1 cm path length). CD amplitudes at 230 and 340 nm were plotted against the excess enantiomeric of arginine. (230 nm: y =0.3462x+0.75, R^2 = 0.9936; 340 nm: y = -0.05566x-0.442, R^2 = 0.9936).

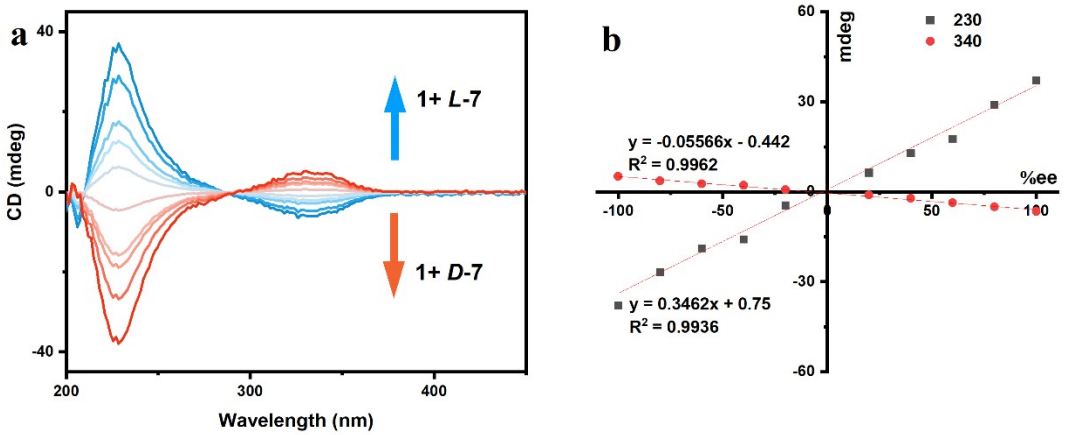

Figure S120. (a) Chiroptical response of probe **1** to scalemic samples of arginine **7**. (b) CD amplitude at 230 and 340 nm *vs*. sample ee.

Simultaneous determination of concentration and enantiomeric composition

Ten samples of phenylethylamine at varying concentrations and enantiomeric composition in ACN were prepared and subjected to simultaneous analysis of the concentration, enantiomeric excess, and absolute configuration using probe **1**. First, a UV spectrum was obtained as described above and the concentration was calculated using the intensities at 230 and 340 nm, and the equation shown in Figure S120. Then, a CD spectrum was obtained as described above. The CD intensities were normalized to the concentrations obtained from UV analysis and the ee was calculated using the intensities at 230 and 340 nm, and the equation shown in Figure S108. The absolute configuration was determined using the sign of the Cotton effect.

S Table 1. Concentration, enantiomeric ratio, and absolute configuration (AC) of samples of arginine determined by simultaneous UV and CD responses of probe **1**.

Entry	Sample composition			Sensing results						
	AC	Conc.[mM]	*L*/*D*	AC	Conc.[mM] at 230 nm	Conc.[mM] at 340 nm	Conc.[mM] (averaged)	*L*/*D* at 230 nm	*L*/*D* at 340 nm	*L*/*D* (averaged)
1	*L*	5.0	20.0:80.0	*L*	4.8	5.0	4.9	20.6:79.4	21.6:78.4	21.1:79.9
2	*D*	3.0	82.0:18.0	*D*	2.8	3.2	3.0	81.6:18.4	82.8:17.2	82.4:17.6
3	*D*	2.5	60.0:40.0	*D*	2.8	2.4	2.6	60.2:39.8	60.6:39.4	60.4:39.6
4	*D*	3.5	70.0:30.0	*D*	3.6	3.5	3.55	70.8:28.2	72.2:27.8	71.5:28.5
5	*D*	4.0	90.0:10.0	*D*	4.1	4.3	4.2	91.7:8.3	90.7:9.3	91.2:8.8
6	*L*	4.0	60.0:40.0	*L*	3.9	4.2	4.05	58.9:41.1	60.9:39.1	59.9:40.1
7	*L*	4.0	35.0:65.0	*L*	4.0	4.2	4.1	36.5:63.5	35.7:64.3	36.1:63.9
8	*L*	2.0	55.0:45.0	*L*	2.3	1.7	2.0	58.0:42.0	56.0:44.0	57.0:43.0
9	*L*	4.0	5.0:95.0	*L*	4.1	3.8	3.95	3.8:96.2	4.8:95.2	4.3:95.7
10	*D*	2.5	60.0:40.0	*D*	2.3	2.9	2.6	59.0:41.0	61.0:39.2	60.5:39.5

The determination of chiral analytes at low concentration

Due to low label reactivity and high background noise, chiroptical sensing of low concentration analytes remains a difficult challenge for existing methods. We were pleased to find that our method worked well for a range of arginine concentrations (6.25×10^{-7}~1.25×10^{-3} M) under the same operating conditions with the same amount (3.13×10^{-4} M) of OPA and sensor **1** and a mixing time of 5 min. As shown in figure S121, excess amounts of chiral reagents had a negligible effect on the CD and UV signals at 330 nm due to the unique signal amplification mechanism of this method.

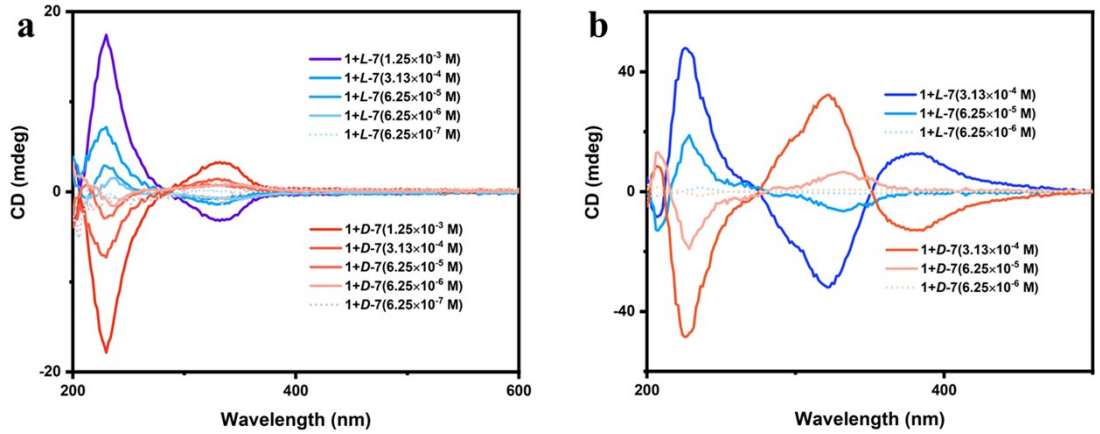

Figure S121. Chiroptical response of probe **1** (3.13×10^{-4} M) to for a range of arginine **7** concentrations (6.25×10^{-7}~1.25×10^{-3} M) with a quartz cuvette (0.1 cm path length)). (a) in ACN (b) in ACN/H_2O (1:4).

References

1. L. K. Ji, Y. T Sang, G. H. Ouyang, D. Yang, P. F. Duan, Y. Q. Jiang, M. H. Liu. Cooperative chirality and sequential energy transfer in a supramolecular light-harvesting nanotube. *Angew. Chem. Int. Ed.* **2019**, *58*, 844-848.
2. L. Lin, X. Lin, H. Guo, F. Yang, Diphenylacrylonitrile-connected BODIPY dyes: fluorescence enhancement based on dark and AIE resonance energy transfer. *Org. Biomol. Chem*., **2017**, *15*, 6006-6013.
3. J. Li, H. K. Bisoyi, J. Tian, J. Guo, Q. Li, Optically rewritable transparent liquid crystal displays enabled by light-driven chiral fluorescent molecular switches. *Adv. Mater*., **2019**, *31*, 1807751.
4. Z. W. Zhang, J. T. Li, W. Y. Wei, J. Wei and J. B. Guo, A luminescent dicyanodistyrylbenzene-based liquid crystal polymer network for photochemically patterned photonic composite film. *Chin. J. Polym. Sci.*, **2018**, *36*, 776-782.
5. Abraham, M. J.; Murtola, T.; Schulz, R.;Páll, S.; Smith, J. C.; Hess, B.; Lindahl, E., GROMACS: High performance molecular simulations through multi-level parallelism from laptops to supercomputers. *SoftwareX* **2015**, 1, 19-25.
6. Wang, J.; Wolf, R. M.; Caldwell, J. W.; Kollman, P. A.; Case, D. A., Development and testing of a general amber force field. *J. Comput. Chem.* **2004**, 25 (9), 1157-1174.
7. Frisch, M.; Trucks, G.; Schlegel, H.; Scuseria, G.; Robb, M.; Cheeseman, J.; Scalmani, G.; Barone, V.; Petersson, G.; Nakatsuji, H., Gaussian 16, Revision B.01. 2016.
8. Lu, T.; Chen, F., Multiwfn: A multifunctional wavefunction analyzer. Journal of computational chemistry 2012, 33 (5), 580-592.
9. Martínez, L.; Andrade, R.; Birgin, E. G.; Martínez, J. M., PACKMOL: A package for building initial configurations for molecular dynamics simulations. J. Comput. Chem. **2009**, *30* (13), 2157-2164.
10. Berendsen, H. J.; Postma, J. v.; Van Gunsteren, W. F.; DiNola, A.; Haak, J. R., Molecular dynamics with coupling to an external bath. *J. Chem. Phys.* **1984**, 81 (8), 3684-3690.